INFORMATION TO USERS

This manuscript has been reproduced from the microfilm master. UMI films the text directly from the original or copy submitted. Thus, some thesis and dissertation copies are in typewriter face, while others may be from any type of computer printer.

The quality of this reproduction is dependent upon the quality of the copy submitted. Broken or indistinct print, colored or poor quality illustrations and photographs, print bleedthrough, substandard margins, and improper alignment can adversely affect reproduction.

In the unlikely event that the author did not send UMI a complete manuscript and there are missing pages, these will be noted. Also, if unauthorized copyright material had to be removed, a note will indicate the deletion.

Oversize materials (e.g., maps, drawings, charts) are reproduced by sectioning the original, beginning at the upper left-hand corner and continuing from left to right in equal sections with small overlaps.

ProQuest Information and Learning
300 North Zeeb Road, Ann Arbor, MI 48106-1346 USA
800-521-0600

Université d'Ottawa · University of Ottawa

The Steady State and Transient Behaviour of 2D Braiding

Albert Mazzawi

A thesis submitted to the Faculty of Graduate and Postdoctoral Studies
in partial fulfilment of the requirements of the degree of

DOCTOR OF PHILOSOPHY
in Mechanical Engineering

Ottawa-Carleton Institute for Mechanical and Aerospace Engineering
University of Ottawa
Ottawa, Canada

December 2001

to my Chéro

Age is just a number

ABSTRACT

Two-dimensional braiding of fibre-reinforced composite components is a promising process for automation. Control of the braiding equipment when the braid angle is changing (transient braiding) is currently achieved either by trial and error or by using simplistic theories. One major contribution of this work is the development of a device and associated mathematical model that allows measurement of the braid angle on-line. This work has also explained the discrepancy between desired and measured braid angles reported in the literature. Finally, a mathematical model to predict the structure of the braid during transient braiding was developed. The experimental data presented strengthen the validity of the analytical expressions developed.

Un processus d'automation prometteur est celui du tissage à deux dimensions des matériaux composés. On obtient le contrôle de l'équipement du tissage en modifiant l'angle du tissage qui se fait présentement soit par essai ou erreur, soit par l'utilisation de theories simplistiques. Cette étude contribue d'une manière importante au développement d'un instrument et de son modèle mathématique qui permettent de mesurer l'angle de tissage 'on-line'. Cette étude explique egalement la différence dans les angle de tissage anticipés et mesurés auquels se réfère la littérature. Finalement, cette étude a permis de developper un modèle mathématique déstiné à prévoir la structure du tissage durant la phase transitoire. Les résultats expérimentaux présentés renforcent la validité des formules analytiques développées.

ACKNOWLEDGMENTS

I wish to express my gratitude to my supervisors, Drs Fahim and Munro, for their constant encouragement, for their critical discussions, for the valuable suggestions given throughout this work and, in particular, for the required space to grow and to innovate that was freely provided.

Also, many thanks are due to Mr. Makasare, head of the workshop of the Department of Mechanical Engineering and his team, for the extensive use of the facilities during the different phases of this research.

Albert Mazzawi

TABLE OF CONTENTS

LIST OF FIGURES

LIST OF TABLES

NOMENCLATURE

r	instantaneous radius of mandrel
R_m , R	radius of the mandrel at the point of braid formation for cylindrical braiding (used in this work and in[5,9,19]).
r_1 , r_2	radii of a conic mandrel.
γ	half cone angle of a tapered mandrel.
R_G	the radius of the formation ring at the guide plane. The average radius of the bobbin carrier payout eye if no guide ring is used.
R_R	variable radius of a guide ring.
λ	ratio of R_m / R_R
v, v_t	mandrel linear speed. Sometimes referred to as the mandrel transverse speed (used in this work and in[5,9,19]).
v_r , ω	carrier rotational speed.
N_c , N	number of braider spools (used in this work and in[5,19]).
w, W_y , w_c	strand width on the mandrel surface (used in this work and in[5, 9, 10,19]).
K , F_ω	fabric cover factor (ratio of area covered to total area).

θ	braid angle at the point of formation of the braid on the mandrel. It describes the strand orientation (see Glossary for additional explanation).
D, H	length of the convergence zone (used in this work and in[9,10]).
$D\infty$	length of the convergence zone at steady state.
z	distance from a reference point on the mandrel to the deposit plane (braid length).
V_f, V_v	volume fraction (used in this work and in[5,19,9,10]). (see Glossary for additional explanation).
P	pitch of a helix.
ζ	the strand interlacing parameter. This angle quantifies the displacement of the deposit plane due to interlacing of fibre strands near the deposit plane.

GLOSSARY

Axis of braiding:

The average direction of all strands in a braided fabric. In this work, it is the centre line of the tubular mandrel mounted in the mandrel drive.

Braid angle:

The acute angle measured from the axis of the braided fabric to a braiding strand (Figure 1.1). It describes the strand orientation along the mandrel length. For this thesis, the following interpretations are considered:

– desired angle — typically calculated using machine parameters, $\tan^{-1}\left(\omega \cdot r / v\right)$.

– measured angle — usually measured (or calculated) from the braided fabric, $\tan^{-1}\left(2 \cdot \pi \cdot r / pitch\right)$ (Figure 5.1).

– derived angle — a function of the coordinates of the point where the swinging arm of the cone angle measurement device lies over the cone shaped outline of the strands in the convergence zone.

Braiding system :

A manufacturing facility consisting of a braiding head and a mandrel drive (Figure 1.1).

Braid, Two-dimensional:

A braided fabric with two braiding strands in the through thickness direction.

Circular braiding:

A textile process for forming tubular fabrics. This process has been extended to produce a range of structural shapes for composite applications.

Convergence zone:

The zone where the fibre strands converge onto the mandrel (Figure 1.2). The convergence zone starts from the guide plane and ends at the deposit plane.

Deposit plane:

The plane where all the fibre strands first come in contact with the mandrel surface (Figure 1.2).

Fabric cover factor:

The fabric cover factor of a fabric is defined as the ratio of the area covered by the strands to the total surface of the workpiece (for simplicity, also called cover factor).

Fell:

The point of braid formation on the mandrel, defined as the point at which the strands in a braid system cease movement relative to one another.

Guide plane:

The plane of the guide ring. However, the guide plane could be the plane of the carrier track if no guide ring is installed (Figure 1.2).

Helix angle:

The complement of the braid angle.

Jammed state:

The state of a braided fabric under tension where the deformation of fabric is

dominated by the deformation properties of the strand.

Plait:

A plait is one repeat of the "braid weave" measured along the braid axis (Figure 2.1).

Spool:

A cylinder or slightly tapered barrel, with or without a flange, for holding fibre strands on the braiding head (Figure 1.1).

Unit cell:

A geometrical representation of a section of a braided fabric that is repeated throughout the structure.

Strand:

Continuous bundle of textile fibres or filaments in a form suitable for knitting, weaving or intertwining to form textile fabrics. Also, referred to in other publications as yarn or tow.

Volume fraction:

The **fibre** volume fraction, V_f, is a standard measure of the average volume of the fibre in a strand relative to the total volume of the composite strand.

The **fabric** volume fraction, V_v, is the volume of the fibre relative to the total volume of the composite braid.

Transient State:

Machine — Period in which the braiding head drive and the mandrel drive reach steady state. This occurs typically in a few milliseconds.

Fabric	Period in which the braided fabric reaches steady state. This occurs typically after few revolutions depending on the start-up position of the braid.

Chapter 1

Presents a brief discussion of relevant publications as well as an outline of the thesis.

INTRODUCTION

1.1 Literature Review

Manufacturers of fibre-reinforced composite material components are increasingly turning to textile fabrics fibres in order to increase fibre deposition rates, thus reducing manufacturing costs. The most commonly used fabric is the traditional flat satin whose fibre strands run over and under one another at right angles. For closed tubular structures, textile fabrics produced by 2D braiding[1] are used. This permits the interlaced fibres to be placed at any braid angle.

Braids of circular cross-section are typically formed by 2D braiding machines. A schematic arrangement of this type of machines is shown in Figure 1.1. As shown in the figure, two sets of strand spools are positioned with their axes normal to the braiding head plane. One set travels in the clockwise direction, the other in the counter clockwise direction along intersecting serpentine paths. A braid is formed when the two groups of strands alternately cross over and under each other causing an interlaced pattern on the surface of the braided fabric. These braids may be used to cover a mandrel as it traverses at a right angle to the braiding head during the braiding operation, they may be made as flexible tubing to be later placed over a centre core, or they may be flattened and used as a tape of double thickness. The fabric structures produced by braiding are commonly used in applications such as cordage, electrical cable covers, ornamental textile articles and, more recently, reinforcements in composite material applications.

Fibre placement by braiding is emerging as an important process for fibre reinforced

---

[1] Throughout this thesis, the term "braiding" will refer to the two-dimensional braiding process.

composite materials manufacturing. During this process, an integral fibre-reinforced structure can be created all at once, impregnated with an appropriate matrix and then cured. The braiding process is viewed as a potentially cost-effective alternative to filament winding given its potential for higher fibre deposition rates. Unlike filament winding, the strands in a braid are mechanically locked. This locking does not limit the placement of the strands to non-slip (geodesic or friction-stabilized) paths as in filament winding [1,2]. In both processes, a thin shell-type structure is produced.

Braiding is widely used for the production of straight cylindrical sock-like fabrics. As discussed below, attempts by others to braid over conic or axially symmetrical mandrels were inconclusive. Machine speeds are usually determined by trial and error or by using simplistic assumptions about the structure and operating parameters. Manual control of the braiding process becomes impractical when conic or other complex profile braids are required. Braiding system control and automation is the most plausible solution.

Detailed data on braids and on the braiding process is scarce as compared to that for flat unidirectional hand lay-up and some woven fabrics. A brief overview of published literature on 2D braiding is presented in the remainder of this section. Some of the articles will be discussed in more detail in the following sections due to their particular applicability.

There are a number of general articles and papers that describe applications of braided fibre reinforced composites; however, there are few published articles that detail the braiding process and the resulting braided structures. The work by Brunnschweiler [3, 4] in the 1950's is still the most referenced research to date. The author attempted to determine the load-strain behaviour of circular braids without cores by analytical and experimental techniques. Ko *et al* [5-7] calculated the area percentage of fibre coverage on the core (fabric cover factor) and developed stiffness matrices for predicting the engineering properties of the braid. Michaelli and Rosenbaum [8] developed an

algorithm for the control of a braiding machine. Their algorithm only relates the machine speeds and the shape of the mandrel to the braid angle, but did not include consideration of other braid parameters pertaining to the braided structure such as the fabric cover factor.

In 1990, Du and Popper [9, 10] published the most comprehensive work to date on the braiding process. They developed a mathematical model to describe the braiding process as applied to axially symmetric shapes, and to relate the process variables to the overall shape of the part and its micro-structure. Their model uses a set of geometric and kinematic relationships to predict the braid geometry assuming that the strand is straight in the convergence zone (Figure 1.2). They reported that the measured braiding angles on a cylindrical mandrel are always lower than those predicted by their model. They suggested that the predictability could be improved by including consideration of strand curvature in a small region of the convergence zone near the deposit plane.

In 1999, Zang *et al* [11, 12] investigated the validity of the assumption that a strand of fibre could be represented by straight lines in the convergence zone. The authors considered the effect of friction forces introduced by the relative sliding of the strands during their interlacing motion. Their proposed a model predicts the braid angle when interlacing forces are considered. Predicted braid angles for different machine speeds and different spring tensions were compared to their steady state values and the observed discrepancies (3 to 4 degrees) were attributed, among other factors, to the change in the deflection of the tension spring during the serpentine path of the spools. It was concluded that the effect of friction forces is more pronounced in larger braiding machines with more than 64 spools. Although the results of this study supports, to a degree, the assumption that the fibre strands can be represented by straight lines in the convergence zone, it did not consider the strand curvature due to strand interlacing in the small region near the deposit plane which is relevant to this work.

The preceding survey of pertinent open literature reveals that the development of models for 2D braiding has been limited. Simple mathematical expressions have been used to compute a range of braiding head-to-mandrel speed ratios for steady state braiding. The effect of braiding during the transient state, where the braid formation per revolution changes, is typically ignored since it could be dealt with either by removing the start-up part of the braided fabric, or by locating the starting position of the braiding process as close as possible to its theoretical steady state value. However, for conic or other complex profile braids where the braid angle must change continuously while braiding, existing models are inaccurate. Typically, one has to revert to trial-and-error procedures to overcome this problem. Thus, any predictive model should accurately account for the transient state in braiding.

1.2 Outline of the Thesis

This thesis consists of seven chapters. A general review of predictive models for braiding and a brief discussion of published results is presented in this introduction.

Chapter 2 is devoted to a detailed analysis and evaluation of published models most relevant to the current study. The predictive models are re-constructed here.

Chapter 3 deals with the geometry of the "unit cells" as defined by various authors and used to calculate the fabric cover factor. As well, a new general expression is developed to express the fabric cover factor and a comparison with published expressions using a tapered mandrel is made.

The steps taken to prepare the University of Ottawa braiding machine for conducting reliable and repeatable operations are presented in Chapter 4. Modifications to the existing braiding machine are discussed, computer programs for speed control as well as

mandrel displacement are described, and finally experiments for calibration of the different sensors are documented and their results are discussed.

The results of experimental braiding over both cylindrical and conic surfaces under different operating conditions are presented in Chapter 5. The adopted strategies for braiding are discussed, the computer programs used to support the experiments are documented, and the experimental results are evaluated.

In Chapter 6, an analysis of braid formation during the transient state is conducted. It shows that a steady state operation can be practically reached perspective after a small but measurable distance from the beginning of mandrel shape transition. However, if the mandrel shape is continuously changing, as in the case of a cone or other more complex shapes, steady state operational conditions are never reached. In addition, any perturbation due to changes in friction or tension in the springs would reintroduce a transient state in the process The experimental data presented strengthen the validity of the analytical expressions developed.

Finally, conclusions are given in Chapter 7. An outlook for future work is also presented in this chapter.

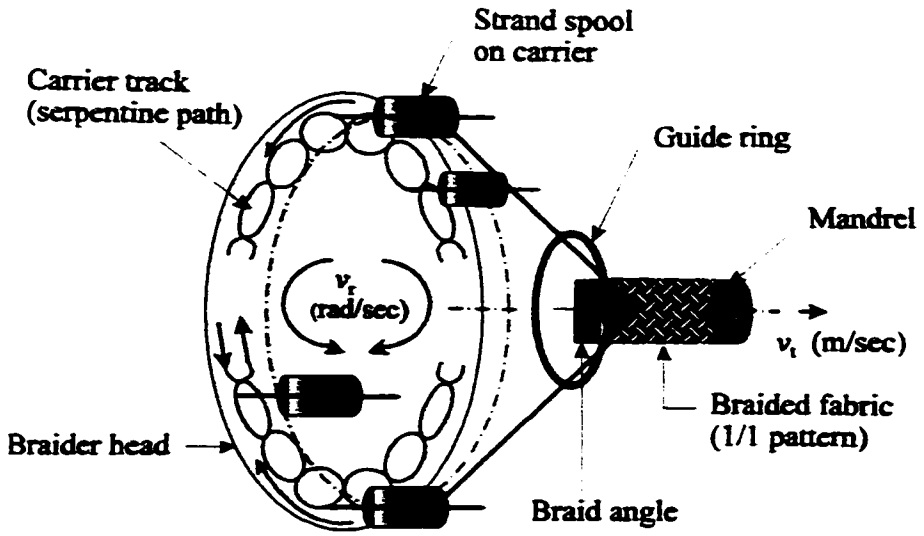

Figure 1.1 Schematic of a 2D braiding machine

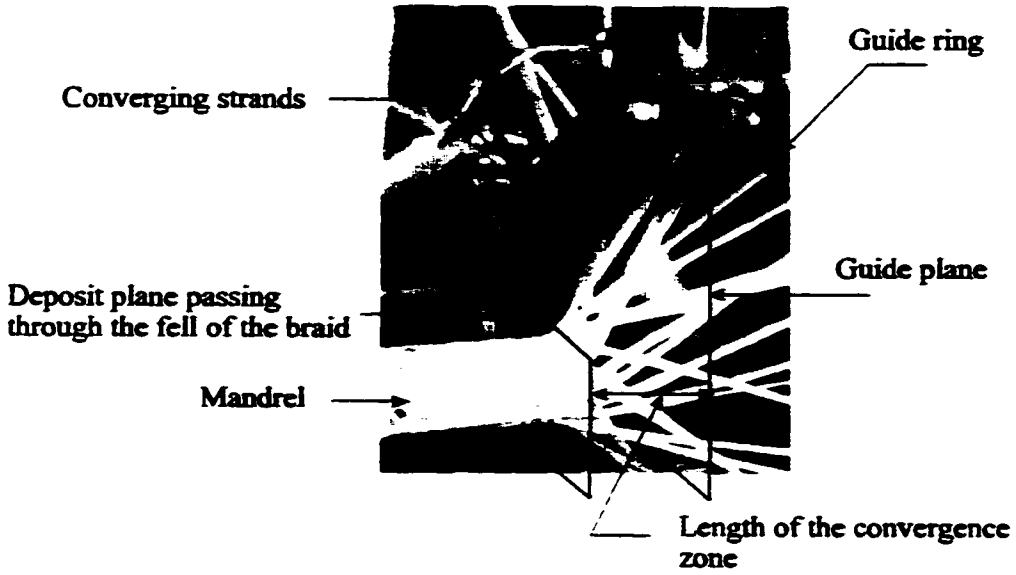

Figure 1.2 The convergence zone

Chapter 2

Detailed analysis and evaluation of published models most relevant to the proposed study are presented in this chapter.

ANALYSIS AND EVALUATION OF EXISTING MODELS FOR BRAIDED STRUCTURES

The geometry of a braid is directly related to the machinery or the mechanism which forms the fabric. By understanding the relationship between the machine and the strands, it is possible to construct a model which describes the structure of the braid. In general, these models were classified by Ko *et al* [5] as follows:

a) A topological model relates the fundamental aspects of the braiding system as a mathematical entity to the mechanism of braiding. These models include a study of the braid pattern and the geometry of the unit cell of the fabric assuming ideal strand properties.

b) A geometric model correlates the physical properties of strands and fabrics with a topological model to produce a realistic model of the fabric which includes fabric dimensions, fibre volume fraction and spatial orientation.

c) The mechanical model relates the geometry of the fabric to the mechanical response of the composite structure using a variety of approaches including those based on Classical Laminate Plate Theory.

This work focuses on the geometric model approach as followed by other studies, in particular, Brunnschweiler [3], Ko et al [5] and Du and Popper [9], all of which are widely referenced. Their models are comprehensive and warrant detailed review and discussion.

2.1 D. Brunnschweiler Model

The first systematic analysis of the structure and formation of braids was presented in 1953 by Brunnschweiler [3]. He introduced the definition of braiding as "the production of ribbon-like textures by the interlacing of one set of threads in such a manner that no two adjacent threads make a complete turn about each other". He stated that an almost unlimited variety of interlacing patterns can be created, and added that every braid pattern consists of repeating units termed "plaits" (also, "stitches" or "picks"). Among these patterns, three have acquired general recognition and are used frequently in the textile industry: the Diamond braid (1/1), the Regular braid (2/2), and the Hercules braid (3/3). In Figure 2.1 the diamond and regular braid patterns are illustrated. The term x/x defines the method of interlacing, thus, if a strand continuously passes over two strands and then under two other strands, then the braid structure is designated as having a 2/2 pattern.

The investigation of such patterns is simplified by formulating geometrical relationships which assume ideal strand properties. The plait geometry can be idealized as a diamond trellis. Thus for a 1/1 pattern (Figure 2.2), the diamond trellis geometry is defined by x and α where x is the plait and α is the cross-over angle bisected by the braid axis. Assuming that the strands are flexible, inextensible, and incompressible, the trellis can be distorted to a variety of extended and contracted positions until the strands jam against each other, thus preventing any further motion. In the extreme positions, all strands are lying side by side and the pattern is said to be "closed". Any orientation between the two locked positions is said to be an "open" pattern. For typical strands, jamming angles vary between ± 15 and ± 75 degrees.

Brunnschweiler has analytically investigated braid geometry for the simple case of 1/1 two-dimensional braids. His model relates the jamming angle to the cross-sectional shape of the strands.

2.2 Ko and Pastore Model

Ko *et al* [5-7] developed their model as part of a CAD/CAM system. Their geometric model correlates the physical properties of the strands and fabrics with a topological model to produce a realistic geometric model of the fabric which predicts cover factor, fabric volume fraction and spatial orientation. In traditional textile engineering, the cover factor of the fabric is a standard design parameter which defines the density of the fabric.

After identification of a repeating geometric or unit cell defining the fabric structure (Figure 2.1), the cover factor of the fabric within the cell can be expressed as a function of the geometry of the cell and strand orientation. The fabric cover factor, or simply the cover factor, is defined as the projected strand area in a unit cell divided by the area of the cell. The orientation of the strand can be related to machine parameters namely, the rotational speed of the braiding head, v_r, and transverse speed of the mandrel, v_t. Typically, the rotational braiding head speed is fixed. Thus the manufacturer would have one degree of freedom, transverse mandrel speed, to control the machine operation. When braiding over a complex shaped mandrel (modelled as a series of concentric circular cross sections Ko *et al*) the instantaneous radius is expressed as a function of the length of the mandrel. A summary of the mathematical expressions derived by Ko *et al* is detailed in Appendix A. The authors reported that several mandrels ranging from simple cylinders and cones to complex coupling rods and turbine rotor bodies were successfully braided at their research laboratories. Their published work included a photograph, shown in Figure 2.3, of a coupling rod being braided with their system. No other information relating to the process was given.

2.3 Du and Popper Model

In 1991 Du and Popper published their work "Process Model of Circular Braiding [9]" followed, in 1994, by a complementary publication on the same topic entitled "Analysis of a Circular Braiding Process for Complex Shapes [10]". In these works, a mathematical model, as applied to axially symmetric shapes, was developed to describe the braiding process, and to relate the process variables to the overall shape of the part and its structure.

Their analysis was based on the following assumptions:

a) The mandrel shape is a surface of revolution, and the process is axially symmetric; therefore, one strand can represent all others.

b) The strand is straight in the convergence zone. This assumption neglects the interlacing effect between strands.

c) The strand does not slip relative to the mandrel. The interlacing pattern permits the strand to follow non-slip paths on the mandrel. Since no strand-mandrel slippage after strand deposit was assumed, the braid angle, θ, must equal the angle formed between the converging strands and the axis of the braid.

The braid angle, θ, as defined in their model describes the strand orientation along the mandrel length and is selected according to the loading direction of the composite part in its particular application. Since no strand-mandrel slippage after strand deposit was assumed, the braid angle, θ, must equal the strand inclination angle made between the strand and the generatrix of the cone tangent to the workpiece at the deposit point.

Their model consisted of a differential equation for the time variation of the convergence zone length, an integral equation to give the position along the braided mandrel at any time, and a geometric relation for the local braid angle at the current braiding point. Expressions for the fabric cover factor and the strand volume fraction as they relate to

the part profile were also presented. In addition, two criteria were also derived, namely, the limit of the process due to strand jamming where the maximum braid angle is given as a function of the strand width and the number of carriers, and the limit of the process due to mandrel geometry where the mandrel slope should not exceed a certain level depending on the direction of braiding. A special case of a sudden change in the mandrel diameter was also considered.

The experimental results reported by these researchers were as follows:

i) A series of 2D braiding experiments were conducted, with and without the use of a guide ring, to braid over a cylindrical mandrel with the machine operating at constant rotational speed, v_r, and transverse mandrel speed, v_t. The speed ratios were determined according to a desired braid angle and kept constant for each experiment. While braiding, the convergence length was allowed to expand, shrink or remain unchanged until a steady state was reached. This behaviour usually depends primarily on the initial value of the convergence length given at the start of the braiding process. Two cases of initial convergence length, h_o, were investigated; one longer and the other shorter than the predicted length at steady state operation. Measurements were made as follows: the deposit plane at every time increment was marked on the mandrel, the braid angle corresponding to the process time increment was measured from the mandrel (no details were given) and the convergence length was photographically recorded and measured after braiding.

   The desired and measured values of the convergence length showed good agreement (Figure 2.4a). The measured and desired braid angles along the mandrel are presented in Figure 2.4b. The results showed that the measured angle, at steady state, was always smaller by about 5° than the predicted value. The authors concluded that since "the model assumes that the strands lie in a

straight lines in the convergence zone and that they are tangential to the over braided mandrel at the deposit plane, these assumptions cause the predicted braid angles to be somewhat larger than measured values", and suggest that "the predictability could be improved by including yarn curvature in a small region of the convergence zone near the deposit plane [10]".

ii) Two other simulations were also reported, when braiding at a constant rotational and mandrel transverse speeds over a mandrel with a conic transition step. Two different transition cone slopes (18° and 38°) were used to illustrate the effect of the transition angle. Initial convergence lengths were set to obtain a uniform braid angle on the cylindrical portion to eliminate the transient phase at start-up. Instead of an anticipated uniform change in the braid angle during the transition zone, irregularities were observed during transition from small to large diameters, as shown in Figure 2.5. When the velocity profile was changed, by trial and error, to compensate for the undesired highly irregular behaviour, better results were claimed; however, no details were given.

iii) A baseball bat was also braided with the mandrel transverse speed maintained at a constant value along the bat length. The initial convergence length was set to produce a 45° braiding angle. The carrier rotational speed was first set to a constant value then dropped by half as the deposit plane moved to the beginning of the conic section. The previously observed 5° discrepancy between the desired and measured braid angle was still noticeable. However, this discrepancy gradually increased to about 10° along the tapered part of the bat.

It was not clear whether the reduction in carrier rotational speed to half its original value was chosen due to the profile of the bat or whether this drop was introduced to compensate for the irregularities in the braid angle mentioned in item 'ii'. It was also noticed that the bat was positioned on the mandrel where the

braiding of the conic section is from the larger diameter to the smaller one. Such positioning, according to the author, produces good agreement between desired and measured results.

2.4 Problem Definition

It follows from the above review that available information in the published literature is sometimes incomplete or inaccurate and experimental details are missing. In order to evaluate the reliability of the available predictive models and the relevance of their simplified assumptions, it is important to conduct a thorough analytical and experimental investigation. Consequently, a large set of experiments involving braiding over cylindrical and conic mandrels was performed, and the inherent problems in the existing models were identified, quantified and corrected.

The main objectives of this research were:

a) to contribute to the fundamental understanding of the dynamics of two-dimensional braiding along constant and varying mandrel cross sections and,
b) to develop an accurate predictive model for the reliable of the 2D braiding process along varying mandrel cross sections.

In order to accomplish these objectives, a number of tasks were performed. The topological models for braiding were reviewed in detail. This requires that the definition of the unit cell be revisited. This is the subject of the next chapter. As well, the mathematical expression relating the braid angle to the machine parameters were verified. The braiding machine located at the University of Ottawa was modified to perform reliable and repeatable operations. Computer programs were developed to support the required experiments, and finally, experiments were conducted and the results assessed.

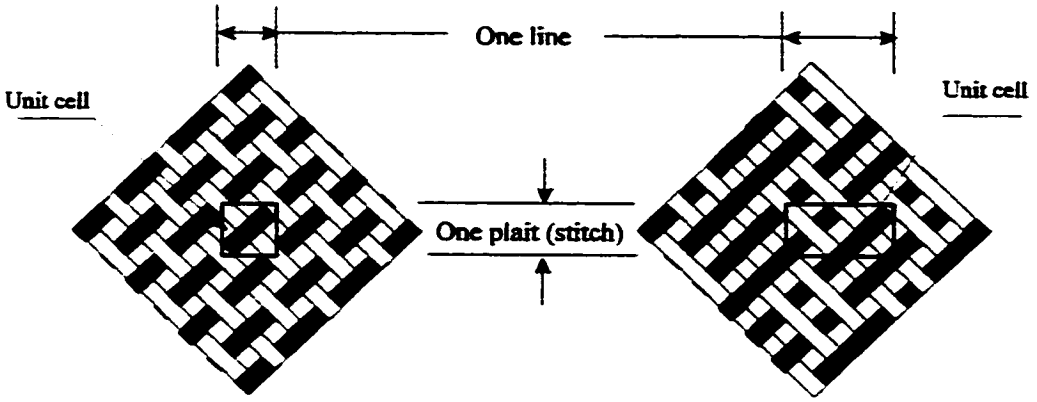

Figure 2.1 Representation of braid patterns

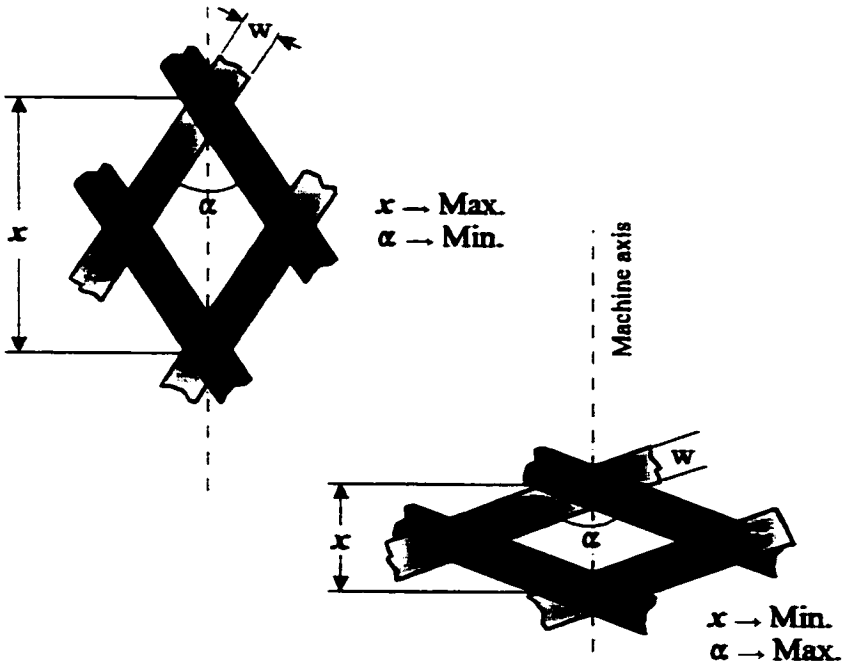

Figure 2.2 Strand jamming conditions

Figure 2.3 Formation of a braid around a mandrel (Courtesy of Atkins and Pearce [19])

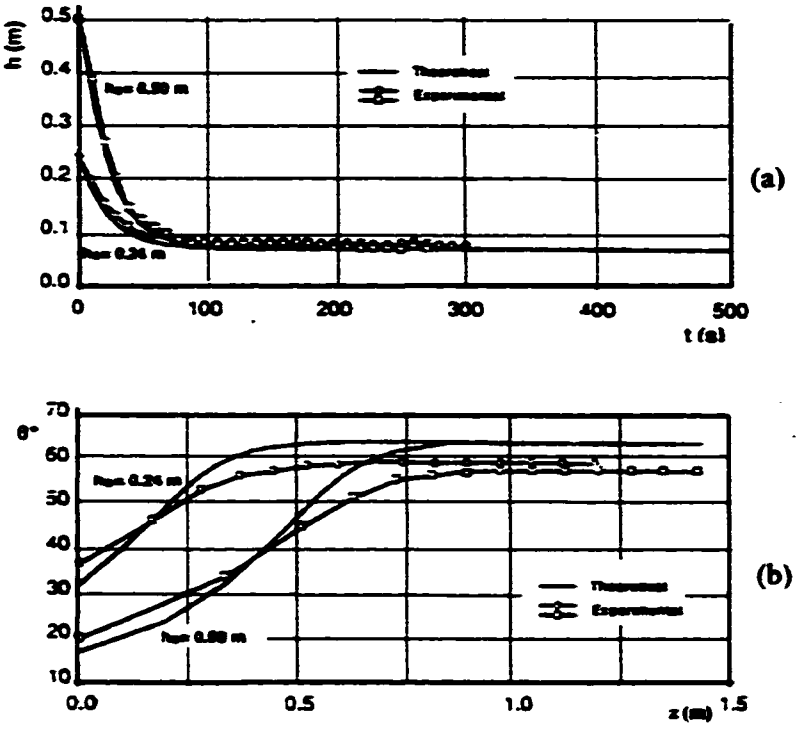

Figure 2.4 Convergence length and braid angle, measured vs predicted, (Du and Popper, [9,10])

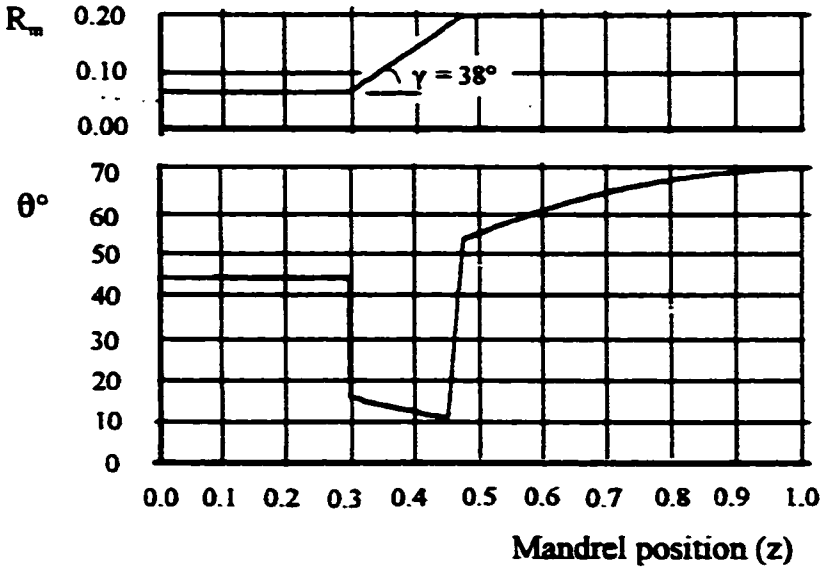

Figure 2.5 Variation of the braid angle for $\gamma = 38°$, (Du and Popper [10])

Chapter 3

In this chapter a review of the geometry of the 'unit cell' used to calculate the 'cover factor' as defined by various authors is conducted. Furthermore, a new general expression is developed to predict the cover factor on conic shapes and the results are compared with existing models.

THE UNIT CELL IN TWO-DIMENSIONAL BRAIDING

A fibre-reinforced composite component is normally designed in terms of its fibre volume fraction and the fibre orientation required to meet the mechanical and thermal loadings of the component. The fibre volume fraction, V_f, is a standard measure of the volume of fibre in a composite relative to the total volume of the composite. Although this parameter plays a critical role in the performance of the composite structures, it was noted by Atkins and Pearce [19] "that it does not translate directly to a fabric structure". For this case, the term fabric volume fraction is a more appropriate parameter. In braiding, the fabric volume fraction is an important parameter that affects the liquid flow in resin transfer moulding (RTM), a process in which a low viscosity resin is forced under pressure through a dry fabric preform. The fabric volume fraction is a function of the cover factor. The braid angle can also be expressed in terms of the cover factor. Thus, the cover factor is an important parameter for 2D braiding.

In this work, a preliminary evaluation of the formulae used to calculate the cover factor by Pastore and Ko [5] and Du and Popper [9, 10] as compared to experimental measurements on braided tubes revealed a substantial difference between the predicted and the experimental values. These differences were found later to be attributed to errors in the published formulae. Thus, the geometry of braided cells and the resulting expressions for the cover factor, as defined by Pastore and Ko and Du and Popper, was reviewed in detail. In addition, a new expression for calculation of the cover factor in conic surfaces will be developed and compared with the existing models.

3.1 The Unit Cell as Described by Pastore and Ko

Pastore and Ko [5] developed relationships for cylindrical braiding using a rectangular unit cell to represent the fabric structure as shown in Figure 3.1. They investigated the

geometry of a 1/1 two-dimensional braid where y and x represent the repeat of the pattern measured along the braid axis and normal to the braid axis, respectively. They calculated the area covered by the fibre strands and took into consideration the areas of fibre overlap at the centre and the overhang beyond the cell boundaries. They expressed these relationships mathematically as follows:

$$V_f = K + \left(\frac{2 \cdot w^2 \cdot \cos^2 \theta}{x^2} \right) \tag{3.1}$$

$$K = \frac{\left(2.x.w.\cos\theta - w^2\right)}{\left(x^2.\cos^2\theta\right)} \tag{3.2}$$

The orientation that will produce the desired cover factor can be calculated in terms of machine parameters and fabric structure as shown in Appendix A and is given by:

$$\theta = \cos^{-1}\left[\frac{N_c.w_y.\left\{1 + \sqrt{(1-K)}\right\}}{4.\pi.K.R_m} \right] \tag{3.3}$$

Furthermore, the authors stated that in the case of a mandrel with a complex shape consisting of concentric circular cross-sections, the radius, R_m, and the braid angle, θ, change with the length along the mandrel. This approach was considered in this study for comparison purposes.

3.2 The Unit Cell as Described by 'Du and Popper'

The relationship between the cover factor and the fabric volume fraction for a frustum of a cone has also been discussed by Du and Popper [9,10]. In developing the mathematical

expressions relating these parameters to the geometry of the braided fabric, they considered a segment of the braid formed in time, ∂t. It should be noted that the partial symbol "∂" is used to indicate that the variation is not multi dimensional. By cutting the braided cone along the line AB, then opening up the cone, the braided fabric becomes flat, as illustrated in Figure 3.2.b. The unit cell, as defined by the authors, includes a $+\theta$ and a $-\theta$ yarn, and a spacing of ∂s between two neighbouring cells. Expression relating the fabric volume fraction, $V_y(z)$, and the fabric cover factor, $F(z)$, to machine and mandrel parameters were developed and are as follows:

$$V_y(z)=\frac{w_y.\sin\gamma(z)}{2.R_m(z).\cos\theta(z).\sin\left\{\frac{2.\pi.\sin\gamma(z)}{N_c}\right\}} \tag{3.4}$$

and;

$$F(z)=1-\{1-V_y(z)\} \tag{3.5}$$

The unit cell relates the spacing ∂s between two neighbouring strands to the incremental length of the fibre. Also in their analysis, it was stated that on the plane developed by cutting the cone along the generatrix, the braided strands become straight lines. This would lead to approximate results since a strand, when braided over a cone-shaped mandrel, follows a spiral (helix) path which climbs up the side of a circular cone. Therefore, the strand in the unit cell should have been represented by a curve rather than a straight line. In addition, since the position of the $-\theta$ strand, as presented, lies outside the time element ∂t, it may not have the same length as of the $+\theta$ strand. Therefore, the unit cell, as defined, may not accurately represent the braided structure.

3.3 An Alternate Method for Defining the Unit Cell – a 'Comprehensive Model'

The fact that the path of the strand over the cone-shaped mandrel should be represented

by a conic helix instead of a straight line, this can be taken into consideration when developing the general representation of the unit cell and hence provide for a more accurate method to calculate the cover factor. Furthermore, other quadratic surfaces of revolution can be approximated as a series of frustum of cones with different slopes, and their cover factor calculated using the proposed alternative method.

In order to properly define the unit cell, the conic section of the braid formed during one complete revolution is considered. The number of strands that can be laid on such a surface is limited to the number of braiding strands and, consequently, the number of spools, N_c. On the plane developed by cutting a 1/1 biaxial braided structure along its generatrix, the deposited strands can be identified as two sets of $N_c/2$ helices, starting at the base of the arch AA, as shown in Figure 3.3. As can be seen, the developed surface represents a grid of $(N_c/2)^2$ cells.

Each cell lies on a particular segment of the cone of defined width, radius, and slope. The distance between the four corners of the cell can be mathematically determined, since they depend on the geometry of the particular frustum of the cone on which they sit. The geometry of the cell is repeatable across the grid and, therefore, the suggested definition accurately represents the entire braided structure.

The dimensions of the unit cell can be calculated as follows:

a) length of the arc between the bottom corners $= \dfrac{4.\pi.r_1}{N_c}$

b) length of the arc between the top corners $= \dfrac{4.\pi}{N_c}\left(r_1 + \dfrac{2.P}{N_c}\tan\gamma\right)$

c) width of the element $= \dfrac{2.P}{N_c.\cos\gamma}$

Once the boundaries of the cell are defined, its area, the length of the segment of the spiral that runs diagonally across the cell, the area covered by the fibre strand, and the fibre strand orientation at any point can be derived. The derivation of the mathematical expression for the cover factor as well as other relevant expressions are given in Appendix B.

3.4 A Simplified Configuration of the Comprehensive Model (a 'Simplified Model')

The equations derived in Appendix B for the Comprehensive Model are more complex than those of the previous two models. It was therefore of interest to evaluate a simplified comprehensive model. The changes resulting from simplifying the unit cell configuration to one of a trapezoid-shaped cell, Figure 3.4, are as follows: (a) the braid angle is defined with respect to the centre of the trapezoidal cell, (b) the radius, a_3, represents the location of the cell within the fabric grid, and **c**) the length of the main strands when stretched would be considered equal to the diagonal of the trapezoid. The mathematical expressions arising from this change in configuration are derived and presented in Appendix B.6.

3.5 Comparison of Cover Factor Models

The structural geometry of a braid is described by a number of parameters used by composites designers, including the fabric cover factor. Pastore and Ko [5] proposed a rectangular cell and considered the strands running diagonally across the cell. On the other hand, Du and Popper, proposed a fabric cell consisting of two straight strands; one positively oriented and the other negatively oriented, arranged in the form of a parallelogram. In this work, comprehensive and simplified models were developed. A

unit cell resembling a sector of an annulus was assumed in the Comprehensive Model while a trapezoidal-shaped unit cell was considered for the Simplified Model.

As noted previously, the Comprehensive Model should provide the most accurate prediction of the cover factor. In order to evaluate the accuracy of the other three models, calculated values of cover factor were compared for the four models; the Comprehensive and Simplified expressions proposed in this work and the formulae in the published works of Pastore and Ko and Du and Popper.

The computed cover factor values using the Pastore and Ko, Du and Popper, and the Simplified Model expressions showed insignificant differences when compared to the results obtained from the Comprehensive Model as shown in Table 3.1. Although the results shown pertain to a specific conic profile of $2\gamma = 16.5°$, the same overall result was obtained for other angles .

3.6 Conclusions

The preceding analysis provides the designer with a method to predict the cover factor along the length of a cone-shaped structure. Therefore, in developing the geometric model for fabric structures, when braiding over conic surfaces, any of the four unit cell approaches can be used to give accurate values of the cover factor.

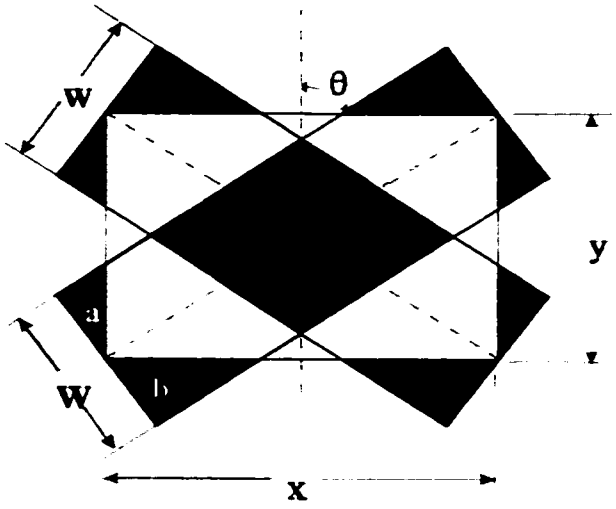

Figure 3.1 Overlap and overhang of strands in the unit cell (Pastore and Ko [5])

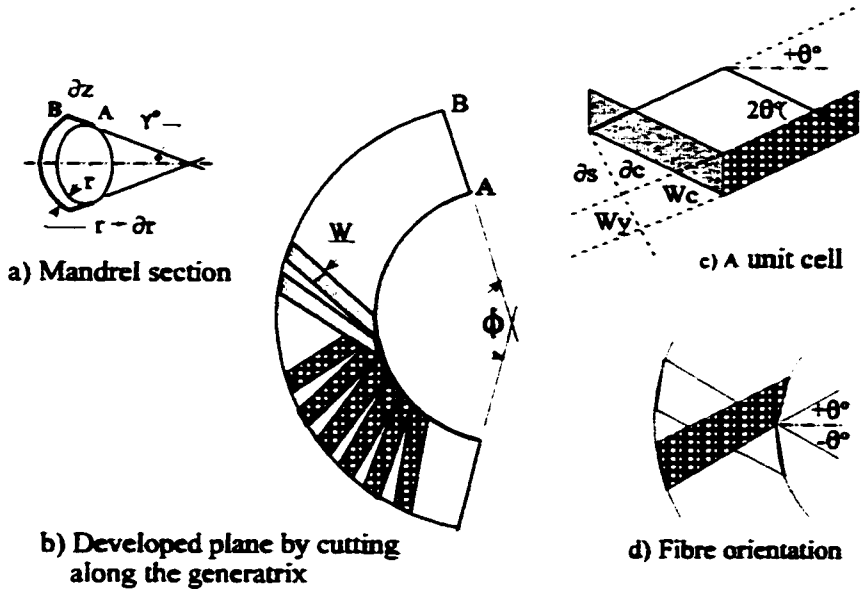

Figure 3.2 Formulation of local strand geometry on a conical segment (modified figure from Du and Popper [9,10])

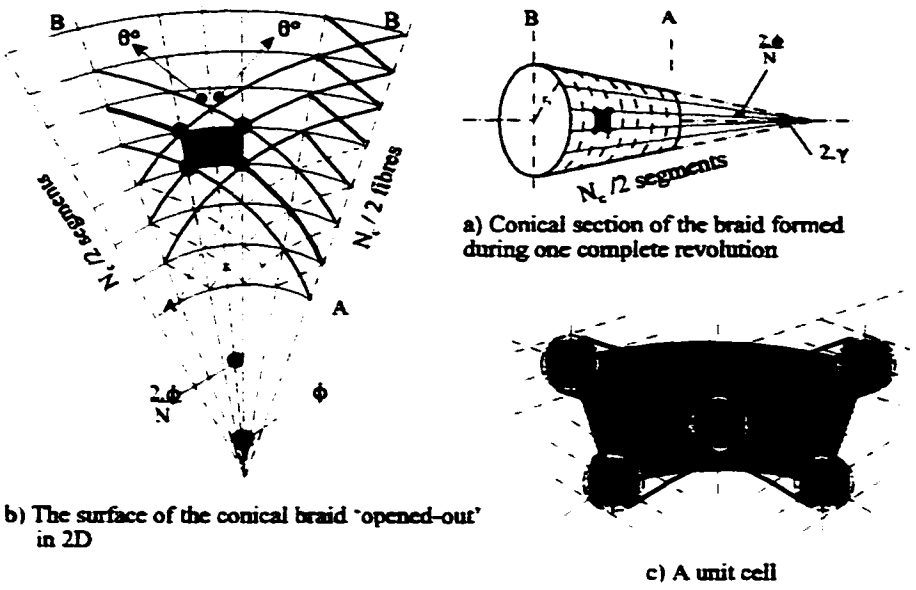

a) Conical section of the braid formed during one complete revolution

b) The surface of the conical braid 'opened-out' in 2D

c) A unit cell

Figure 3.3 The unit cell showing the main and auxiliary fibre contributing to the cell coverage

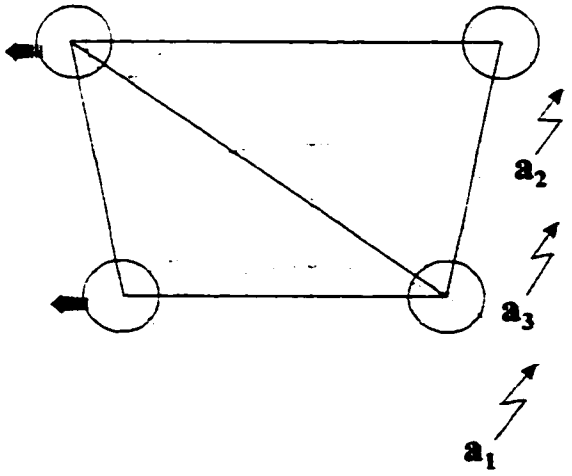

Figure 3.4 The simplified model of the unit cell

TABLE 3.1 **Comparison of the Values of the Cover Factor Calculated Using the Four Models.**

A tapered cone with the following geometry was considered in this comparison:

- Cone radius, r_1 = 1.585 cm
- Cone angle, 2γ = 16.5 °
- Distance travelled in one complete revolution = 7.62 cm
- Number of carriers N_c = 36

Cell	Head rotation	Distance travelled	Cone angle	Radius of segment	Fibre orientation	Fabric Cover Factor models			
	degrees	cm	degrees	cm	degrees	Comprehensive	Simplified	Popper	Pastore
1	20	0.424	8.307	1.585	52.286	0.9938	0.9938	0.995	0.995
2	40	0.846	8.306	1.646	53.341	0.9917	0.9917	0.993	0.993
3	60	1.270	8.307	1.709	54.347	0.9895	0.9896	0.991	0.991
4	80	1.694	8.307	1.770	55.305	0.9874	0.9874	0.989	0.989
5	100	2.116	8.307	1.831	56.22	0.9852	0.9852	0.986	0.986
6	120	2.540	8.307	1.895	57.093	0.9831	0.9831	0.984	0.984
7	140	2.964	8.306	1.956	57.926	0.981	0.981	0.982	0.982
8	160	3.386	8.307	2.017	58.723	0.979	0.979	0.98	0.98
9	180	3.810	8.307	2.080	59.485	0.9771	0.9771	0.978	0.978
10	200	4.234	8.307	2.141	60.214	0.9753	0.9753	0.976	0.976
11	220	4.656	8.307	2.202	60.911	0.9735	0.9735	0.974	0.974
12	240	5.080	8.306	2.266	61.58	0.9718	0.9718	0.973	0.973
13	260	5.504	8.307	2.327	62.221	0.9701	0.9701	0.971	0.971
14	280	5.926	8.307	2.388	62.836	0.9686	0.9686	0.969	0.969
15	300	6.350	8.307	2.451	63.426	0.9671	0.9671	0.968	0.968
16	320	6.774	8.307	2.512	63.993	0.9657	0.9657	0.966	0.966
17	340	7.196	8.306	2.573	64.537	0.9643	0.9643	0.965	0.965
18	360	7.620	8.307	2.636	65.061	0.963	0.963	0.964	0.964

Chapter 4

The steps taken to prepare the braiding machine for conducting reliable and repeatable operations are presented. This includes details of the necessary computer interfaces, measuring devices and sensors.

DESCRIPTION OF THE UNIVERSITY of OTTAWA BRAIDING SYSTEM

The design of machines to produce braids originated in France and Germany during the eighteenth century [3]. Early braiding machines were used to make simple tapes and cords for garments and shoe laces. Later, many complex braids were created and used mainly for dress trimmings. In the nineteenth century, the use of braids to cover electrical conductors challenged inventors to accelerate development of new techniques. The basic principles of early braiding machines are still in use today. One concept in particular, the concept of thread interlacing, is still found in the majority of modern machines. Fibre spools move in a plane along intersecting serpentine paths. Interlacing of the fibre strands occurs as they are withdrawn from the spools as shown in Figure 4.1. Similarities between the paths traced by Maypole dancers about a vertical pole, and that of the spools around the centre of the braiding machine resulted in the name 'Maypole braiders' being given to these machines.

4.1 The Existing 2D Braiding Machine

The 2-D braiding machine currently installed in the Composite Materials Laboratory at the University of Ottawa (see Figure 4.2) consists of a 36-carrier Steeger braiding head and a mandrel drive designed and fabricated in-house. On this braiding head it is possible to produce bi-axial braided structures with a standard 2/2 interlock pattern as shown in Figure 2.1b. This pattern can be changed to a 1/1 pattern (Figure 2.1a) by using only one-half of the spools. Fibre tension is controlled by compression springs in the spool carrier assemblies. The mandrel drive is equipped with a 15 cm guide ring to allow the formation of the braid nearer to the braiding head when small braid angles are required.

As the braid is formed, it is pulled by the mandrel, drive which guides the mandrel along an axis perpendicular to the plane of the rotating spool carriers. The existing mandrel drive was equipped with an independent motor drive; both braiding head and mandrel drives were equipped with open loop control.

The existing braiding machine can be operated either manually or by computer. In manual mode, the machine is controlled from a control cabinet. As a safety feature, a switch on the cabinet must be activated before control can be handed to the computer. General information and the technical specifications of the braiding head and the mandrel drives are provided in Appendix C.

4.2 The Data Acquisition System

The Keithley Data Acquisition System (Model KDAC-500) used in this work is a modular scientific workstation capable of acquiring, measuring and interpreting data via its different modules. Most of the hardware components of the system are already in use for another purposes and any expansion to the existing modules is limited. Four of the five high-speed analog output channels are used for setting the direction of rotation of both motor drives. One of the two 32 bit event counters is used, for the time being, to detect the rotational speed of the braiding head. Twenty of the thirty-two I/O channels are used to service the up-down counter attached to the mandrel drive and seven of the sixteen single-ended analog input channels are used for the measurement of analog input signals. The remaining analog input channels are earmarked for an eventual 'Frequency to Volt' converter application.

Communication between the Keithley Data Acquisition System and the PC dedicated to the braiding system is based on a memory-mapped input/output system where each command function is mapped to a location in system memory. The specific locations of

these commands are set by the use of dip switches on the PC interface card to which the KDAC system is hooked. It is worthwhile mentioning that the location of the memory map is different for every computer. Presently, the IBIN interface card is configured with a CFF80 address. If this interface card has to be installed on another computer, the memory map location will have to be re-configured. In general, the memory map command locations are automatically handled by the Keithley data acquisition system's software at initialization.

The software component of the data acquisition system in-use is a 'KDAC-500/M' compiler. This product was designed to run under, among others, Microsoft 'Quick-C v2.5'and earlier versions. Unfortunately, upgrading of this compiler was never considered by the manufacturer, thus limiting the application's programming capabilities to 1980's vintage compilers. The KDAC500 commands are given specific information instructions by means of command parameters.

4.3 Modifications to the Existing 2D Braiding System

During this work enhancements and modifications were necessary to improve the accuracy of the braiding system. The first task was to align the mandrel bed with respect to the braiding head. The braiding head and the structure that supports the mandrel do not share the same base or foundation. This made it very difficult to align the centre of the pull fixture of the mandrel with the centre line of the braiding head over the entire length of the mandrel. There is a discrepancy of -0.2 to +2.0 degrees in reading the braid angle over the 1.5 m traverse distance of the mandrel (readings were done using the cone angle measuring device, see section 4.3.4). However, an accuracy of $\pm 0.2°$ is obtained when braiding short lengths along the 0.5 m of the mandrel nearest to the guide ring.

The major effort in modifying the existing braiding system was the addition of new sensors and the introduction of closed loop control for the braiding head drive, the mandrel drive, and the coordination of the two drives. In order to be able to control the braiding operation, five sensors and their associated electronic circuitry were installed. Two tachometers were added to provide information regarding the mandrel transverse speed and the braiding head angular speed during the braiding process. Two encoder were added to provide on-line measurement of mandrel position and rotational position of the braiding head. A final sensor was included for the on-line measurement of the braid angle.

4.3.1 Measuring the speed and travel of the mandrel

A synchronous AC motor is used to drive the mandrel through a belt system and a lead screw. The lead screw is equipped with a tachometer and an encoder. These sensors are used for measuring the speed and the travel of the mandrel.

4.3.1.1 Measuring the Transverse Speed

The tachometer produces an analog signal proportional to the rotational speed of the shaft. This signal is detected and measured by the data acquisition system and converted to a linear speed value. Due to noise in the signal, a low pass filter, shown in Figure 4.3, that was tuned so that its corner frequency lies beyond the useful operating parameters, was constructed and installed. A reduction in signal noise was achieved; however, it should be noted that there is a trade-off in the form of slower response.

4.3.1.2. Measuring the Linear Travel

The optical encoder module is used to detect the rotary position of the mandrel drive shaft. The encoder module incorporates an LED light source and a monolithic photodetector array to produce two output signals. These signals were initially fed to the 32-bit frequency up-counter of the Data Acquisition. This connection permitted tracking of the mandrel movement for a distance up to 0.416 m only before the counter turns back to zero.

An interface board was later designed, constructed and tested using five 4-bit UP/DOWN counters and a 'Quadrature Encoder to Counter' interface chip. This chip allows the incremental shaft encoder to drive standard up/down counters. This arrangement permits the measurement of the mandrel position for a distance up to ±3.33 m before it returns to zero. Appendix D.1 shows the detailed wiring arrangement of the board.

4.3.2 Measuring the Angular Speed of the Braiding Head

In order to measure the angular speed of the braiding head a frequency to voltage circuit is used. It was decided to convert the frequency signals generated by the encoder mounted on the motor of the braiding head into voltage. For that purpose, the appropriate electronic circuit, shown in Appendix D.2, was designed and implemented.

4.3.3 On-line Measurement of the Braid Angle

Simple mathematical expressions have previously been developed for cylindrical braiding to predict the braid angle based on braiding head and mandrel speeds [5-7]. Similarly, for complex axially symmetric structures, a series of differential equations

were developed to evaluate the length of the convergence zone and hence calculate the braid angle [9, 10]. In both cases, measurements to confirm experimental results were made after the completion of the braid. No attempts have been made to measure the braid angle, either directly or by proxies, during the braiding process.

In addition, the braid angle changes as the diameter of the component changes when braiding complex structures. This cannot occur instantly, therefore, a transition zone exists in which the braid angle changes from its original value to the new desired angle.

An in-depth study of the topography of the convergence zone has led to an innovative approach to measure the braid angle. This approach is based on the ability to measure the coordinates of the point where the strand crosses the plane perpendicular to the guide plane passing through the centre of the guide ring. Once the coordinates of this point are determined, the angle of the cone-shaped profile of the converging strands and the length of the convergence zone can be computed and consequently, the braid angle can be determined. Thus for the purpose of on-line measurement of the braid angle, a measuring device (Figure 4.4) was designed and constructed. A brief description of its design and its mathematics are discussed below.

4.3.3.1 Cone Angle Measuring Device Configuration

The cone angle measuring device consists of a swinging arm, a potentiometer and an analog to digital converter. As shown in Figure 4.4 , the device is mounted on top of the guide ring. The free end of its swinging arm is held on the interlacing strands with an elastic band that forces the swinging arm to rest gently on the cone-shaped outline of the convergence zone. A high precision potentiometer is attached to the axle of the arm and is capable of sensing its rotational position. As the convergence zone expands and contracts, the swinging arm reacts accordingly, and the voltage difference caused by the

rotation of the arm is read by the data acquisition system and converted to an angle in degrees.

As shown in Figure 4.5, the movement of the swinging arm of the measuring device describes a circle on the *x-y* plane, and intersects the path of a pair of strands at a point *C*. Also, the point *C* on a strand revolving around the centre line of the workpiece will describe a circle (locus of the point '*C*') on a plane parallel to the guide ring at a distance x_c from the deposit plane.

Two methods were used to determine the relationship between the coordinates of the point *C* where the free end of the swinging arm rests on the converging strands, and the length of the convergence zone, *D*. These relationships are then used to deduce the braid angle, θ. The first method uses conventional geometry. Details of the derivation are given in Appendix E.1. Highlights of the derivation follow:

With reference to Figure 4.5, the coordinates of point *C* with respect to the deposit plane can be written in terms of the geometry of the swinging arm as follows:

$$x_c = D - L \cdot \cos(\alpha + \alpha_o) + p$$

and,

$$R_c = R_G - L \cdot \sin(\alpha + \alpha_o) - q$$

Furthermore;

$$y_{c'} = \sqrt{\left(R_G - L \cdot \sin(\alpha - \alpha_o) - q\right)^2 - \left(r_1 + x_c \cdot \tan\gamma\right)^2}$$

but;

$$\tan\theta = \frac{\cos\gamma \cdot y_{c'}}{x_c} = \frac{\cos\gamma \cdot \sqrt{R_G^2 - \left(r_1 + D \cdot \tan\gamma\right)}}{D} \qquad (4.1)$$

Substituting for y_c and x_c into Equation 4.1 and solving for θ gives;

$$\theta = \tan^{-1}\left(\frac{\cos\gamma \cdot \sqrt{\left(R_G - (L \cdot \sin(\alpha + \alpha_o) - q)\right)^2 - \left(r_1 \cdot \left(D - (L \cdot \cos(\alpha + \alpha_o) + p)\right) \tan\gamma\right)^2}}{D - \left(L \cdot \cos(\alpha + \alpha_o) + p\right)} \right) \quad (4.2)$$

Equation 4.2 is verified using the vector analysis method as shown in Appendix E.2.

4.3.3.2 Calibration of the Cone Angle Measuring Device

As shown in Figure 4.6a, the "zero" position of the device, α_o, was set by placing a rectangular gauge mounted on a sleeve that slid freely over the mandrel such that the free edge of the gauge was always parallel to the axis of the mandrel. When placed inside the guide ring, the top edge of the gauge barely made contact with its inner surface.

The rectangular gauge was then replaced by a set of triangular gauges of known angles. These gauges represented various angles for calibrating the device. Readings were made and recorded for angles 15, 30, 36.87, 45, 53.13, 60, 75 degrees. In all cases, measurement accuracy was within ± 0.1°. These tests showed that the device is reliable and has an acceptable accuracy.

4.4 Determination of Delays in Response to Commands.

Once the braiding machine was equipped with its new sensors and measuring devices, it was necessary to assess their resolutions and accuracies. In particular, it was important to determine the time difference between the issuance of a command to change the speed

and the time at which the desired speed was attained. This is due to the computer model used and the damping factor in the filter's components. A series of experiments were conducted in which the readings of both braiding head and mandrel tachometers were recorded. These experiments explored the following situations:

a) The mandrel drive, with no strands attached, starts from rest and runs at speeds equal to 10, 20 ...., 100% of the maximum speed of the drive.

b) Same as item 'a' but strands were attached to the mandrel. This series of tests was intended to investigate the effect of the tension in the springs of the carriers.

c) Same as item 'a', as applied to the braiding head .

d) Full braiding on cylindrical mandrel starting with a specific speed ratio. The mandrel speed is then incrementally increased by 10% every 1.5 seconds until its maximum value is reached. The mandrel speed is then reduced by 10% until it reaches zero.

The results of these experiments showed that it takes approximately 2.2 seconds for the mandrel drive and 3.4 seconds for the braiding head drive to reach 80% of their maximum speeds. However, for more typical speed changes, it was found that it takes approximately 0.2 seconds to reach the next 10% incremental change in speed of the drives.

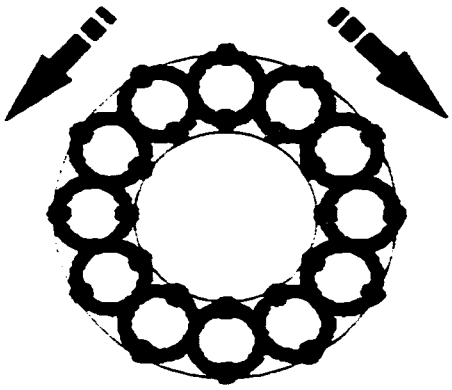

Figure 4.1 Schematic of fibre interlace – Spools travelling along a serpentine path

Figure 4.2 University of Ottawa braiding machine

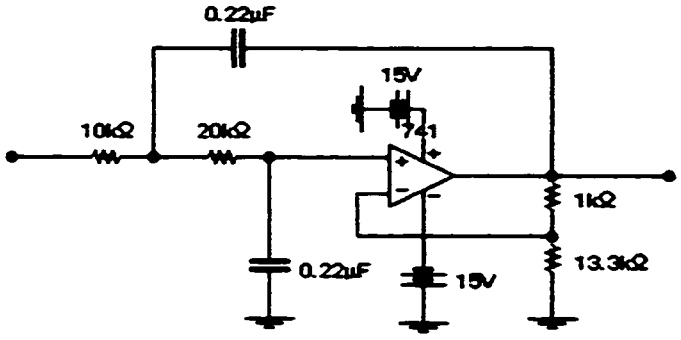

Figure 4.3 Low pass filter used with the mandrel's tachometer

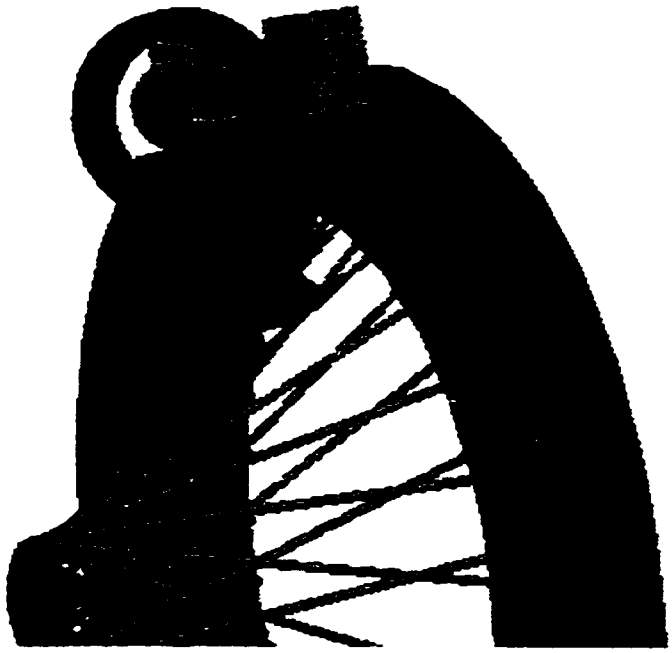

Figure 4.4 Cone angle measuring device mounted on a guide ring

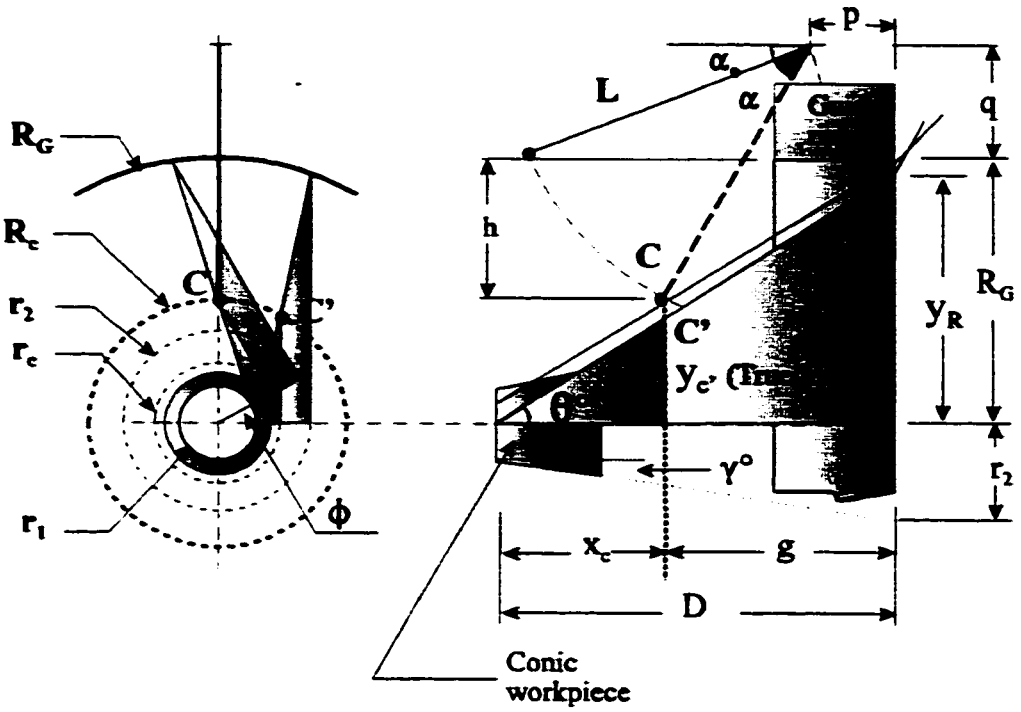

Figure 4.5 Geometric relationships in the convergence zone

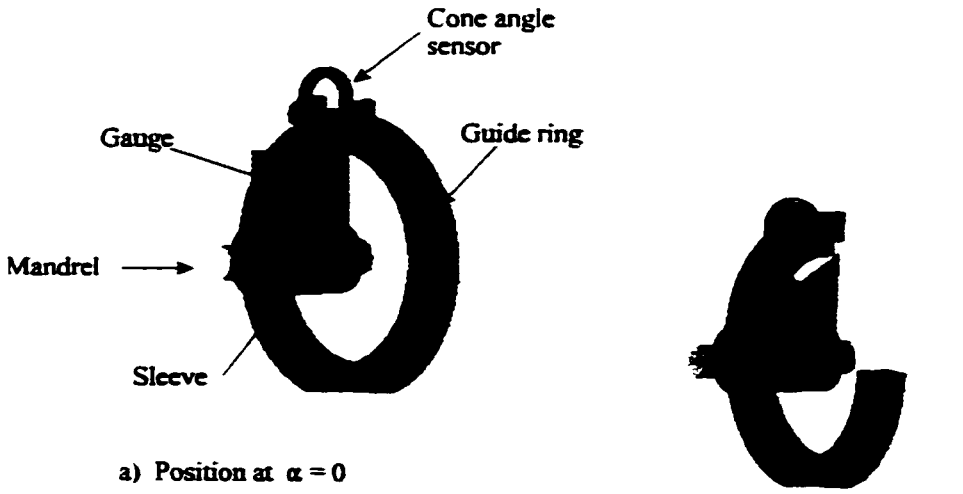

Figure 4.6 Calibrating the cone angle measurement device

Chapter 5

The results of actual braiding over cylindrical and conic surfaces are discussed. As well, a fibre strand interlacing parameter is introduced

RESULTS FROM BRAIDING TRIALS ON CYLINDRICAL AND CONIC SURFACES

As previously mentioned, published information on 2D braiding is often incomplete or inaccurate. In the case of cylindrical braiding, Du and Popper reported a five degree difference between the predicted and measured values of the braid angle. They also suggested that predictability could be improved by including the effect of strand curvature in a small region of the convergence zone near the deposit plane. This discrepancy between the desired and measured values of the braid angle, after upgrading the University of Ottawa facilities, could now be investigated using the improved braiding facilities. Braiding over both cylindrical and conic surfaces was evaluated.

5.1 Braiding on Cylindrical Surfaces

A simple strategy was first adopted for cylindrical braiding. A basic model to describe the braid structure was formulated based on that of Pastore and Ko [5]. Full coverage was considered the most important factor since it would be easier to visually assess the quality of the braided structure.

In developing the model, only braiding parameters with a major influence were considered. Each strand consists of many fibres. The cross-section of the strand is approximated by a rectangle of a given width and thickness. The individual strands that constitute the braid are treated as helices wound around a cylindrical core. At steady state, if a piece of cylindrical braided fabric in which a strand makes one complete revolution is cut along the axis of the braid, the rectangle obtained, as shown in Figure 5.1, would contain all the geometrical parameters of the braid. Thus, the braid angle, θ, can be expressed in term of machine and mandrel parameters as follows:

$$\tan\theta = \frac{\omega \cdot r}{v_t} \tag{5.1}$$

where, $r = R_m$ is the instantaneous radius of the mandrel at the point of measurement.

The convergence zone extends from the guide plane (the back side of the guide ring) to the deposit plane where all the strands first come into contact with the mandrel. In the absence of a guide ring, the guide plane passes through the payout eyes on the spool carriers. The convergence length, D, remains constant during steady-state operation. Assuming that strand curvature due to interlacing can be neglected, the strands in the convergence zone will be considered straight and under uniaxial tension. Based on these assumptions, the path of the strand in the convergence zone is tangent to the helical path of the braid and, therefore, the braid angle, θ, must be equal to the inclination of the strand to the axis of the braided structure as shown in Figure 5.2. Thus for a uniform cylindrical mandrel, the braid angle expressed is given by:

$$\tan\theta = \frac{\sqrt{R_G^2 - R_m^2}}{D} \tag{5.2}$$

Substitution for $\tan\theta$ from Equation 5.1 into the above equation, and solving for D gives;

$$D = \frac{v_t}{\omega} \cdot \frac{\sqrt{1-\lambda^2}}{\lambda} \tag{5.3}$$

where, $\lambda = R_m / R_G$.

The fabric cover factor, K, is defined as the ratio of the area covered by the strands over the total area of the fabric. According to Pastore and Ko [5], the braid angle can be expressed in terms of the cover factor as shown in Equation 3.3. For full coverage, i.e. when $K = 1$, this equation reduces to:

$$\theta = \cos^{-1}\left(\frac{N_c \cdot W}{4 \cdot \pi \cdot R_m}\right)$$
$$= \tan^{-1}\left(\sqrt{\left(\frac{4 \cdot \pi \cdot R_m}{N_c \cdot W}\right)^2 - 1}\right) \quad (5.4)$$

The speed ratio for full coverage can therefore be expressed in term of fabric structure as follows;

$$\frac{\omega}{v_t} = \sqrt{\left(\frac{4 \cdot \pi}{N_c \cdot W}\right)^2 - \frac{1}{R_m^2}} \quad (5.5)$$

A computer program was developed to calculate the speed ratios which correspond to a desired cover factor. Usually in braiding, the angular speed of the braiding head is fixed while the transverse speed of the mandrel drive is calculated as a function of the number of carriers, the mandrel diameter and the width of the fibre strand. A typical output of the developed program is shown in Appendix F.1.

Several experiments were conducted using Kevlar 49 strands of 0.314 cm width and different combinations of machine speeds which would produce a fully covered braided structure, i.e. $K = 1$. After steady-state braiding was reached, the braiding process was stopped. The actual braid angle was measured directly from the braided structure and compared to the desired braid angle. At first, overhead transparencies were used for measurement. A transparency was wrapped tightly around the braided mandrel, a particular strand (pre-coloured) was identified and its path traced while spiralling around the mandrel. The transparency was then unwrapped and measurements were taken. This method was replaced by directly measuring the pitch from the braid structure by means of a divider. The relationship, $\tan\theta = 2\pi R_m / pitch$, was used to compute the braid angle. This second method was used, where applicable, in all subsequent experimental work requiring direct measurement of the braid angle of the braided structure. The measured

braid angles were within 1% of the desired angles; however, during the transient state, a non-uniform pattern of the braided fabric was formed.

The length of the convergence zone was also measured off the mandrel and compared to the predicted steady-state value. There was a difference of approximately 12 mm (maximum of 25 mm) between the measured and the calculated values of the convergence zone length. This difference was believed to be either due to the braiding process being terminated before reaching steady-state or the inability to determine exactly the location of the fell of the fabric. These results confirm that, during braiding, it is important to determine accurately the location of the deposit plane.

5.2 Braiding on Conic Surfaces

The profile shown in Figure 5.3 was chosen as the mandrel to conduct experiments on braiding onto conic surfaces.

A simple open loop control braiding strategy was adopted. At incremental positions along the full length of the mandrel, the braid angles were calculated and their corresponding speed ratios (braiding head angular speed vs mandrel transverse speed) and the steady-state value of the convergence lengths at these locations were computed and stored in a data table. The braiding head speed was set at a constant value and the corresponding mandrel speed computed. During the braiding process, the incremental position along the mandrel was monitored using the pulse count generated by the mandrel drive encoder. When a desired position was reached, the braiding head was stopped, and the mandrel moved to pre-calculated steady-state position (i.e. convergence length) of the next increment of the mandrel. Braiding then resumed with a new set of speeds for that increment.

In order to implement this strategy, relationships used to predict the parameters required for machine control, namely, mandrel speed and length of the convergence zone, are presented in the following section.

5.2.1 Prediction of Mandrel Speed for Braiding on Conic Surfaces

The derivation of braid angle in the fabric structure is discussed in Appendix B. It was found that the braid angle can be expressed as a function of the pitch as follows:

$$\cos(\theta) = \frac{1}{\cos\gamma \cdot \sqrt{\frac{4 \cdot \pi^2 \cdot r_1^2}{P^2} + \frac{4 \cdot \pi \cdot r_1}{P} \cdot \beta_z \cdot \tan\gamma + \beta_z^2 \cdot \tan^2\gamma + \tan^2\gamma + 1}} \tag{5.6}$$

however, $P = {}^{2 \cdot \pi \cdot v_t}/_{\omega}$

for a given mandrel speed, v_t, (braiding head speed, ω, is predetermined), and a given radius, r_1, the fibre orientation is given by:

$$\theta = \cos^{-1}\left(\frac{1}{\sqrt{\cos^2\gamma \cdot \left(r_1 \cdot \frac{\omega}{v_t} + \beta_z \cdot \tan\gamma\right)^2 + 1}}\right) \tag{5.7}$$

$$= \tan^{-1}\left(r_1 \cdot \cos\gamma \cdot \frac{\omega}{v_t} + \beta_z \cdot \sin\gamma\right)$$

On the other hand, if a desired pattern of braid angles along the mandrel is given, then the pitch of the spiral can be expressed in terms of fibre orientation as follows:

$$P = \frac{2 \cdot \pi \cdot r_1 \cdot \cos\gamma \cdot \cos\theta \cdot (\beta_z \cdot \sin\gamma \cdot \cos\theta + \sin\theta)}{\left(\sin^2\theta - \beta^2 \cdot \cos^2\theta \cdot \sin^2\gamma\right)} \tag{5.8}$$

and by inference the mandrel speed can be deduced and expressed as follows:

$$v_t = \frac{\omega \cdot r_1 \cdot \cos\gamma \cdot \cos\theta \cdot (\beta_z \cdot \sin\gamma \cdot \cos\theta + \sin\theta)}{(\sin^2\theta - \beta_z^2 \cdot \cos^2\theta \cdot \sin^2\gamma)} \tag{5.9}$$

5.2.2 Prediction of Length of Conversion Zone for Braiding on Conic Surfaces

The Vector Analysis approach described in Appendix G was used to develop an algorithm relating the point of braid formation and the geometry of the mandrel. It was found that, for given values of braid angle, θ, and mandrel geometry, the length of the convergence zone, D, can be represented as;

$$D = \frac{-r_1 \cdot \sin\gamma \cdot \cos\gamma + \sqrt{(R_G^2 - r_1^2) \cdot \tan^2\theta + R_G^2 \cdot \sin^2\gamma}}{\tan^2\theta + \sin^2\gamma} \tag{5.10}$$

5.2.3 The Computer Program

An interactive computer program was written to generate the required parameters for braiding over a coned-shaped object. A sample output is shown in Appendix F.2. Two features of the program are worthwhile highlighting: first, the profile of the guide ring mounted on the mandrel drive, shown in Figure 5.4, was taken into consideration. The large radius rounded edge intended to reduce fibre damage causes the radius of the ring, R_G, at the point of tangency to be a variable which depends on the value of the braid angle, θ. Thus, an iterative routine was introduced in the program to determine the point of tangency. Secondly, testing at each incremental position was conducted to verify whether or not the strands were still touching the guide ring. The salient steps in the program for both features are summarized in Appendix F.3.

5.2.4 Braiding Experiments for a Conic Mandrel

Several braiding experiments were conducted using Kevlar fibre strands of 3.14 mm width for a full coverage condition, i.e. $K = 1$. The angular speed of the braiding head was limited to 30% of its maximum value. This speed was selected in order to permit a detailed examination and a close observation of the braiding process as it progressed along the work piece. Each experiment included three phases; a front-end braiding phase, where braiding over the cylindrical portion of the mandrel is performed; braiding over the cone-shaped mandrel (this phase used the off-line generated information in the data table), and a back-end braiding over the cylindrical mandrel.

The front-end braiding phase is a prelude to the experiment. It involves positioning the mandrel in preparation for braiding. Its purpose is to ensure that, at the start of the braiding process over the conic section of the mandrel, the deposit plane would be at its predicted steady state position, thus avoiding braiding in the transient state. The mandrel is first moved so that the fibre contact point is located at a predetermined distance (length of the convergence zone) from the guide plane. The braiding process starts by braiding over this distance to ensure that when the conic section is reached the process is at steady state.

During the braiding process, the pulse counts generated by the encoder to monitor the displacement of the mandrel are recorded every 50 milliseconds and the distance travelled is compared to the appropriate information in the data table. Whenever a new increment is reached, a software interrupt is generated. The rotation of the braiding head is stopped while the fibre contact point on the mandrel is repositioned to its predetermined value in preparation for braiding the next increment. Braiding then resumes with a new set of corresponding speeds for that new increment. A sample of the braiding process session and the operation monitoring information screen are shown in Appendix F.4.

Braiding results from the preliminary set of experiments were unsatisfactory. As shown in Figure 5.5, coverage of the mandrel was incomplete, and a jamming condition was observed at the tail end of the braided structure. It was noted that the actual incremental positions of the conic mandrel did not coincide with the desired locations of the deposit planes.

Various remedial actions were taken to increase the accuracy of the process. For example, the stop and start action of the braiding head used to locate the deposit plane at the beginning of each increment was replaced by rotating the braiding head at its lowest speed in order to reduce the inertia forces associated with the stopping and starting action of the braiding head. Also, it was noticed that there was a period of two interrupts (100 milliseconds) between the initiation of an instruction and its execution. Adjustments to the computer program were made to take into consideration this delay. In spite of these remedial actions, no improvement to the quality of the braided fabric was noticeable.

5.3 Evaluation of the Interlacing Effect

The unsuccessful attempts to braid over conic surfaces first led to a study of the interlacing effect when modelling the braiding process. Brunnschweiler pointed out that frictional forces acting between the strands of fibres as they slide over and under each other cause displacement of the deposit plane nearer to the carriers than would otherwise be expected.

Du and Popper [9,10] assumed, in developing their model, that the strands are straight in the convergence zone. As a result of their experiments, they concluded that the predictability of the braid angle could be improved by including in their model strand curvature in a small region of the convergence zone near the deposit plane.

Zang et al [11,12] also investigated the validity of the assumption that the strands could be represented by straight lines in the convergence zone. The straight line assumption is based on an ideal braiding condition where no frictional force exists when a strand moves over or under other strands to form a braid. They assumed only one warp or weft strand needs to be analysed because other strands simply repeat the same motion at different locations. They proposed a model that predicts the braid angle when interlacing forces are considered. They conducted experiments at different machine speeds and with different spring tensions. They compared the braid angles produced at steady state to those calculated by their model as well as Du and Popper's model. Measurements of the braid angle were made with a flexible plastic protractor that was held by hand on the braided mandrel. Five to ten braid angle measurements were taken per test, and the measured angle generally varied no more than ±2 to ±3 degrees from the average, which is less than found by Du and Popper. They attribute the discrepancies between measured and desired braid angles to the change in the deflection of the tension spring while moving around the serpentine path of the braiding spools. They conclude that the effect of friction forces is more pronounced in larger braiding machines with more than 64 spools.

Previously, there was no method available to measure or to compute the strand curvature in the region of the convergence zone near the deposit plane. In an attempt to do so, an experimental investigation was conducted. The 36-carrier braiding machine, equipped with a 0.152 m. internal diameter guide ring was used to conduct a series of experiments. The carrier track was arranged to produce a braid structure with a standard 2/2 interlock pattern. Kevlar strands were used in all spools except for one spool in which a fibreglass strand was used to provide a marker in the braided fabric. A 0.025 m cylindrical diameter mandrel was used with the machine operating at constant braiding head and mandrel speeds. No initial positioning was used to set the convergence zone lengths to their steady state values. The original lengths were allowed to expand and contract until the process reached steady state.

One set of experiments was conducted in which a cylindrical mandrel was covered by strands from carriers moving in one direction only. The carriers moving in the reverse direction ran empty. This arrangement was chosen to eliminate the effect of interlacing strands. A second set of experiments was carried out with all the carriers filled. The second set was used as a control set to compare with the first set.

During these experiments, on-line measurements using the cone angle measuring device were recorded every 50 milliseconds. Also, it was noticed that the recorded measurements fluctuated with the passage of the fibre strands in the convergence zone, in particular when the measured braid angles were relatively small. Therefore, a moving average method was adopted to reduce the fluctuation in the recorded data. The length of the convergence zone as well as the inherent braid angles were computed and their moving average values were stored in a database.

Some additional information was also gathered for each case. During braiding, the linear transverse speed of the mandrel and rotational speed of the braiding head were recorded. After braiding, the pitch of the braided fabric was measured directly from the mandrel. As well, the diameter of the braided mandrel was measured to determine the average thickness of the braided fabric. These measurements were used to calculate the value of the braid angle from the speed measurements using Equation 5.1 ($\tan\theta = \omega r/v$), and from the pitch and radius measurements using helix geometry (i.e. $\tan\theta = 2\pi r/pitch$). Both were compared with the braid angles calculated from the cone angle device measurements. Table 5.1 presents the measurements and the different braid angle calculations based on these measurements. A plot of the braid angles is shown Figure 5.6. The parameters of the fitting polynomials are also presented. A number of conclusions can be made based on these results.

First, it is of interest to note that the differences in the braid angles measured from the braided fabric using helix geometry and those obtained from speed measurements

(Equation 5.1) in both sets of experiments are less than 0.5° for all speed ratios. This confirms the applicability of both expressions. More importantly, it shows that the final braid pattern is not affected by strand interlacing.

In addition, results from the first set of experiments (1-7), where the carriers moving in one direction were empty, showed excellent agreement between the desired and derived angles (a percentage difference of less than 2.5 %). This confirms that the cone angle measuring device is accurate.

The effect of strand interlacing can now be quantified. From the second set (8-14) of experiments, the 3 to 8° difference between the desired and derived braid angles at various speed ratios represents the effect of strand interlacing in the convergence zone near the deposit plane. Thus, when strand interlacing occurs, the deposit plane moves nearer to the guide ring. This leads to the conclusion that the trajectory of the strand in the convergence zone does not follow the tangent to the helical path of the strand along the mandrel but is bent towards the braiding head at a steeper angle, as shown in Figures 5.7 and 5.8. It is believed that the displacement of the deposit plane is one of the reasons for the inaccurate results obtained when using open loop control for braiding over conic surfaces as mentioned in Section 5.2.3. Since the angles calculated from the cone angle measuring device were always greater than the desired value, this discrepancy quantified by the angle ζ (Figure 5.6), should be considered whenever mathematical models describing the geometry in the convergence zone are developed.

Thus, in computing the length of the convergence zone, D, when braiding over a cylindrical surface one should consider the effect of that displacement as follows;

$$\tan(\theta + \zeta) = \frac{\sqrt{R_G^2 - R_m^2}}{D} \tag{5.11}$$

Furthermore, since $\tan\theta = \omega \cdot r / v_t$, this relation could be further developed to yield the following expression;

$$D = \left(\frac{v - \omega \cdot r \cdot \tan\zeta}{\omega \cdot r + v \cdot \tan\zeta} \right) \cdot \sqrt{R_G^2 - r_m^2} \qquad \textbf{(5.12)}$$

where ζ, the strand interlacing parameter, quantifies the displacement of the deposit plane due to interlacing.

$$\tan\theta = \frac{2 \cdot \pi \cdot r}{pitch} \longrightarrow \tan\theta = \frac{\omega \cdot r}{v_t}$$

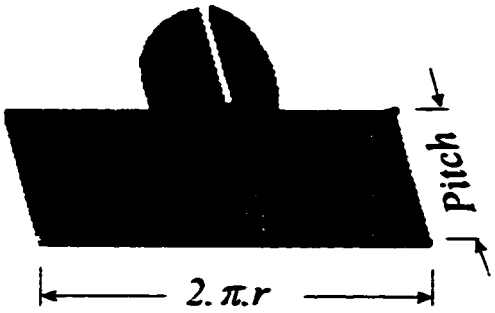

Figure 5.2 Geometry of the braided fabric as related to machine and mandrel parameters

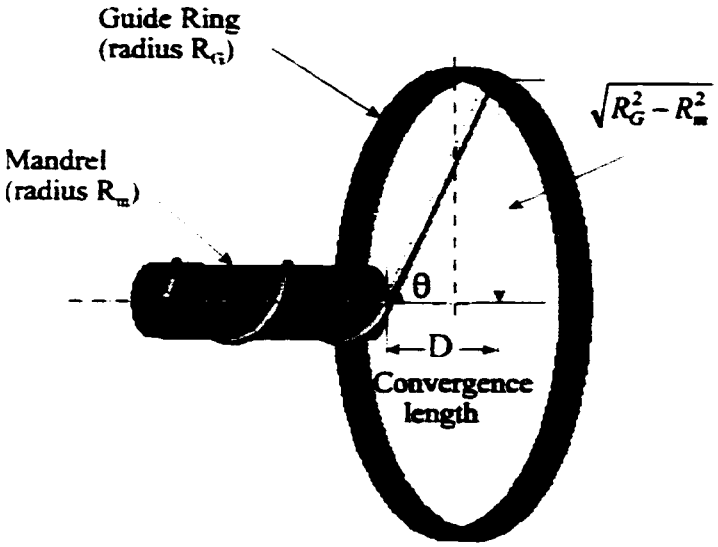

Figure 5.1 Geometry of the convergence zone

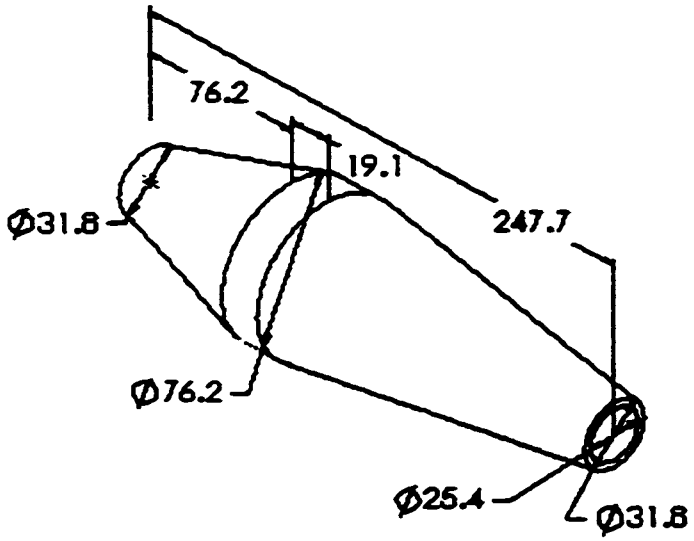

Figure 5.3 Conic mandrel (all dimensions in mm.).

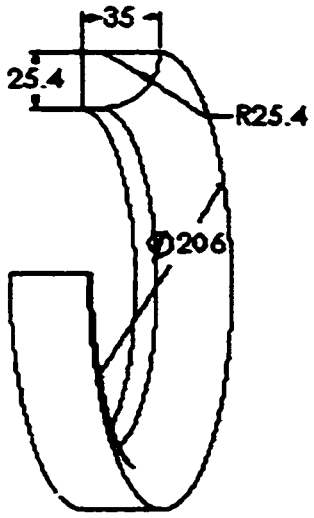

Figure 5.4 Guide ring with rounded edge to reduce fibre damage.

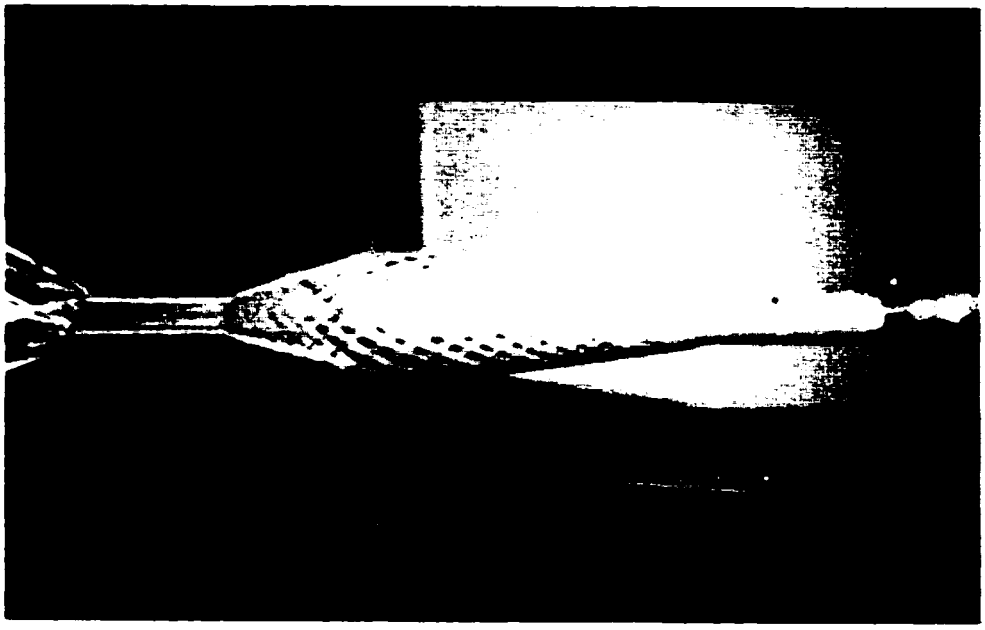

Figure 5.5 Braiding over a conic mandrel

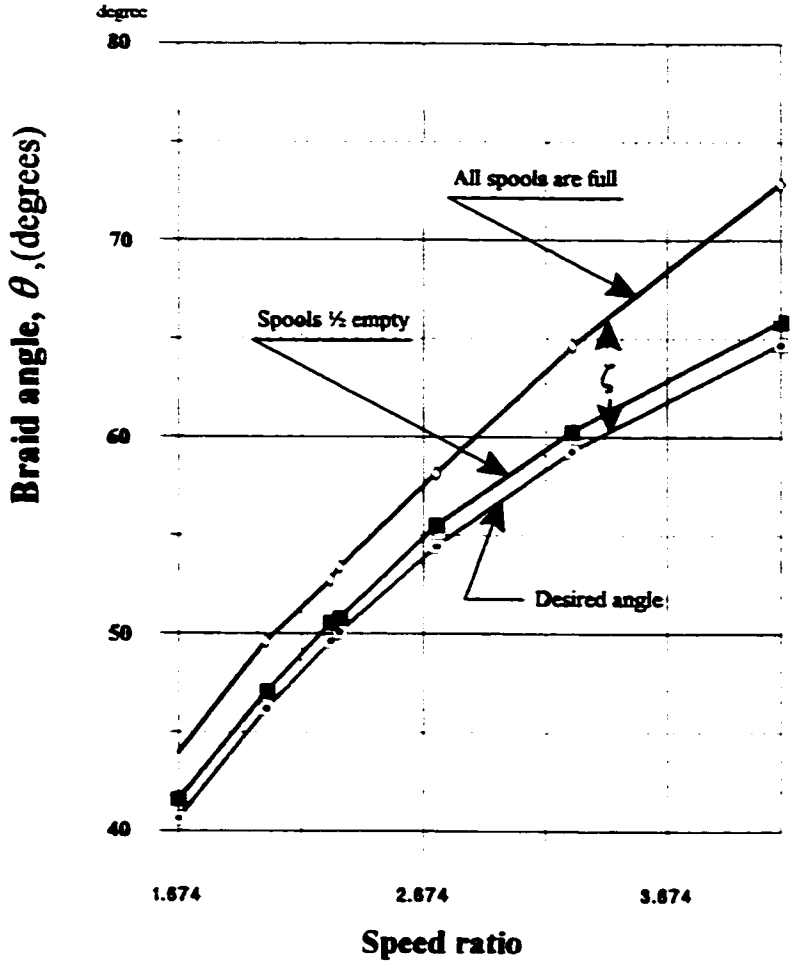

The curve fitted polynomials for the three curves are:

Theta – desired → $y = 9.66168 + 22.95901 * x - 2.27011 * x^2$ ($r^2 = 0.99956$)

Theta – ½ full → $y = 8.57207 + 23.15900 * x - 2.32243 * x^2$ ($r^2 = 0.99951$)

Theta – all full → $y = 16.13512 + 18.76701 * x - 1.21320 * x^2$ ($r^2 = 0.99966$)

Figure 5.6 Experimental results – comparison between desired and derived braid angles

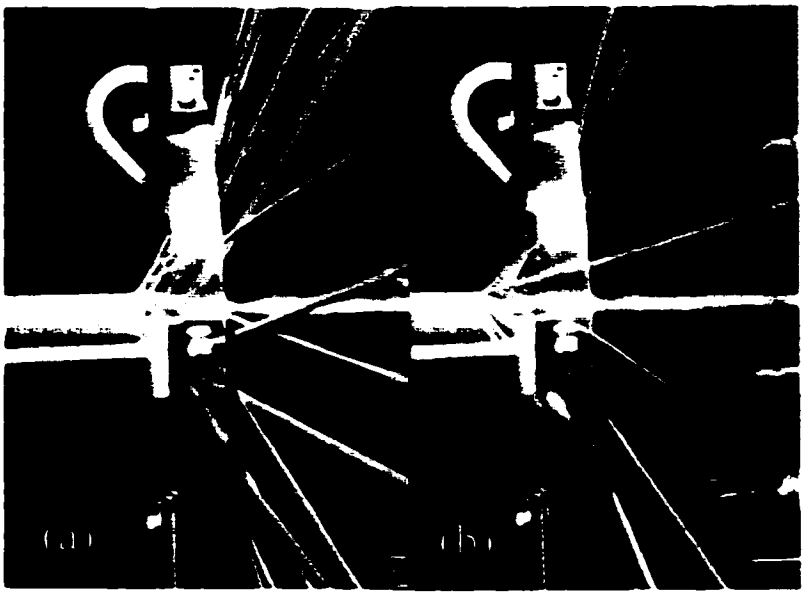

Figure 5.7 The effect of fibre interlacing in the convergence zone;
a) with interlacing
b) without interlacing

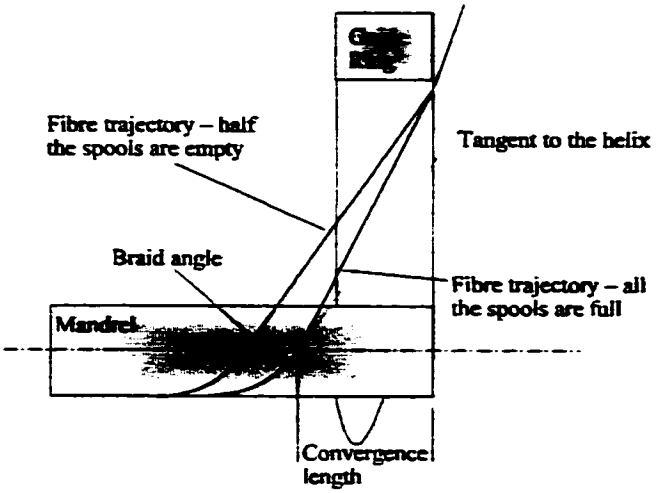

Figure 5.8 Fibre trajectory in the convergence zone

Table 5.1: **Braid angle ' θ ' – derived from the cone angle measurement device vs computation using recognized formulas.**

exp #	B. Head speed rpm	Mandrel rpm	Ratio ω/v	PITCH p (cm.)	THETA (Degree) tanθ = ω.r/ v desired	2.π.r/ p measured	Cone Angle Device α derived [1]	ζ difference [2]	% difference [3]
Lines 1 to 7, represent the results of the set of experiments where carriers moving in one directions are running empty (no interlace).									
1	674.5	119.2	2.331	6.91	50.07	49.8	50.78	0.71	1.42
2	674.5	101.9	2.727	5.95	54.45	53.9	55.53	1.08	1.98
3	674.9	136.7	2.034	7.78	46.19	46.4	47.07	0.88	1.91
4	675.1	67.4	4.127	3.89	64.70	64.6	65.84	1.14	1.76
5	590.2	145.3	1.674	9.53	40.63	40.6	41.59	0.96	2.36
6	761	136.7	2.294	6.83	49.62	50.1	50.55	0.93	1.87
7	675.4	84.8	3.281	4.89	59.26	59.1	60.26	1	1.69
Lines 8 to 14, represent the results of the set of experiments where all carriers are full (with interlace).									
8	673.9	119.1	2.331	6.87	50.07	49.9	53.37	3.3	6.68
9	673.5	101.9	2.723	5.88	54.38	54.3	58.12	3.74	6.94
10	673.3	136.6	2.031	7.86	46.15	46.2	49.59	3.44	7.47
11	673.9	67.3	4.126	3.89	64.69	64.6	72.86	8.17	12.73
12	588.7	145.3	1.669	9.53	40.54	40.6	43.87	3.33	8.06
13	759.5	136.5	2.292	6.91	49.59	49.8	52.71	3.12	6.04
14	674.9	84.6	3.287	4.89	59.31	59.1	64.64	5.33	9.15

Note 1. Cone angle measuring device (derived from Equation 4.1)

2. difference = (θ derived – θ desired)

3. % difference = $\frac{(\theta \text{ derived} - \theta \text{ desired})}{\theta \text{ desired}} * 100\ \%$

Chapter 6

In this chapter, the analysis was directed to study the braid formation during the transient state. The experimental data presented strengthen the validity of the analytical expressions developed. In addition, this chapter presents a solution to the problem of manufacturing 2D cylindrical braids of variable pitch.

A MODEL FOR BRAID FORMATION DURING THE TRANSIENT STATE

The helix geometry relationship given by Equation 5.1 is generally used for 2D steady state cylindrical braiding. The assumptions underlying this simple relationship are that the spools follow a circular path and that there is no friction due to interlacing effects between the strands until they reach the point of formation of the braid. Du and Popper [9, 10] evaluated the geometry of the braid during the transient state of braiding. They developed a differential equation to describe the time-dependence of the location of the deposit plane on cylindrical and conic mandrels. They reported that "when braiding over a conic section, manual adjustments to the mandrel velocity beyond those dictated by the conic geometry were necessary to produce better results".

There is a growing need to produce complex (varying cross-section or braid angle) braided structures. Consequently, during the braiding process the changes to the machine speed ratios required to produce complex structures would result in transient periods that would, if not accounted for, produce unacceptable products. The existence of transient zones could be another factor, in addition to strand interlacing, that contributed to the unacceptable braiding result shown in Figure 5.5.

6.1 Braiding process during the transient state

A uniform helix, like a thread, is produced when a tool traverses at a constant speed along the surface of a cylinder rotating at constant speed, as in a lathe. Similarly, if a strand passing through a payout eye replaces the tip of the cutting tool (with the payout eye touching the cylindrical mandrel), the strand winds around the mandrel in a spiral of equal pitch all along the mandrel. On the other hand, if the payout eye is moved away

from the mandrel, the spiral formation goes through a transient stage during which the strand pitch on the mandrel varies until, at steady state, a spiral of constant pitch is again obtained. This behaviour is associated with the position of the payout eye at start up.

In order to confirm this hypothesis, the braiding machine was equipped with a guide ring having an internal diameter only slightly larger than the diameter of the braided mandrel. Once braiding was completed, the distance travelled by the strand per revolution (pitch) was measured all along the braided structure. The result was a braid with a negligibly small transient state. Thus, the desired braid angle was obtained throughout the braided fabric.

The experiment was then repeated to explore the effect of a sudden change in the speed of the mandrel drive on the desired braid angle of the braid. It was found that the desired braid angle was attained as soon as the change in speed was made. Accordingly, the production of braided structures of varying braid angle (for example production of catheters with variable stiffness along the length) could be easily accomplished using a guide ring that is very close in diameter to that of the intended catheter or mandrel.

In a second set of experiments, a standard metal lathe was set up to form a helical thread of 2.54 cm pitch length. Two polished rods of 2.54 and 1.27 cm diameter were used as the mandrels. A special tool, shown in Figure 6.1, replaced the metal cutting tool. The special tool was designed to trace a spiral contour on the rotating mandrel by mean of a stylus, as well as wind a strand onto the rotating mandrel using an adjustable payout eye. The stylus was always kept in contact with the cylindrical surface, while the distance of the centre point of the payout eye from the mandrel surface was adjustable.

As expected, when both the stylus and the payout eye were touching the mandrel, the contact points of the stylus and the strand would be always in the same plane, and two matching helical profiles each of 2.54 cm pitch length were obtained. When the payout

eye was placed at a distance from the surface of the mandrel, the helix angle gradually changed until steady state was reached. Consequently, the spiral formed by the strand had a variable pitch before reaching the desired length of 2.54 cm at steady state. To investigate the possibility of slippage of the fibre while spiralling along the polished mandrel, the experiments were repeated with the mandrel covered with double sided tape. The measurements of the helical profiles in both cases were identical. The same observations are valid regardless of the mandrel diameter. The results for the 1.27 cm diameter mandrel are shown in Figure 6.2.

6.2 Model Development for Braiding During the Transient State

The path of a strand along a 2D braided structure can be modelled as the tip of a vector, $\vec{V}_1$, (at the fell of the fabric), that moves at uniform angular and transverse speeds around and parallel to the axis of the braid, thus describing a helix (Figure 6.3). Similarly, the point of contact of the strand at the guide ring can also be modelled as the tip of a vector, $\vec{V}_2$, moving at the same uniform angular and transverse speeds as the mandrel, describing a helix inside and along the axis of an imaginary tube representing the guide ring. The passage of a strand into the convergence zone can be represented by a vector, $\vec{V}_3$, tangent to the helix at the fell point and passing through the point of contact of the strand with the guide ring. The magnitude of the vector, $\vec{V}_3$, represents the relative distance between the fell point and the point of contact of the strand with the guide ring.

In Figure 6.3 (a), the tips of the vectors $\vec{V}_1$ and $\vec{V}_2$ travelling along two cylinders representing the mandrel and the guide ring of radii, r_1 and R_G, respectively, and rotating at constant angular speed around their common axis, are shown. During the transient state (Figure 6.3 (b)) the axial distance covered by the fell point per revolution

representing the pitch of the strand, $a_1, a_2, a_3, a_4, \ldots a_n, \ldots$, varies until it becomes equal to the mandrel pitch, P, at steady state. Also, since the tangent to the helix at the fell point should pass through the point of contact of the strand and the guide ring, then the distance, a_1, travelled by the tip of the vector $\bar{V}_1$ during one revolution of the braiding head is given by the following relationship:

$$\tan\theta = \frac{2\pi r_1}{a_1} = \frac{\sqrt{R_G^2 - r_1^2}}{P - a_1} \tag{6.1}$$

rearranging, gives;

$$\frac{P - a_1}{a_1} = \frac{\sqrt{R_G^2 - r_1^2}}{2\pi r_1} \tag{6.2}$$

It should be noted that these equations are valid under the assumption that only one braiding strand needs to be considered as a representative of all others (i.e. no interlacing effect). Solving for a_1, the initial pitch distance of the strand gives:

$$a_1 = P \cdot c \tag{6.3}$$

where, $c = \dfrac{2\pi r_1}{2\pi r_1 + \sqrt{R_G^2 - r_1^2}}$

Similarly, the second pitch distance is obtained as follows:

$$\tan\theta_2 = \frac{2\pi r_1}{a_2} = \frac{\sqrt{R_G^2 - r_1^2}}{2P - a_1 - a_2} \tag{6.4}$$

re-arranging gives;

$$\frac{2P - a_1}{a_2} = \frac{2\pi r_1 + \sqrt{R_G^2 - r_1^2}}{2\pi r_1} \tag{6.5}$$

Substituting for c and a_1, from Equation 6.3, gives;

$$a_2 = (2 - c) \cdot a_1 \tag{6.6}$$

in a similar fashion, the third pitch distance of the braid can be shown to be given by;

$$a_3 = \left(3 \cdot P - (a_1 + a_2)\right) \cdot c$$

substituting for a_1 from Equation 6.3 and a_2 from Equation 6.6 and simplifying gives;

$$a_3 = \left(3 - 3 \cdot c + c^2\right) \cdot a_1 \tag{6.7}$$

The fourth and the fifth pitch distances are derived in a similar manner and are given respectively by:

$$a_4 = \left(4 - 6 \cdot c + 4 \cdot c^2 - c^3\right) \cdot a_1 \tag{6.8}$$

and,

$$a_5 = \left(5 - 10 \cdot c + 10 \cdot c^2 - 5 \cdot c^3 + c^4\right) \cdot a_1 \tag{6.9}$$

Thus, the varying strand pitch, a_1, a_2, a_3, ..., a_n, ..., of the braid during the transient state can be represented by following series;

$$\begin{bmatrix} a_1 \\ a_2 \\ a_3 \\ .. \\ .. \\ a_n \\ .. \end{bmatrix} = \begin{bmatrix} 1 & & & & \\ 2 & -c & & & \\ 3 & -3c & c^2 & & \\ 4 & -6c & 4c^2 & -c^3 & \\ 5 & -10c & 10c^2 & -5c^3 & c^4 \\ .. & .. & .. & .. & .. \\ .. & .. & .. & .. & .. \end{bmatrix} \cdot a_1$$

where, its general term is;

$$a_n = \left(n - \frac{n(n-1)}{2!} \cdot c + \frac{n(n-1)(n-2)}{3!} \cdot c^2 - \ldots\ldots \right) \cdot a_1 \qquad \textbf{(6.10)}$$

In order to evaluate the general term of this sequence, consider the binomial expansion of the general expression $(a+b)^n$. This expansion is given by:

$$(a+b)^n = a^n + n \cdot a^{n-1} \cdot b + \frac{n(n-1)}{2!} \cdot a^{n-2} \cdot b^2 + \frac{n(n-1)(n-2)}{3!} \cdot a^{n-3} \cdot b^3 + \ldots. \qquad \textbf{(6.11)}$$

Substituting $a = 1$, and $b = -c$ in the general form of the expansion gives:

$$(1-c)^n = 1 - n \cdot c + \frac{n(n-1)}{2!} \cdot c^2 - \frac{n(n-1)(n-2)}{3!} \cdot c^3 + \ldots\ldots \qquad \textbf{(6.12)}$$

In a matrix form, this expansion is given as follows:

$$\begin{bmatrix} (1-c) \\ (1-c)^2 \\ (1-c)^3 \\ \\ (1-c)^n \\ \\ \end{bmatrix} = \begin{bmatrix} 1 & -c & & & & \\ 1 & -2c & +c^2 & & & \\ 1 & -3c & +3c^2 & -c^3 & & \\ 1 & -4c & +6c^2 & -4c^3 & +c^4 & \\ 1 & -5c & +10c^2 & -10c^3 & +5c^4 & -c^6 \\ .. & \ldots & \ldots & \ldots & \ldots & \ldots \end{bmatrix}$$

Subtracting both sides from 1 and dividing by c, gives;

$$\frac{1-(1-c)^n}{c} \Rightarrow n - \frac{n(n-1)}{2!} \cdot c + \frac{n(n-1)(n-2)}{3!} \cdot c^2 - \ldots\ldots \qquad \textbf{(6.13)}$$

The RHS of Equation 6.13 is identical to the bracketed term of Equation 6.10. Hence, the general term, a_n, of the pitch distance sequence that represents the braided structure

during the transient state can be written as follows:

$$a_n = \frac{1-(1-c)^n}{c} \cdot a_1 = \left(1-(1-c)^n\right) \cdot p \tag{6.14}$$

In the above analysis, the two vectors $\vec{V}_1$ and $\vec{V}_2$ started from the same reference axial position. However, when the vector $\vec{V}_2$ leads or lags vector $\vec{V}_1$ by an axial distance, X, (Figure 6.4) as usually occurs in 2D braiding, the derivation of the series follows a similar development to that presented earlier and proceeds as follows:

$$\tan\theta_1 = \frac{2\pi r_1}{a_1} = \frac{\sqrt{R_G^2 - r_1^2}}{X + P - a_1} \tag{6.15}$$

Thus, the first pitch distance of the braided fabric is given by:

$$a_1 = X \cdot c + P \cdot c \tag{6.16}$$

where, $c = \dfrac{2\pi r_1}{2\pi r_1 + \sqrt{R_G^2 - r_1^2}}$

Subsequent terms of the series representing the pitches are given by;

$$a_2 = \left[(X+2\cdot P) - (X+P)\cdot c\right]\cdot c$$

$$a_3 = \left[(X+3\cdot P) - (2\cdot X+3\cdot P)\cdot c + (X+P)\cdot c^2\right]\cdot c$$

$$a_4 = \left[(X+4\cdot P) - (3\cdot X+6\cdot P) + (3\cdot X+4\cdot P)\cdot c^2 - (X+P)\cdot c^3\right]\cdot c$$

$$a_5 = \left[(X+5\cdot P) - (4\cdot X+10\cdot P)\cdot c + (6\cdot X+10\cdot P)\cdot c^2 + (4\cdot X+5\cdot P)\cdot c^3 - (X+P)\cdot c^4\right]\cdot c$$

This sequence can be re-arranged as follows;

$$a_1 = X \cdot c + P \cdot c \tag{6.17}$$

$$a_2 = (1-c) \cdot X \cdot c + (2-c) \cdot P \cdot c \tag{6.18}$$

$$a_3 = (1-2 \cdot c + c^2) \cdot X \cdot c + (3-3 \cdot c + c^2) \cdot P \cdot c \tag{6.19}$$

$$a_4 = (1-3 \cdot c + 3 \cdot c^2 - c^3) X \cdot c + (4-6 \cdot c + 4 \cdot c^2 - c^3) P \cdot c \tag{6.20}$$

In matrix notation, this takes the following form;

$$\begin{bmatrix} a_1 \\ a_2 \\ a_3 \\ .. \\ .. \end{bmatrix} = \begin{bmatrix} 1 & & & & \\ 1 & -c & & & \\ 1 & -2c & c^2 & & \\ 1 & -3c & 3c^2 & -c^3 & \\ 1 & -4c & 6c^2 & -4c^3 & c^4 \end{bmatrix} \cdot X \cdot c + \begin{bmatrix} 1 & & & & \\ 2 & -c & & & \\ 3 & -3c & c^2 & & \\ 4 & -6c & 4c^2 & -c^3 & \\ 5 & -10c & 10c^2 & -5c^3 & c^4 \end{bmatrix} \cdot P \cdot c$$

The general term of this sequence can again, be mathematically deduced by comparison to the series $(1-c)^n$. The general term, a_n, of this sequence can be expressed as follows:

$$a_n = (1-c)^{n-1} \cdot X \cdot c + \left(1-(1-c)^n\right) \cdot P \tag{6.21}$$

The length of the convergence zone, D, during the transient state is represented by the projection of the vector, $\vec{V}_3$, on the axis of rotation.

With reference to Figure 6.4, the sequence of the lengths, D_n, during the transient state are given by:

$$D_1 = X + P - a_1$$

$$D_2 = X + P - (a_1 + a_2)$$

and so on.

Substituting for $a_1, a_2, a_3, \ldots$ etc, gives;

$$D_1 = (1-c)\cdot X + (1-c)\cdot P \tag{6.22}$$

$$D_2 = (1-2\cdot c+c^2)\cdot X + (2-3\cdot c+c^2)\cdot P \tag{6.23}$$

$$D_3 = (1-3\cdot c+3\cdot c^2-c^3)X + (3-6\cdot c+4\cdot c^2-c^3)P \tag{6.24}$$

This series can be represented in matrix form as follows;

$$\begin{bmatrix} D_1 \\ D_2 \\ .. \\ .. \\ .. \end{bmatrix} = \begin{bmatrix} 1 & -c & & & \\ 1 & -2c & c^2 & & \\ 1 & -3c & 3c^2 & -c^3 & \\ 1 & -4c & 6c^2 & -4c^3 & c^4 \\ -- & -- & -- & -- & -- \end{bmatrix} \cdot X + \begin{bmatrix} 1 & -c & & & \\ 2 & -3c & c^2 & & \\ 3 & -6c & 4c^2 & -c^3 & \\ 4 & -10c & 10c^2 & -5c^3 & c^4 \\ -- & -- & -- & -- & -- \end{bmatrix} \cdot P$$

The general term of the sequence can be mathematically deduced by comparison with the series $(1-c)^n$, and is given by:

$$D_n = (1-c)^n \cdot X + \left[\frac{1-(1-c)^{n+1}}{c} - 1\right] \cdot P \tag{6.25}$$

A vector approach was used to confirm the validity of Equations 6.21 and 6.25 and to show that the angle between the tangent to the helix and $\vec{V}_3$, in Figure 6.3a, is always equal to zero. An excerpt of the output of a computer program written for that purpose is shown in Appendix F.4.

6.3. Verification of the Series Solution

Three sets of results were generated to verify the accuracy of the developed model. The first set was generated using the lathe with the special tool shown in Figure 6.1. Figures 6.5 and 6.6 compare the calculated and the measured lengths of the spiralling strand travelling along the 2.54 and 1.27 cm diameter mandrels. Measured and calculated data for this set are shown in Appendix H. In the case of the 2.54 cm diameter mandrel, the deviations between the calculated and measured pitches ranged from 8.9 to 2.5%, while in the case of the 1.27 cm. diameter mandrel, the range of deviation was between 14.24 and 0.34 %. In both cases, the highest percent deviation occurred during the first revolution of the braiding head (i.e. at the first data point) and was attributed to the error in measuring the distance, X, of the starting point. Also, it was felt that the high bending deflection of the smaller diameter mandrel caused the higher percent deviation than that of the 2.54 cm diameter mandrel.

The second set of results, given in Table 6.1, shows the data points generated from fourteen 2D cylindrical braiding experiments where the distances travelled per revolution, a_i's, were measured off the mandrel. Experiments 1, 3, 4, 5, 7, 9, 11, 13, and 14 are for $X < D_-$, while experiments 2, 6, 8, 10,12 ... etc., are for $X > D_-$. Table 6.2 presents the calculated values of the pitch lengths during the transient state for the fourteen 2D cylindrical braiding experiments. Tables 6.3 and 6.4 give the corresponding deviations (in cm as well as in %) between the measured and derived values.

Figure 6.7 shows the results of experiment number 1 where the agreement between the derived and the measured pitch lengths along the braided structure is displayed. A complete set of results for all fourteen cases is given in Appendix H.2. The absolute deviations between the measured and derived pitch lengths for all fourteen cases were less than 5.5% as shown in Figure 6.8, except at the first point in six cases, where the percent deviations rose to a maximum of 22%. These specific points were omitted from the figure. These high values were attributed to errors in measuring the starting point for the series and the adjustments that took place until they converged to the steady state. As well, it was noted that the choice of the position of the starting point ($X > D\infty$ or $X < D\infty$) had no significant effect on the magnitude of the deviation between the derived and measured values.

The third set of data was extracted from the Du and Popper publication [10]. These data points, which represent the length of the convergence zone at the beginning of every revolution, were measured from Figure 12 [10]. These data points, as well as the data derived in this work are given in Appendix H.3.

The extracted Du and Popper and the derived data are shown in Figures 6.9 and 6.10. It should be noted that the farther the starting point from its steady state value, the higher the absolute deviation before the series converges to steady state.

It is worthwhile mentioning that the transient state equations used in this thesis are discrete since the data points were measured at every pitch on the actual braid produced and compared to the calculated values at every 360° (one revolution of the braiding head). A simulation was conducted to calculate the series coefficient at shorter intervals (1/10 of the pitch) and compared to the corresponding discrete values. Using the data points from the braid produced in experiment number 7 as a base for the comparison, it was found that the measured difference is 0.12 mm. Figures 6.11 and 6.12 as well as Appendix H.4 show the results of this simulation.

6.4. Considering the Effect of Fibre Interlace when Braiding Occurs During the Transient State

As mentioned in Section 6.2, the variable strand pitch of a braided structure observed during the transient state can be expressed as a function of the machine and mandrel parameters, the desired pitch and the start up length of the convergence zone. The effect of strand interlacing can be incorporated in the transient state solution by introducing the fibre strand interlacing parameter, ζ , obtained from steady state experiments and evaluated experimentally for a specific machine setup. The derivation of a generalized theoretical expression was considered outside the scope of this thesis. However, for the sake of completeness, a graphical representation of a method to determine the effect of the fibre strand interlacing near the deposit plane during the transient state can be determined by referring concurrently to the length of the strand pitch when no interlacing is considered.

The derivation of expressions for the length of the conversion zone, D, and the pitch change parameter, c, for the 2D braiding follows. It will be assumed here that ζ is constant throughout the transient state. Figure 6.13 (a) shows a schematic of the braided structure, considering the interlacing of the fibre strands, after one revolution of the braiding head during which the position of the deposit plane moves from d_1 to d_2. As shown in Chapter 5, the deposit plane is brought nearer to the guide plane due to the effect of the interlacing between the strands and thus a fibre strand interlacing parameter, ζ, (see Table 5.1) applies. Figure 6.13 (b) shows the equivalent position of the braided fabric without consideration of the interlacing of the fibre strands. For a given speed ratio, the desired pitch, P, the strand interlacing parameter for the case of steady state, ζ, and the coefficient of the expression for braiding during the transient state, c, can be determined. Also, for a given cone angle α, the inclination of the interlaced fibre strands in the convergence zone, θ, as well as, the length of the convergence zone, X, at this position can be computed using Equations 4.2 and E.21.

The equivalent inclination of the non-interlaced fibre strands in the convergence zone at start-up, Figure 6.13 (b), can be obtained by considering the fibre strand interlacing parameter ζ. Consequently, the equivalent start-up length of the convergence zone, X_I, can be computed.

Knowing the distance P travelled by the mandrel and the coefficient of the expression for braiding during the transient state, c, the pitch of the braided fabric, a_i, the length of the convergence zone, D_I, and consequently the corresponding new inclination of the non-interlacing strands, θ_I, in the convergence zone after one revolution can be determined. By again considering the parameter, ζ, the equivalent inclination of the fibre strands and the corresponding deposit plane location after one revolution in the case of the interlaced strands can be determined.

The procedure described above is shown in Figure 6.14. This procedure leads to the derivation of the expression for the determination of the length of the convergence zone, D, after one revolution of the braiding head when the effect of fibre strands interlace is considered. This length is given by:

$$\cdots D = \frac{\left[(a.d + P.b)(1-c) - a.b.\tan\zeta\right]}{a.b + (a.d + P.b)(1-c).\tan\zeta} \qquad \textbf{(6.26)}$$

where, $a = \sqrt{R_G^2 - R_m^2}$

$$b = (a - X.\tan\zeta)$$

$$d = (X + a.\tan\zeta)$$

$$c = \frac{2\pi R_m}{2\pi R_m + \sqrt{R_G^2 - R_m^2}}$$ (coefficient of the series with **no** interlace).

And thus, the coefficient of the expression for braiding during the transient state considering the effect of fibre interlacing is given by:

$$c_{\text{with interlace}} = \frac{(X+P)-D}{(X+P)} \tag{6.27}$$

A fourth set of experimental and theoretical results were generated to evaluate the accuracy of the model when considering the effect of fibre strand interlace near the deposit plane during the transient state. The results were obtained for a machine setup similar to those of Experiment number 7 of the second set mentioned in Section 6.2. The compiled information is summarized below:

desired pitch		4.826 cm.	
speed	mandrel (v_l)	84.6 rpm	
	head (v_r)	674.9 rpm	
length of the convergence zone at start up (X)		2.057 cm.	
strand interlacing parameter, ζ, (Table 5.1)		5.33°	
coefficient of the series, c (without interlace)		0.51021	(Equation 6.3)
c (with interlace)		0.57729	(Equation 6.27)

The measured braid pitches $a_1, a_2, a_3, \ldots, a_n$ of the braided structure (with interlace), as well as, the prediction of the variable strand pitch during the transient state are given in Appendix H.5. Figure 6.15 shows the degree of agreement between the derived and measured data. It shows that the percent absolute deviation was less than 0.7 % all along the braided structure.

Since only one set of experimental data was used to demonstrate the accuracy of the predictive model for braiding during the transient state, no general conclusions for the time being are made. However, the results obtained so far show that the assumption that the fibre strand interlace parameter, ζ, is constant throughout the transient state, is plausible.

6.5. Algorithm Developed to Respond to a Desired Change in Fibre Orientation – A Practical Example

In order to demonstrate the process of adjusting the braiding parameters (speeds and deposit plane location) in response to a desired change in the braid angle during a 2D cylindrical braiding exercise the following procedure is developed. Assume that while braiding over a cylindrical mandrel at a certain speed, the cone angle measuring device estimated the length of the convergence zone at 2.344 cm. It is required to change the fibre orientation to a new value of 58.65° (based on data of Experiment number 7, given in Appendix H.2), and thus, the following input data are utilized:

- length of convergence zone (X) 2.344 cm (Cone angle measuring device)
- desired braid angle 58.65° (New desired orientation)
- desired pitch length (P) 4.862 cm ($P = \frac{2\pi R_m}{\tan\theta}$)
- desired speed ratio (ω/v) 3.283 ($\frac{\omega}{v_t} = \frac{\tan\theta}{R_m}$)
- conversion factor for the local machine drives 38.735 cm/rev (or 15.25 in/rev)
- desired machine speed drives
  - Head (v_r) 675.1 rpm (chosen)
  - Mandrel (v_t) 84.7 rpm ($P = 38.735 \cdot \frac{v_t}{v_r}$)
- strand interlacing parameter, ζ, 5.33° (Table 5.1)
- coefficient of the series during transient (c) .57729 (Equation 6.28)

A new set of speeds (v_r and v_t, and consequently P_{new}) are determined such that the

outcome of the first sequence of the variable strand pitch of the braid formation during the transient state is equal to the desired pitch, 4.862 cm. Figure 6.16 represents the geometric relationships of the conversion zone. With reference to the figure, the new speed setting for the first revolution of the braiding head is calculated (Equation 6.16).

$$i.e. \quad P_{new} = \frac{4.862}{c} - X = 6.078 \ cm$$

If the speed of the braiding head, v_r, remains unchanged, then the new speed of the mandrel, v_t, can be calculated as follows:

$$P_{new} = 38.735\frac{v_t}{v_r} \quad then \ v_t = 105.9 \ rpm$$

This means that the distance that would be covered by the braided structure once the speed of the mandrel drive changes to 105.9 rpm is equal to 4.862 cm, thus, the desired braid angle is attained directly as braiding continues. After one revolution, the speed of the mandrel drive is adjusted to the desired speed.

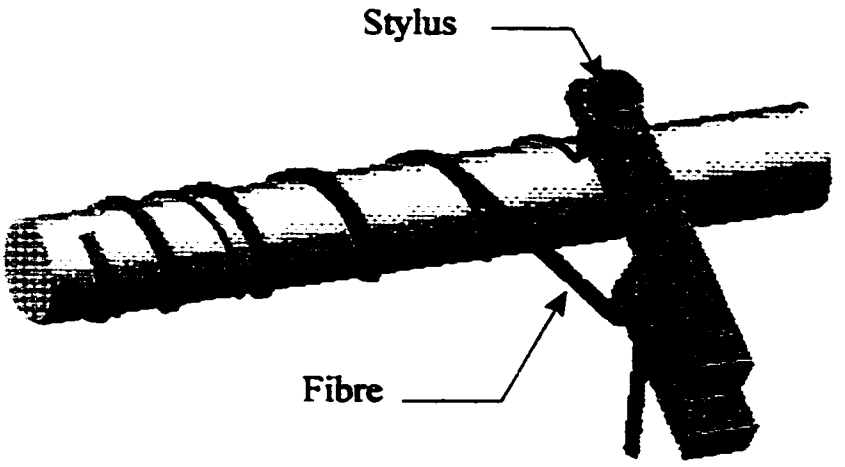

Figure 6.1 Superimposed helix formation during the transient, as well as, the steady state

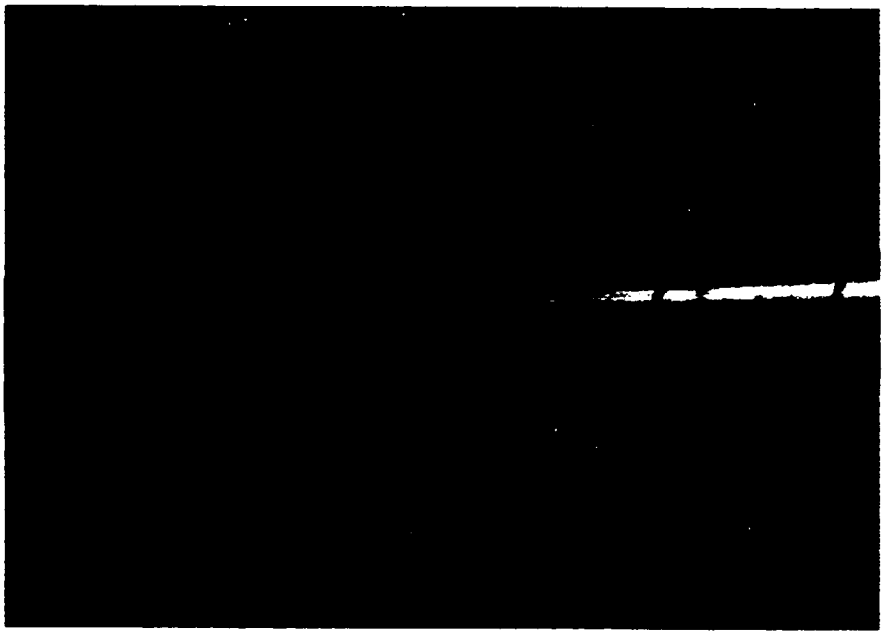

Figure 6.2 Superimposed helix formation during transient state– experimental results using a 1.27 cm diameter mandrel

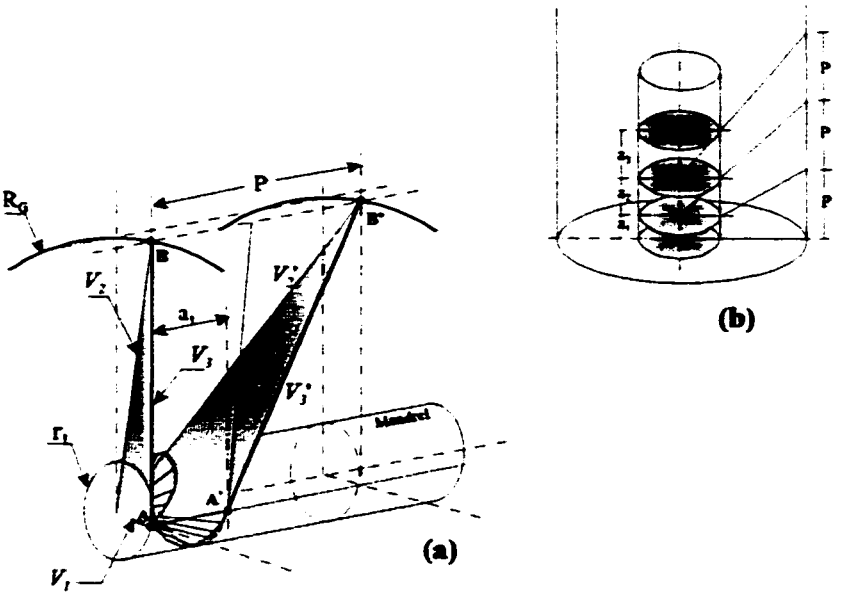

Figure 6.3 Vectorial representation of a fibre strand in the convergence zone during the transient state

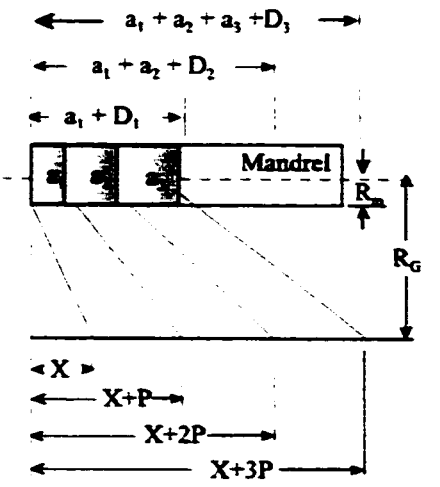

Figure 6.4 Illustration of the series during the transient state when the vectors do not start from the same reference level

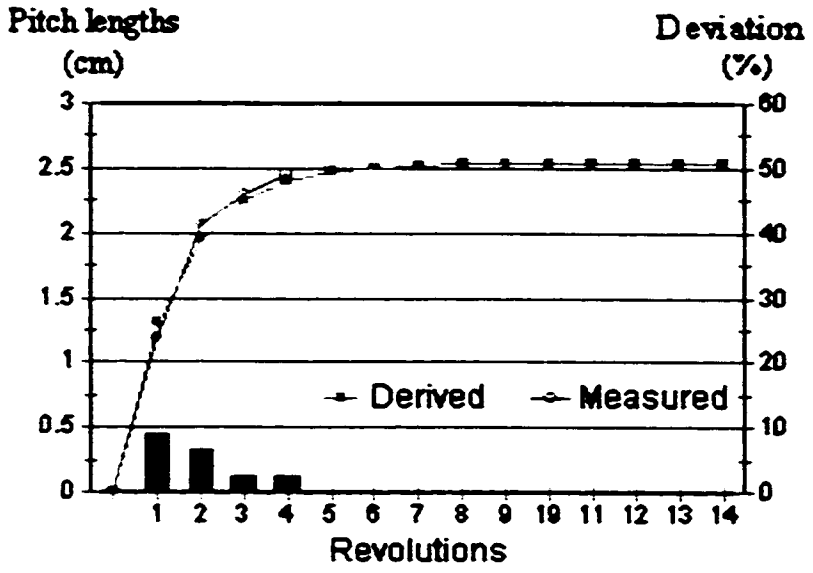

Figure 6.5 Distance travelled per revolution (variable strand pitch) during the transient state – mandrel diameter = 2.54 cm. Percentage deviation given by bars

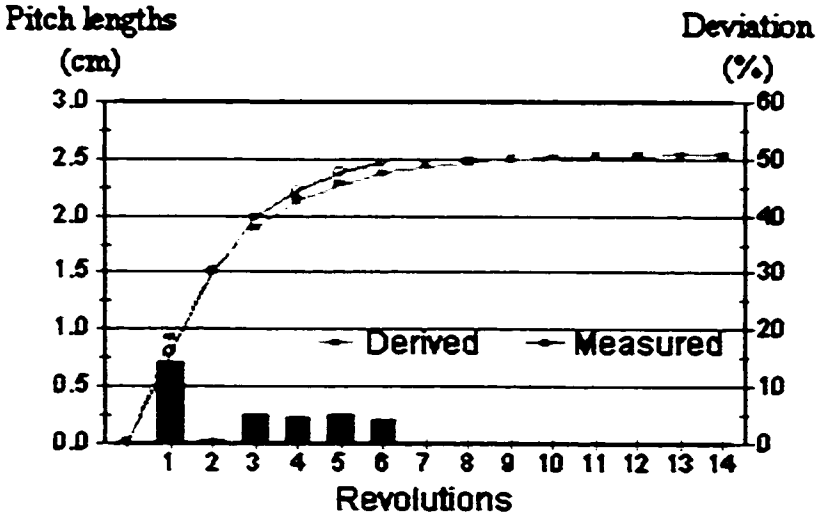

Figure 6.6 Distance travelled per revolution (variable strand pitch) during the transient state – mandrel diameter = 1.27 cm. Percentage deviation given by bars

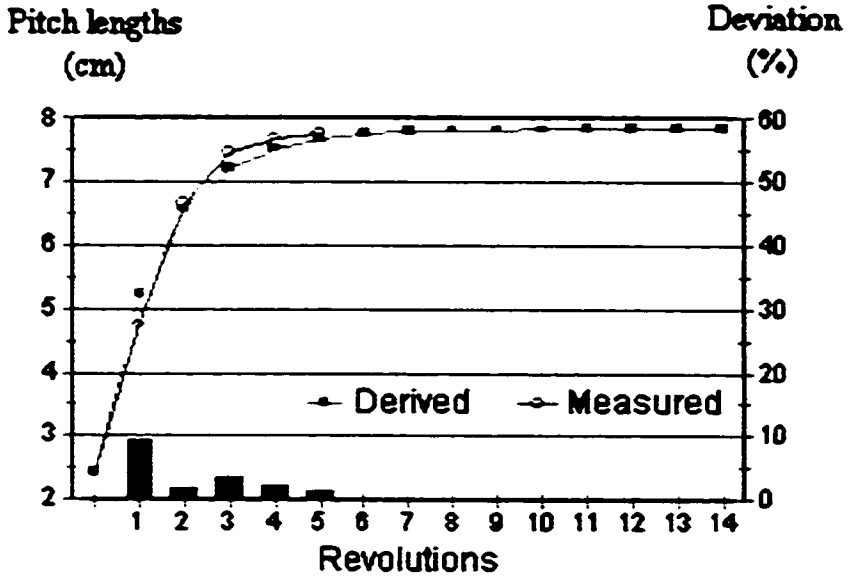

Figure 6.7 Distance travelled per revolution of the braiding head during the transient state (experiment #1). Percentage deviation given by bars

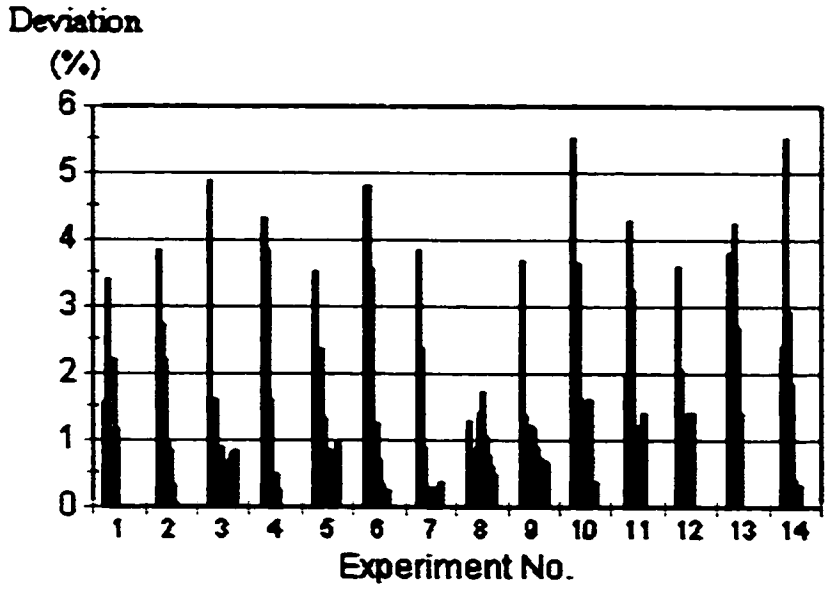

Figure 6.8 Percent deviation for the 14 braiding experiments ignoring the first data point in the set

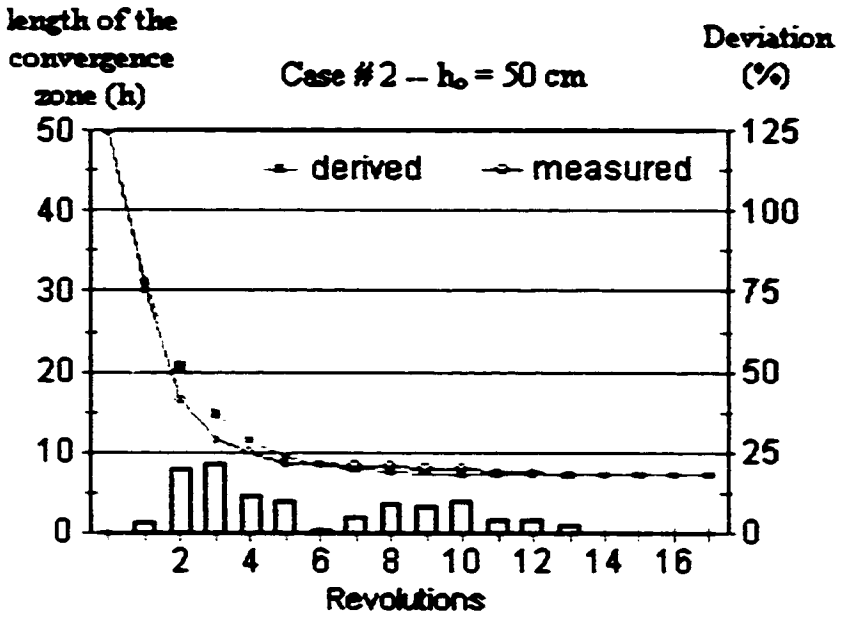

Figure 6.9 Length of the convergence zone during the transient state. (Data extracted from Du and Popper [10] — h_o = 50 cm) Percentage deviation given by bars

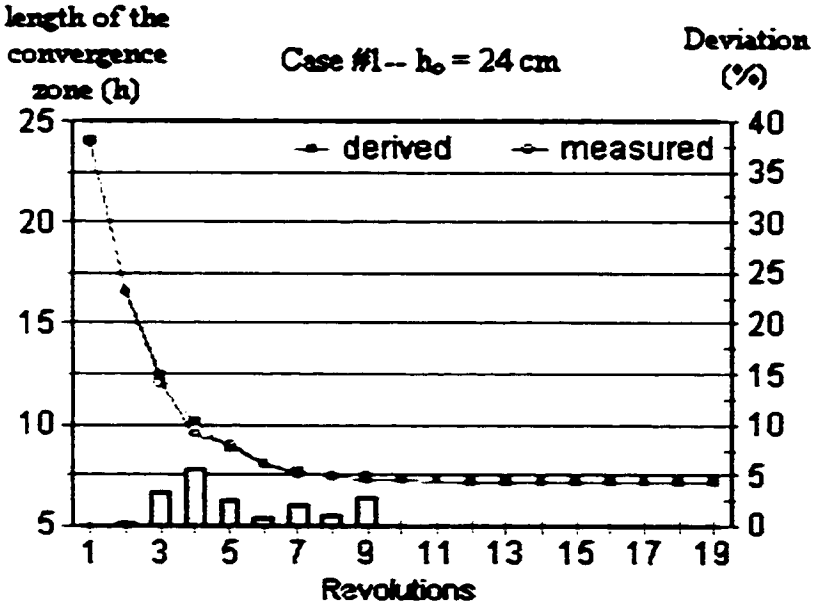

Figure 6.10 Length of the convergence zone during the transient state (Data extracted from Du and Popper [10]– h_o = 24 cm.) Percentage deviation given by bars

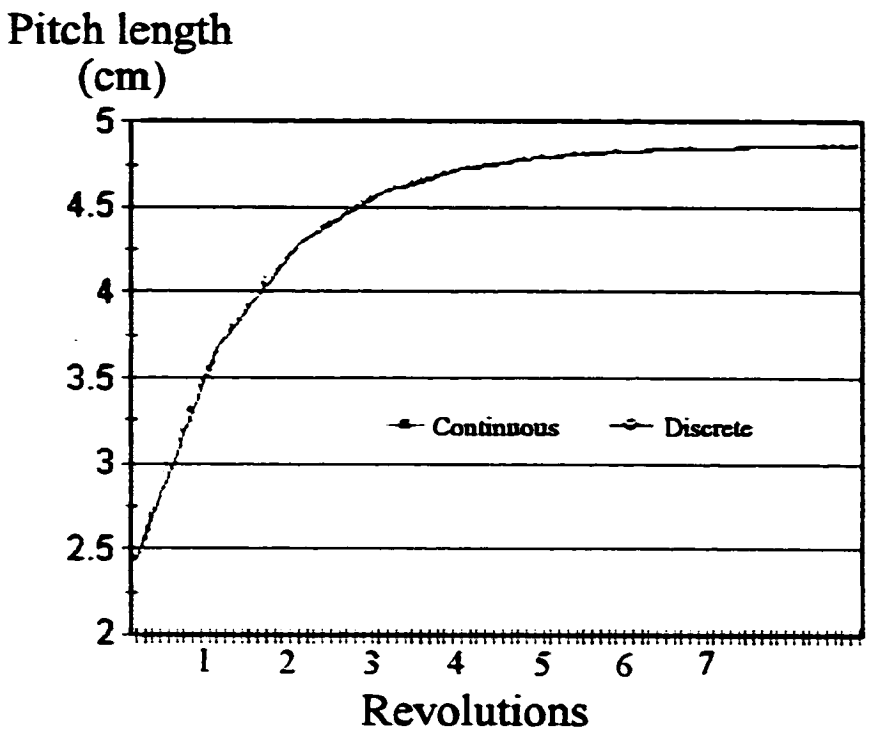

Figure 6.11 Simulation of a continuous and discrete series (Experiment no. 7)

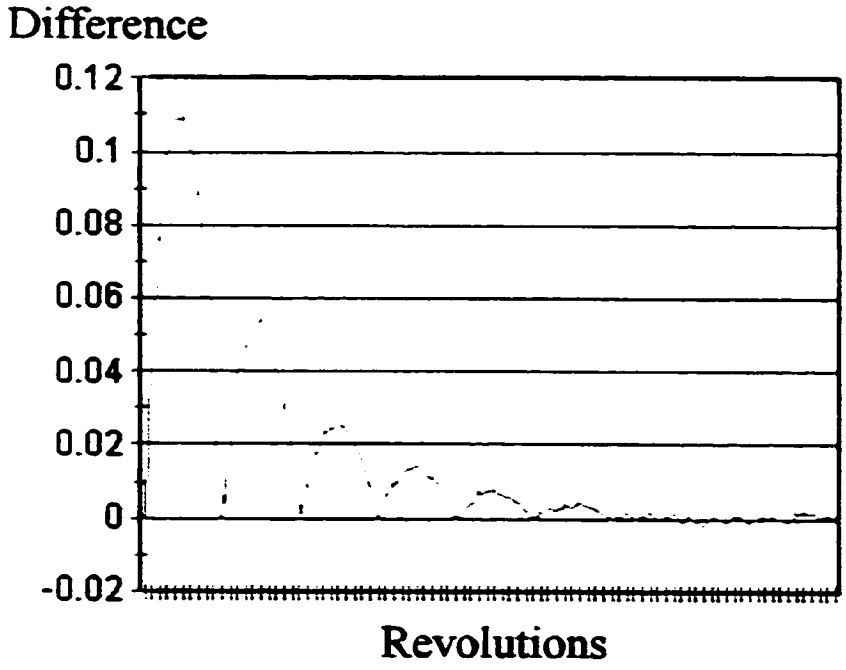

Figure 6.12 Difference between the continuous and discrete series. (Experiment no. 7)

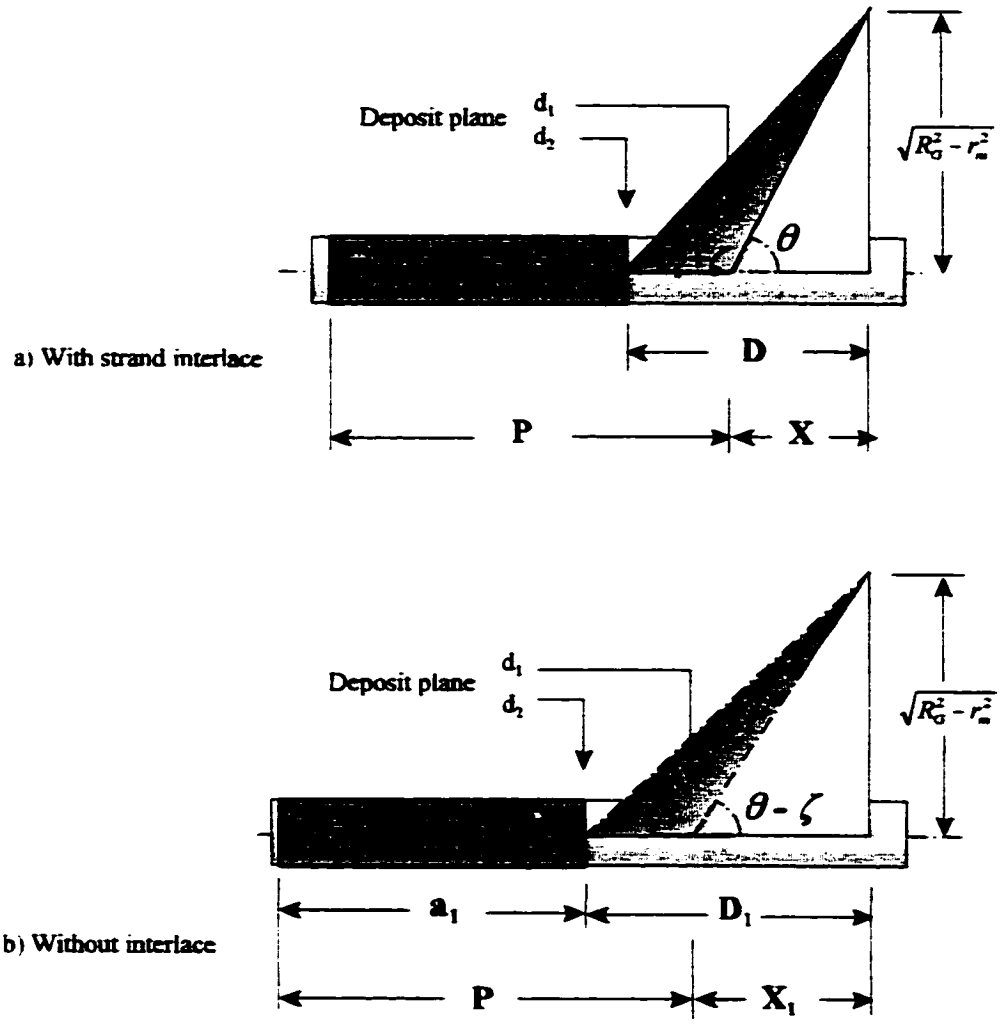

Figure 6.13 Graphical representation of braiding during the transient state considering strand interface near the deposit plane

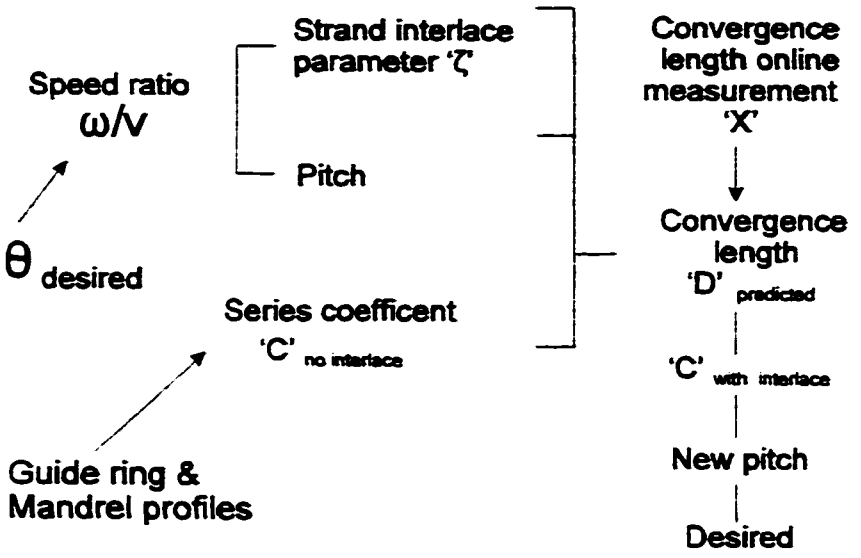

Figure 6.14 Procedures to follow in response to a required change in fibre orientation

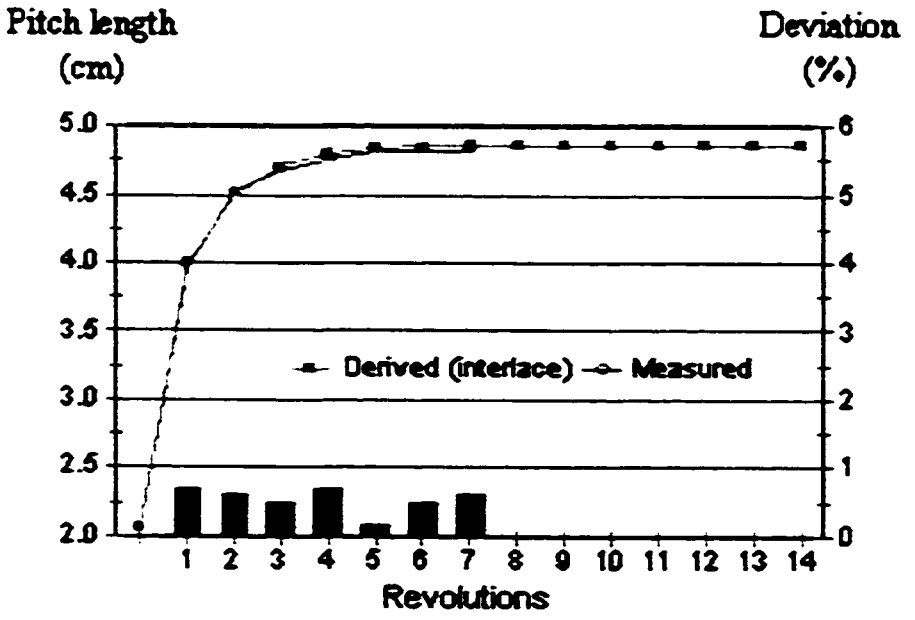

Figure 6.15 Distance travelled during the transient state considering the effect of strand interlace parameter, ζ. Percentage deviation given by bars

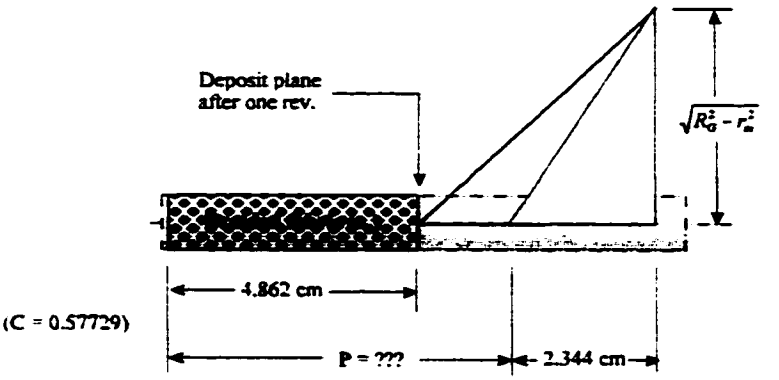

Figure 6.16 Schematic representation of the geometric relationships in the convergence zone

TABLE 6.1 Measurements of pitch lengths for the case where half the spools are loaded -- no fibre strand interlace.

Experiments 1, 3, 5, .. etc., are for X < D and experiments 2, 4, 6, ... etc., are for X > D.

Experiment #	1	2	3	4	5	6	7	8	9	10	11	12	13	14
Velocity % of Max. Head Mandrel Vel. Ratio (ω/v_1)	40/40 % 674.9 rpm 136.6 rpm 2.035		40/35 % 674.5 rpm 119.2 rpm 2.331		40/30% 674.5 rpm 101.9 rpm 2.727		40/25% 675.1rpm 84.7 rpm 3.283		40/20% 675.1 rpm 67.4 rpm 4.127		30/30% 502.3 rpm 101.8 rpm 2.039		25/40% 417.1 rpm 136.4 rpm 1.260	
a_0	0.955	5.3	0.988	0.732	1.447	4.568	0.923	3.565	0.86	3.67	1.052	4.635	0.796	0.097
a_1	1.875	5.281	1.781	1.672	2	4.125	1.5	3.013	1.281	3.125	2	4.125	2.672	2.594
a_2	2.625	3.812	2.407	2.328	2.187	3.031	1.75	2.375	1.422	2.188	2.656	3.625	4.141	3.906
a_3	2.938	3.281	2.531	2.563	2.25	2.5	1.844	2.109	1.468	1.75	2.969	3.219	4.688	4.656
a_4	3.031	3.156	2.641	2.625	2.281	2.422	1.875	2	1.5	1.594	3.063	3.188	4.875	4.844
a_5	3.063	3.125	2.671	2.641	2.312	2.344	1.891	1.937	1.522	1.562	3.062	3.094	4.938	4.938
a_6		3.094	2.671	2.656	2.312	2.322	1.906	1.906	1.531	1.562	3.031	3.062	4.938	4.938
a_7		3.094	2.671	2.688	2.312	2.313	1.969	1.906	1.531	1.562	3.031		4.938	
a_8		3.094	2.717			2.313	1.906	1.906	1.531	1.531	3.031			
a_9			2.688			2.313	1.906	1.906	1.531	1.531				
a_{10}			2.688						1.531					
Pitch P_∞ (computed)	3.087		2.695		2.304		1.914		1.522		3.081		4.987	

TABLE 6.2 Calculated values of pitch lengths (series coefficients) for the case where half the spools are loaded. – – no fibre strands interlace

Experiment #	1	2	3	4	5	6	7	8	9	10	11	12	13	14
Velocity % of Max. Head Mandrel Vel. Ratio ($\zeta/_{VT}$)	40/40 % 674.9 rpm 136.6 rpm 2.035		40/35 % 674.5 rpm 119.2 rpm 2.331		40/30% 674.5 rpm 101.9 rpm 2.727		40/25% 675.1rpm 84.7 rpm 3.283		40/20% 675.1 rpm 67.4 rpm 4.127		30/30% 502.3 rpm 101.8 rpm 2.039		25/40% 417.1 rpm 136.4 rpm 1.260	
a_0	0.955	5.3	0.988	0.732	1.447	4.568	0.923	3.565	0.86	3.67	1.052	4.635	0.796	0.097
a_1	2.062	4.279	1.879	1.749	1.914	3.506	1.447	2.795	1.215	2.649	2.109	3.937	2.951	2.594
a_2	2.585	3.671	2.295	2.231	2.113	2.893	1.686	2.346	1.372	2.074	2.605	3.500	3.990	3.815
a_3	2.841	3.373	2.499	2.468	2.210	2.592	1.802	2.125	1.448	1.792	2.848	3.286	4.498	4.413
a_4	2.967	3.227	2.599	2.584	2.258	2.445	1.859	2.018	1.486	1.654	2.967	3.182	4.748	4.706
A_5	3.028	3.156	2.648	2.641	2.282	2.373	1.887	1.965	1.504	1.587	3.025	3.130	4.870	4.849
A_6	3.058	3.121	2.672	2.668	2.293	2.338	1.901	1.939	1.513	1.554	3.054	3.105	4.930	4.920
A_7	3.073	3.103	2.684	2.682	2.299	2.321	1.908	1.926	1.518	1.538	3.068	3.093	4.959	4.954
a_8	3.08	3.095	2.689	2.689	2.301	2.312	1.911	1.920	1.520	1.530	3.074	3.087	4.973	4.971
a_9	3.084	3.091	2.692	2.692	2.303	2.308	1.912	1.917	1.521	1.526	3.078	3.084	4.980	4.979
A_{10}	3.085	3.089	2.694	2.693	2.303	2.306	1.913	1.915	1.522	1.524	3.079	3.082	4.984	4.983
a_{11}	3.086	3.088	2.694	2.694	2.304	2.305	1.914	1.915	1.522	1.523	3.080	3.082	4.985	4.985
A_{12}	3.087	3.087	2.695	2.695	2.304	2.304	1.914	1.914	1.522	1.522	3.081	3.081	4.986	4.986
a_{13}	3.087	3.087	2.695	2.695	2.304	2.304	1.914	1.914	1.522	1.522	3.081	3.081	4.987	4.987

TABLE 6.3 Differences in the values of strand pitch in cm. (derived vs measured)

Exp. # / Pitch	1	2	3	4	5	6	7	8	9	10	11	12	13	14
a_1	0.475	1.196	0.249	0.194	0.219	1.333	0.133	0.553	0.167	1.526	0.276	0.478	0.707	0
a_2	0.102	0.358	0.284	0.245	0.188	0.0351	0.164	0.057	0.128	0.29	0.13	0.318	0.384	0.231
a_3	0.246	0.233	0.081	0.241	0.101	0.235	0.107	0.042	0.05	0.108	0.308	0.171	0.482	0.617
a_4	0.164	0.181	0.106	0.105	0.136	0.059	0.041	0.045	0.036	0.153	0.244	0.017	0.324	0.351
a_5	0.089	0.077	0.058	0.001	0.077	0.074	0.01	0.07	0.045	0.064	0.093	1.16	0.174	0.226
a_6		0.067	0.003	0.032	0.048	0.04	0.013	0.084	0.045	0.02	0.057	1.39		0.047
a_7		0.024	0.033	0.016	0.044	0.019	0.004	0.051	0.034	0.062	0.093			0.04
a_8		0.002	0.047		0.027	0.002	0.013	0.036	0.028	0.004	0.11			
a_9			0.054		0.055	0.013	0.017	0.028	0.026	0.014				
a_{10}			0.058					0.024	0.024					

TABLE 6.4 Differences in the values of strand pitch in % (derived vs measured)

Exp. # / Pitch	1	2	3	4	5	6	7	8	9	10	11	12	13	14
a_1	9	11	5.22	4.37	4.51	14.97	3.62	7.79	5.41	22.68	5.15	4.78	9.43	0
a_2	1.55	3.84	4.87	4.32	3.50	4.78	3.83	1.26	3.67	5.5	1.96	3.58	3.79	2.38
a_3	3.41	2.72	1.28	3.84	1.80	3.57	2.34	0.78	1.36	2.37	4.26	2.05	4.22	5.5
a_4	2.18	2.21	1.61	1.60	2.37	0.95	0.87	0.88	0.95	3.64	3.24	0.21	2.69	2.94
a_5	1.16	0.96	0.86	0.01	1.33	1.23	0.21	1.40	1.18	1.59	1.21	1.16	1.41	1.83
a_6		0.85	0.04	0.47	0.82	0.67	0.27	1.71	1.17	0.51	0.73	1.39		0.38
a_7		0.3	0.05	0.23	0.75	0.32	0.08	1.04	0.88	1.59	1.19			0.32
a_8		0.03	0.69		0.46	0.03	0.27	0.74	0.73	0.10	1.41			
a_9			0.79		0.94	0.22	0.35	0.58	0.67	0.36				
a_{10}			0.85					0.49	0.62					

Chapter 7

Concluding remarks are made and an outlook for future works is presented.

CONCLUSIONS AND FUTURE WORK

7.1 Conclusions.

There is a growing need to produce complex braided structures with varying cross-sections or stiffness. To meet this demand, accurate and timely identification of the location of the deposit plane, and its relocation with respect to a fixed coordinate, are required. This action is followed by a change in processing speeds to obtain the required fibre orientation. These changes cannot occur instantly, since a change to the braid angle by means of changing the machine speed ratio would evoke a transition period in which the strand orientation produced is not similar to the required and hence, affects the integrity of the braided structure. Thus, the fell of the fabric (in other words the length of the convergence zone) should always be maintained during the braiding process at its desired steady-state value. Therefore, it is essential to predict and/or to control the position of the deposit plane during these transient states as slight errors can accumulate, resulting in inaccurate braided patterns on the component.

From the surveyed literature on 2D braiding, two research works were highlighted as being relevant to this research. The model developed by Du and Popper (1991) used differential equations to locate the deposit plane at all times. This model was based on simplified assumptions that does not take into consideration the strand curvature near the deposit plane due to strand interlacing. On the other hand, Zang *et al* (1999) considered a quasi-static equilibrium approach to study the effect of friction between interlacing fibres in the convergence zone. Similarly, their study did not take into consideration the effect of strand interlacing near the deposit plane. In addition, published experimental results from both studies, were not conclusive, interpretations were not fully supported, methods of measurement were not clearly presented nor understood. Finally the use of

trial and error methods to overcome the encountered braiding problems are not suited for a manufacturing environment. For these reasons these models were revisited.

The results of preliminary investigations and early experimentation, although unsuccessful, were important to understand the intricacy of the braiding process. Various aspects of the braiding process were successfully addressed. It has been proven that the geometry of the unit cells, as described by the various authors and used in the determination of the cover factor, can be simplified without any compromise to accuracy. The existing braiding machine drives were equipped with improved closed-loop feedback controls. The concept of using the angle formed by the cone-shaped profile of the converging strands as a mean to measure online the length of the convergence zone and by inference, the braid angle was introduced. A measuring device was constructed and successfully tested and the algorithm that relates the angle of the cone-shaped profile of the converging strand to the length of the converging zone was developed. This cone angle is used to locate in real time the fell of the fabric the braiding process. The fell location, in turn is used to calculate the braid angle.

The effect of stand interlacing in the proximity of the deposit plane was also considered. The relationship between the machine speed ratios and the measured braid angle (through th cone angle measuring device) has been experimentally determined and successfully tested using both interlacing and non-interlacing strands. For the first time, the effect of fibre interlace has been quantified and applied, as a factor, to a basic model of cylindrical braided structures. It is believed that, for braiding over conic surfaces the same procedures are applicable.

In addition, the time required for the braiding process to reach steady state was investigated. Braiding during the transient state has been modelled and expressions describing the formation of the braided structure have been formulated. The results of experimental investigations that have been presented support the validity of the

analytical expressions developed and have been incorporated the control strategy for complex shaped braided structures.

It is believed that the analysis presented throughout this thesis provides a better understanding of the braiding process as well as a basic tools for its process control. The analysis is aimed at advancing braiding technology for producing parts with complex cross-sections and stiffness variations along their lengths.

7.2 Further Developments

The knowledge gained and the momentum generated in University of Ottawa in the area of 2D braiding cannot pass unnoticed. Therefor, this study cannot be considered complete without suggesting some elements of future work. Three areas are suggested:

a) the development of the coefficient of the expression, c, for braiding over conic surfaces during transient.

b) recalculation of the interlacing parameter, ζ, for different mandrels and formation rings diameters.

c) the study of the effect of fibre strand packing at the deposit plane on the interlacing parameter, ζ.

d) the machine set up can no longer be dedicated to a specific area of research. Therefore, the existing set up should be adjusted to support different sizes of mandrels and formation rings. The braiding head and the mandrel bed should share a common base to facilitate the levelling of the mandrel. The data acquisition could very well be replaced to benefit from the advanced technology in the area of data sampling. Speed sensors could be enhanced by using

frequency convertors. Finally, any or all of the preceding changes would require new computer programs to support the suggested improvement.

References

REFERENCES

1. M. Munro, "Review of Manufacturing of Fibre Composite Components by Filament Winding", Polymer Composites, Vol. 9, No. 5, Oct. 1988.

2. M. Munro and A. Fahim, "A Comparison of Helical Filament Winding and 2D Braiding of Fibre Reinforced Polymeric Components", Materials and Manufacturing Processes, Vol. 10, No. 1, 1995, pp 37-46.

3. D. Brunnschweiler, "Braids and Braiding", J. of Text. Institute, Vol. 44, 1953, pp 666.

4. D. Brunnschweiler, "The Structure and Tensile Properties of Braids", J. of Text. Institute, Vol. 45, 1954, pp T55.

5. C. Pastore and F. Ko, "CIM of Braided Preforms for Composites, Computer Aided Design in Composite Material Technology", Computational Mechanics Publications, 1988, pp 133-156.

6. G. Yang, C. M. Pastore, Y. J. Tsai, H. B. Soebroto, and F. Ko, "CAD/CAM of Braided Preforms for Advanced Composites", ASM International, Metals, 1987, pp 103-107.

7. H. B. Soebroto, T. Hager, C. M. Pastore, F. Ko, "Engineering Design of Braided Structural Fibreglass Composites", 35th International SAMPE Symposium, April 1990, pp 687- 696.

8. W. Michaeli, U. Rosenbaum, "Structural Braiding of Complex Shaped FRP parts - A New Approach for Higher Productivity", 34th International SAMPE Symposium, May 1989, pp 1834.

9. P. Popper, G. Du, Tsu-Wei Chou, "Process Model for Circular Braiding, Processing of Polymers and Polymeric Composites", ASME Materials Division, Vol. 19, 1990, pp 119-133,

10. P. Popper and G. W. Du, "Analysis of a Circular Braiding Process for Complex Shapes", J. of Text. Institute, Vol. 85, No. 3,1994, pp 316.

11. Q. Zang, D. Beale, and R. M. Broughton , "Analysis of Circular Braiding Process, Part 1: Theoretical Investigation of Kinematic of the Circular Braiding Process", Journal of Manufacturing Science and Engineering, Vol. 121, No. 3, Aug. 1999, pp 345-350

12. Q. Zang, D. Beale, R. M. Broughton, and S. Adanur, "Analysis of Circular Braiding Process, Part 2: Mechanics Analysis of the Circular Braiding Process and Experiments", Journal of Manufacturing Science and Engineering, Vol. 121, No. 3, Aug. 1999, pp 351-359.

13. Q. Zang, D. Beale, S. Adanur, R. M. Broughton, and R. P. Walker,"Structural Analysis of Two Dimensional Braided Fabric", J. of Text. Institute, Vol. 88, 1997, pp 41-52.

14. Richard T. Brown, "Through-The-Thickness Braiding Technology", 30th National SAMPE Symposium, March 1985, pp 1509.

15. L. R. Sanders, "Braiding - A Mechanical Means of Composite Fabrication", SAMPE Quarterly, Jan. 1977, pp 38-43.

16. R. H. Hopper, J. W. Grant, P. Popper, "Mechanics of a Hybrid Circular Braid with an Elastic Core", Textile Research Journal, Vol 65, No 12, Dec. 1995, pp 709-722.

17. Roy J Post, "Braiding Composites - Adapting the Process for the Mass Production of Aerospace Components", 22nd National SAMPE Symposium, 1977, pp 486-503.

18. Textile Terms and Definitions, 8th Edition, edited by S. R. Beech *et al*, The Textile Institute, 1986.

19. F. K. Ko, C. M. Pastore, and A. A Head, "Handbook of Industrial Braiding", Published by Atkins and Pearce, Covington, Kentucky, 1990.

20. F. T. Peirce, "The Geometry of Cloth Structure", J. of Text. Institute, Transactions, Vol. 28, Mar. 1937.

Appendices

APPENDIX A – Ko and Pastore's Model – [5, 6, 19]

Summary of the Mathematical Derivation.

The cover factor as defined by the authors is the projected strand area in a unit cell divided by the area of the cell.

In Figure 3.1 the projected area, A_y, of the yarn is equal to two rectangular strips minus the overlap and the overhangs. Thus,

$$A_y = 2 \cdot W \sqrt{x^2 + y^2} - \frac{W^2}{\sin(2 \cdot \theta)} - \frac{W^2(\tan\theta + \cot\theta)}{2} \qquad \text{(A.1)}$$

where x and y represent the dimensions of the cell.

Further simplification to the above equation gives;

$$A_y = \frac{2 \cdot x \cdot W \cdot \cos\theta - W^2}{\sin\theta \cdot \cos\theta} \qquad \text{(A.2)}$$

Since the area of the cell $A = \frac{x^2}{\tan\theta}$, then the Cover Factor, K, can be expressed as follows;

$$K = \frac{2 \cdot x \cdot W \cdot \cos\theta - W^2}{x^2 \cdot \cos^2\theta} \qquad \text{(A.3)}$$

The unit cell width, x, can be expressed in terms of the mandrel size and number of spools as;

$$x = \frac{2 \cdot \pi \cdot R_m}{N/2} \qquad \text{(A.4)}$$

where R_m = radius of the mandrel , and

N = total number of spools.

It should be noted that Equation A.4 differs from that given by Ko and Pastore [5,19]. In their work a typographical error shows the equation as; $x = \frac{2 \cdot \pi \cdot R_m}{N}$.

Substituting for x from Equation A.4 into Equation A.3 gives the fibre orientation in terms of the cover factor as follows:

$$\theta = \cos^{-1}\left(\frac{N \cdot W\left(1 \pm \sqrt{1-K}\right)}{4 \cdot \pi \cdot K \cdot R_m}\right) \qquad \textbf{(A.5)}$$

Equation A.5 yields two positive values for θ. In braiding, the smaller value (resulting from the positive sign) is usually considered since it is associated with the fibre jamming along the axes of the braid due to fibre tension along this direction (see Figure 2.2). On the other hand, the negative sign is associated with fibre jamming in the compression mode. Therefore, the fibre orientation in terms of the cover factor is given by:

$$\theta = \cos^{-1}\left(\frac{N \cdot W\left(1 + \sqrt{1-K}\right)}{4 \cdot \pi \cdot K \cdot R_m}\right) \qquad \textbf{(A.6)}$$

In a simple 1/1 braided fabric, the orientation of the strand can be related to the machine parameters as follows:

$\tan\theta = {}^{2\pi R_m}/_{p}$, where $p = v_t / v_r$

APPENDIX B – An Alternate Method to Calculate the Cover Factor

APPENDIX B -- An Alternate Method to Calculate the Cover Factor

For the development of a general expression for the cover factor, braiding over a conic surface will be considered. Since the braiding carriers and the mandrel are moving at constant rates, then the path of a strand while braiding over a conic mandrel would describe a helix. The lateral area of the cone-shaped braid and, consequently, the area of any unit cell on its surface can be mathematically formulated. As well, the properties of a helix passing along the side of the cone can be determined. Hence, its length (or any segment of its length) and the tangent to the helix at any point can be located, and the braid angle can be determined.

With reference to Figure B.1, a cone has the property that for any point, Q, on its surface, the vector OQ lies entirely on its surface. As well, if the point, Q, moves at a constant rate both around and along the axis of the cone, then the point, Q, describes in the domain $z_1 \le z \le z_2$ a helix whose equation, in the case of a circular cone is given by:

$$f_z = (r_z.\cos\beta_z)\vec{i} + (r_z.\sin\beta_z)\vec{j} + z.\vec{k} \qquad \textbf{(B.1)}$$

The tangent T_z in the same domain is determined by differentiating f_z with respect to z. This tangent could be described as follows;

$$T_z = \left\{\left(-r_z \cdot \sin\beta_z \cdot \beta_z^{\bullet} + r_z^{\bullet} \cdot \cos\beta_z\right), \left(r_z \cdot \cos\beta_z \cdot \beta_z^{\bullet} + r_z^{\bullet} \cdot \sin\beta_z\right), 1\right\} \qquad \textbf{(B.2)}$$

For the point Q the relationships for the angle of rotation, β_z, and the radius, r_z, are be derived as follows;

$$r_z = r_1 + \frac{r_2 - r_1}{z_2 - z_1} * (z - z_1)$$

Differentiating r_z with respect to z gives;

$$r_z^{\bullet} = \frac{r_2 - r_1}{z_2 - z_1}$$

Furthermore,

$$\frac{\beta_z}{2 \cdot \pi} = \frac{z - z_1}{z_2 - z_1}$$

Solving for β_z and differentiating with respect to z gives;

$$\beta_z^{\bullet} = \frac{2 \cdot \pi}{z_2 - z_1}$$

B.1. Length of the Conic Helix

The length of the conic helix, L, in the domain $z_1 \le z \le z_2$, is given by;

$$L = \int |T_z| \, dz \qquad \textbf{(B.3)}$$

By substituting the values of r_z, $r_z^{\bullet}$, β_z *and* $\beta_z^{\bullet}$ in the Equation B.3 and integrating, the length of the spiral across a segment of the cone is found to be as follows;

$$L = \frac{1}{(z_2 - z_1)^2} \left[\frac{2 \cdot a \cdot z + b}{4 \cdot a} \sqrt{c + b \cdot z + a \cdot z^2} + \frac{4 \cdot a \cdot c - b^2}{8 \cdot a \cdot \sqrt{a}} \ln\left(2 \cdot \sqrt{a} \cdot \sqrt{c + b \cdot z + a \cdot z^2} + (2 \cdot a \cdot z + b) \right) \right] \quad z_1 \le z \le z_2 \qquad \textbf{(B.4)}$$

where $a = 4 \cdot \pi^2 \cdot (r_2 - r_1)^2$

$$b = 8 \cdot \pi^2 \cdot (r_1 \cdot z_2 - r_2 \cdot z_1)(r_2 - r_1)$$

$$c = 4 \cdot \pi^2 \cdot (r_1 \cdot z_2 - r_2 \cdot z_1)^2 + (z_2 - z_1)^2 (r_2 - r_1)^2 + (z_2 - z_1)^4$$

When $r_1 = r_2 = r$, i.e. a cylindrical mandrel, the terms a and b vanish. Furthermore, $z_2 - z_1 = P$. Substituting these values in Equation B.4 gives $L = \sqrt{4\pi^2 r^2 + P^2}$.

B.2. Fibre Orientation in a Conic Cell

The fabric axis in conic braiding is generally taken along the generatrix of the cone. When the fabric is formed on the mandrel along an axis normal to the plane of carriers motion, it is expected that the angle formed between the converging strands and the fabric axis represents the braid angle. The braid angle, θ, as shown in Figure B.2, is hence the angle between the tangent of the helix and the generatrix of the cone. From theories of analytical geometry and vectors, the angle between two vectors is given by:

$$\cos\theta = \frac{a_1 \cdot b_1 + a_2 \cdot b_2 + a_3 \cdot b_3}{|a| \cdot |b|}$$

where the a's and the b's

$$a = a_1 \cdot \vec{i} + a_2 \cdot \vec{j} + a_3 \cdot \vec{k}, \quad \textit{and}$$
$$b = b_1 \cdot \vec{i} + b_2 \cdot \vec{j} + b_3 \cdot \vec{k}$$

are the components of the two vectors.

Utilizing the helix equation and its tangent as given by Equations B.1 and B.2, the braid angle, θ, can be derived and is given by;

$$\cos\theta = \frac{1}{\cos\gamma \sqrt{\frac{4 \cdot \pi^2 \cdot r_1^2}{P^2} + \frac{4 \cdot \pi \cdot r_1}{P} \beta_z \cdot \tan\gamma + \beta_z^2 \cdot \tan^2\gamma + \tan^2\gamma + 1}} \qquad \textbf{(B.5)}$$

Equation B.5 shows that for a given mandrel speed (represented by the pitch, P), a cone

angle, γ, and frustum radius, r_l, the orientation of strand can be determined. For the particular case of cylindrical braiding when $\gamma \to 0$, Equation B.5 reduces to:

$\cos\theta = P/\sqrt{4 \cdot \pi^2 \cdot r^2 + P^2}$.

B.3. The Surface Area of the Unit Cell

The general formula to calculate the surface area generated by revolving a straight line around an axis is given by:

$$s = \oint 2.\pi . f_z \sqrt{1 + (T_z)^2}\, dz \qquad \textbf{(B.6)}$$

With reference to Figure B.3, the surface area of the conic segment is given by:

$$s = \pi . (r_2 + r_1) \sqrt{(z_2 - z_1)^2 + (r_2 - r_1)^2} \qquad \textbf{(B.7)}$$

Since each segment of the cone can only hold N_c 2 cells, then:

$$Area\ of\ each\ cell = \frac{2.\pi}{N_c} (r_2 - r_1) \sqrt{(z_2 - z_1)^2 + (r_2 - r_1)^2} \qquad \textbf{(B.8)}$$

B.4. Area in a Conic Cell Covered by Strands

There are six strands that contribute to the area covered in a cell. In Figure B.4, strands 1 and 2 are considered the main strands running diagonally through the cell. Strands 3, 4, 5 and 6, the auxiliary strands or corner strands, also contribute to the covered area. However, their contribution is reduced since they overlap with the main strands. Assuming constant width strands, the mathematical expression relating the covered area to the total area of the cell can be derived by considering the area of the main strands, minus the overlap at their intersection and the cutoff of the overhanging parts at the

corners.

The interlacing of two straight strands creates a diamond-shaped area of overlap. However, when the two strands involved are curved the area of overlap becomes warped as if the diamond shaped area is under bending, as shown in Figure B.5. The study of the geometry of such an area is simplified by simplifying its contour and subdividing the area into standard geometric elements.

As shown in Figure B.6, part of the diamond triangles, a and b, will open-up while triangles, c and d, will overlap. Therefore, to calculate the area covered by the strands in the cell, triangles, A. B, C, and D, will be used. The areas of these triangles respectively are given by;

$$A = \frac{w^2}{8} \cdot \cot(\theta + \eta)$$

$$B = \frac{w^2}{8} \cdot \tan(\theta)$$

$$C = \frac{w^2}{8} \cdot \tan(\theta)$$

$$D = \frac{w^2}{8} \cdot \cot(\theta + \eta)$$

Where η relates to the curvature at the centre. By using simple geometric relationships, η is given by $\sin^{-1}\left(\frac{w \cdot \sin\gamma}{4 \cdot r \cdot \cos\theta}\right)$

It should be noted that the value of the angle, θ, differs from point to point along the helix. Thus the notations, θ_1, θ_2 and θ_3, are adopted thereafter. Also, it should be noted that since the helix is continuous between two consecutive cells then θ_2 of cell_{i-1} should be equal to θ_1 of cell_i.

Thus, the area of strand overlap at the centre of the cell is equivalent to twice the area of triangles 'A + B + 2·E' and twice the area of the triangles 'C + D - 2·E'

$$\textit{overlap at the centre} = 2\frac{w^2}{8}\left[2\tan\theta_3 + \cot(\theta_3+\eta) + \cot(\theta_3-\eta)\right]$$

$$= \frac{w^2}{4}\cdot\left[2\cdot\tan\theta_3 + \frac{1-\tan\theta_3\cdot\tan\eta}{\tan\theta_3+\tan\eta} + \frac{1+\tan\theta_3\cdot\tan\eta}{\tan\theta_3-\tan\eta}\right]$$

$$= \frac{w^2}{4}\cdot\left[\frac{2\cdot\tan^3\theta_3 + 2\cdot\tan\theta_3}{\tan^2\theta_3-\tan^2\eta}\right]$$

Hence,

$$\textit{area of overlap} = \frac{w^2}{2}\cdot\left[\frac{\tan\theta_3\cdot\left(\tan^2\theta_3+1\right)}{\tan^2\theta_3-\tan^2\eta}\right] \qquad \textbf{(B.9)}$$

Similarly, the area of cutoff for the top corners of the cell, Figure B.7, is equivalent to twice the area of triangles, B + D. Hence,

$$\textit{area of cutoff at the top corners} = 2\cdot\left[\frac{w^2}{8}\cdot\tan\theta_2 + \frac{w^2}{8}\cdot\cot(\theta_2-\eta)\right] \qquad \textbf{(B.10)}$$

Also, the area of cutoff for the bottom corners of the cell is equal to twice the area of triangles, A + B. Hence,

$$\textit{the area of cutoff at the bottom corners} = 2\cdot\left[\frac{w^2}{8}\cdot\tan\theta_2 + \frac{w^2}{8}\cdot\cot(\theta_2-\eta)\right] \qquad \textbf{(B.11)}$$

Therefore, the total area of overlap and cutoffs is given by;

$$\textit{total area} = \frac{w^2}{2}\cdot\left[\frac{\tan\theta_3\left(\tan^2\theta_3+1\right)}{\tan^2\theta_3-\tan^2\eta}\right] + \frac{w^2}{4}\cdot\left[\tan\theta_1 + \cot(\theta_1+\eta_1)\right] + \frac{w^2}{4}\cdot\left[\tan\theta_2 + \cot(\theta_2-\eta_2)\right] \qquad \textbf{(B.12)}$$

When $\eta = 0$, the angles θ_3, θ_2, θ_1 are equal to θ (i.e., cylindrical braiding), the above expression reduces to $\frac{w^2}{\sin\theta \cdot \cos\theta}$. This formula has been reported in various publications.

B.5. Determination of the Cover Factor

The cover factor, K, is given by:

$$K = \frac{\text{Twice the length of the strand* strand width - Area of cutoff and overlap}}{\text{Area of Cell}}$$

Where:

Equation B. 4, represents the *length of the main strand* in the cell

Equation B.11, represents the total *area of overlap and of cutoffs*, and

Equation B.7, represents the *area of the cell.*

B.6. Simplification of the Unit Cell

As previously shown, a unit cell with a specific geometry was defined to faithfully represent the braided fabric. Mathematical expressions to calculate the necessary components of the cover factor were derived, namely, the length of the strand within the cell, areas of overlap and cutoffs and the total area of the cell.

In this section, the simplification of the unit cell configuration to one of a trapezoidal-shaped cell, Figure B.8, is examined. In doing so, the braid angle, as previously defined, would be defined at the centre of the trapezoidal cell. The radius, a_3, would represent

the location of the cell within the fabric grid, and the length of the main strands, when stretched, would be considered equal to the diagonal of the trapezoid.

a) Geometry of the Trapezoid

The distance between the adjacent corners of a trapezoid is equal to the length of the corresponding arcs. Hence, the distances between the bottom and top corners are given by $4 \cdot \pi \cdot r_1 / N_c$ and $4 \cdot \pi \cdot r_2 / N_c$ respectively.

The height of the trapezoid is given by;

$$a_2 - a_1 = (r_2 - r_1)/\sin\gamma = \sqrt{(z_2 - z_1)^2 + (r_2 - r_1)^2}$$

Therefore, the diagonal of the trapezoid can be represented by;

$$\sqrt{\left(\frac{2 \cdot \pi}{N_c}(r_2 + r_1)^2\right) + (z_2 - z_1)^2 + (r_2 + r_1)^2} \qquad \textbf{(B.13)}$$

and its area is given by;

$$\frac{2 \cdot \pi}{N_c}(r_2 + r_1) \cdot \sqrt{(z_2 - z_1)^2 + (r_2 + r_1)^2} \qquad \textbf{(B.14)}$$

b) Braid Angle, θ

The braid angle, θ, is the same as the angle between the centreline and the diagonals of the trapezoid:

$$\tan\theta = \frac{2 \cdot \pi}{N_c}(r_2 + r_1) \Big/ \sqrt{(z_2 - z_1)^2 + (r_2 + r_1)^2} \qquad \textbf{(B.15)}$$

c) Cutoff and Overlap

For the trapezoid the simplification of Equation B.12 gives;

$$\textit{the area of cutoff and overlap} = w^2 \cdot \left[\frac{\tan\theta \cdot \left(\tan^2\theta + 1\right)}{\tan^2\theta - \tan^2\eta} \right] \qquad \textbf{(B.16)}$$

$$\textit{where} \quad \eta = \sin^{-1}\left(\frac{w \cdot \sin\gamma}{4 \cdot r \cdot \cos\theta} \right)$$

d) The Cover Factor

The cover factor was defined earlier and is given by;

$$\frac{\textit{Twice the length of the strand* strand width - Area of cutoff and overlap}}{\textit{Area of Cell}}$$

for the case of the trapezoid, the elements of the above expression are given by;

Equation B.13, represents the *length of the main strand* in the cell,
Equation B.16, represents the *areas of overlap and cutoffs*, and
Equation B.14, represents the *area of the cell.*

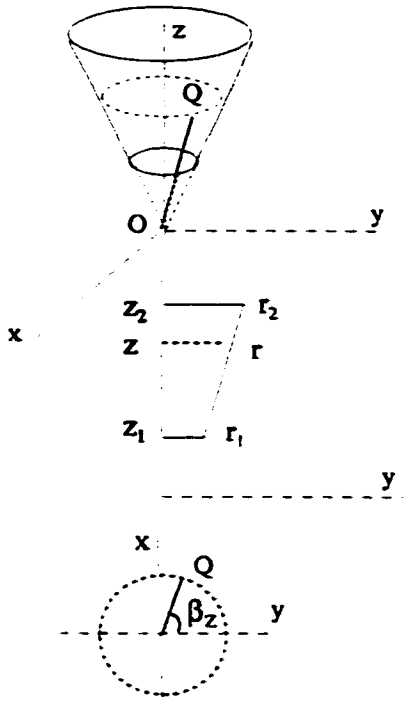

Figure B.1 Vectorial representation of a conic helix

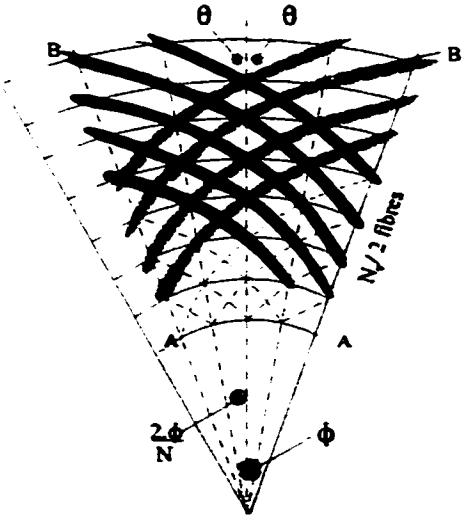

Figure B.2 Braid angle, θ, shown on the plane developed by cutting the conic fabric section along the generatrix

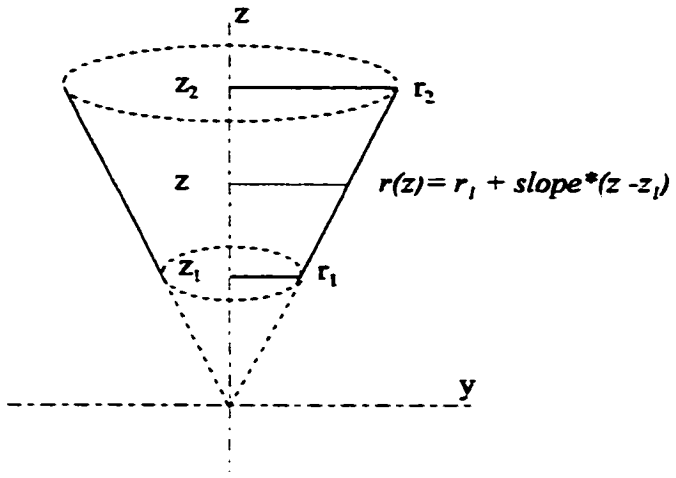

Figure B.3 Lateral surface area of cone segment

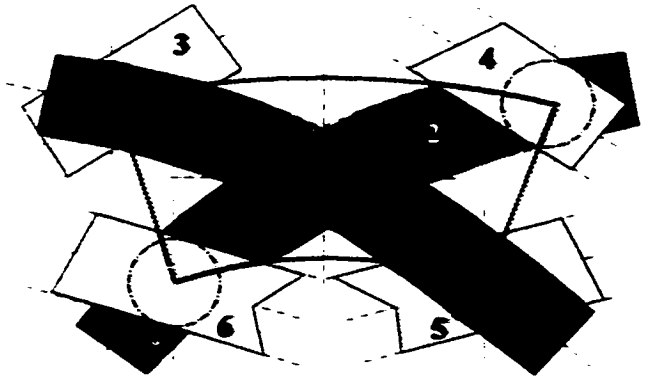

Figure B.4 The unit cell

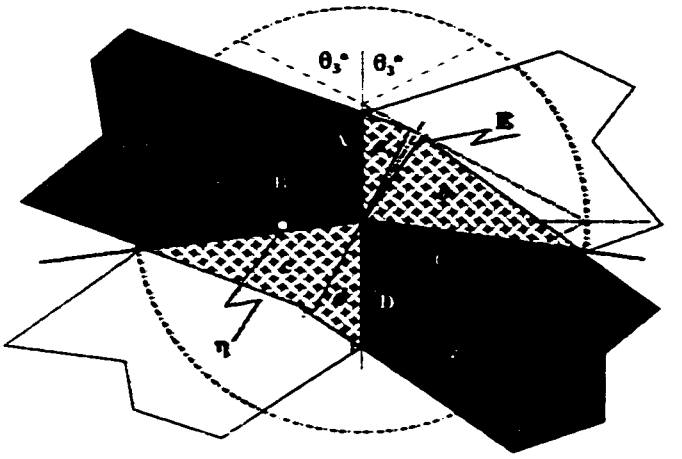

Figure B.5 Strand overlap at the centre of the cell

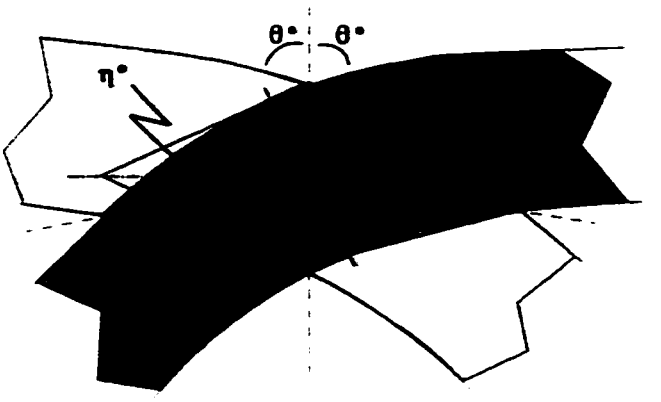

Figure B.6 Overlap between two curved strands

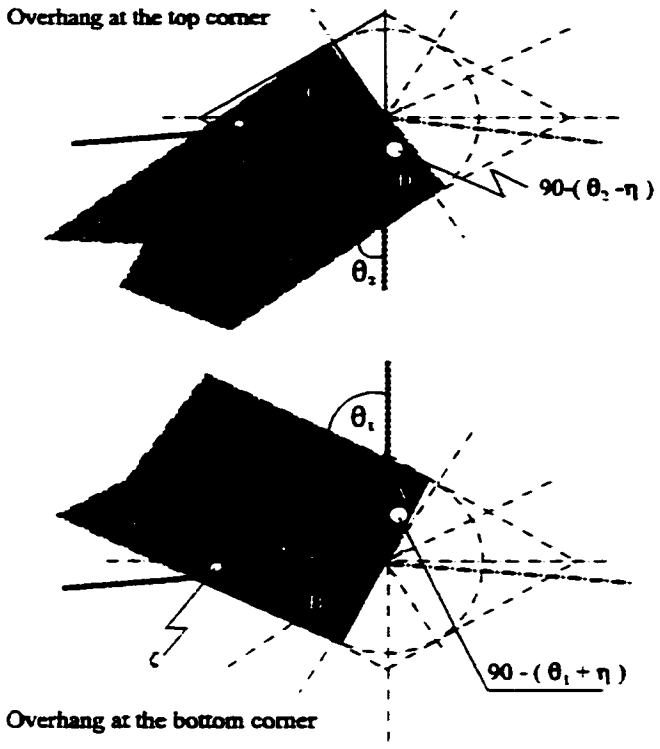

Figure B.7 Overhang at top and bottom corners

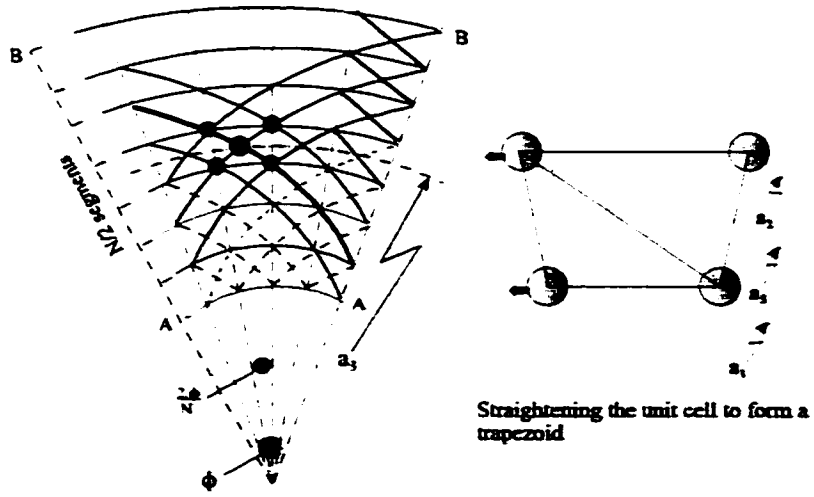

Figure B.8 Unit cell – Simplified

APPENDIX C – Mechanical and Technical Specifications of the Braiding Machine

Motor drive: (braiding head and mandrel drive)

Model SK 02F-80L14

2 three-phase synchronous AC motor

Power = 1 HP

Volt = 220 volts

Speed reduction (motor : bobbin) = 122:1

Mechanical system (loaded):

$J = 5.85$ kg/m^2

b = 5.79 N-m/rad/sec

Break torque = 1.976 N-m

Tachometer

direct current

V_{max} = 1.57 volts @ 1800 rpm

Encoder

US Digital Optical Shaft Encoder (S1)

Filter (Low Pass)

Amplifier model: LM741

R1 = 2200 ohms

R2 = variable set at 1050 ohms

C = 100 μF

Position filter

Amplifier model: LM741

R_{diode} = 475 ohms

R1 = 2680 ohms

R2 = 1000 ohms

APPENDIX D – Wiring Arrangements for the Braiding Setup

D.1 Wiring Arrangement for the Up-down Counter

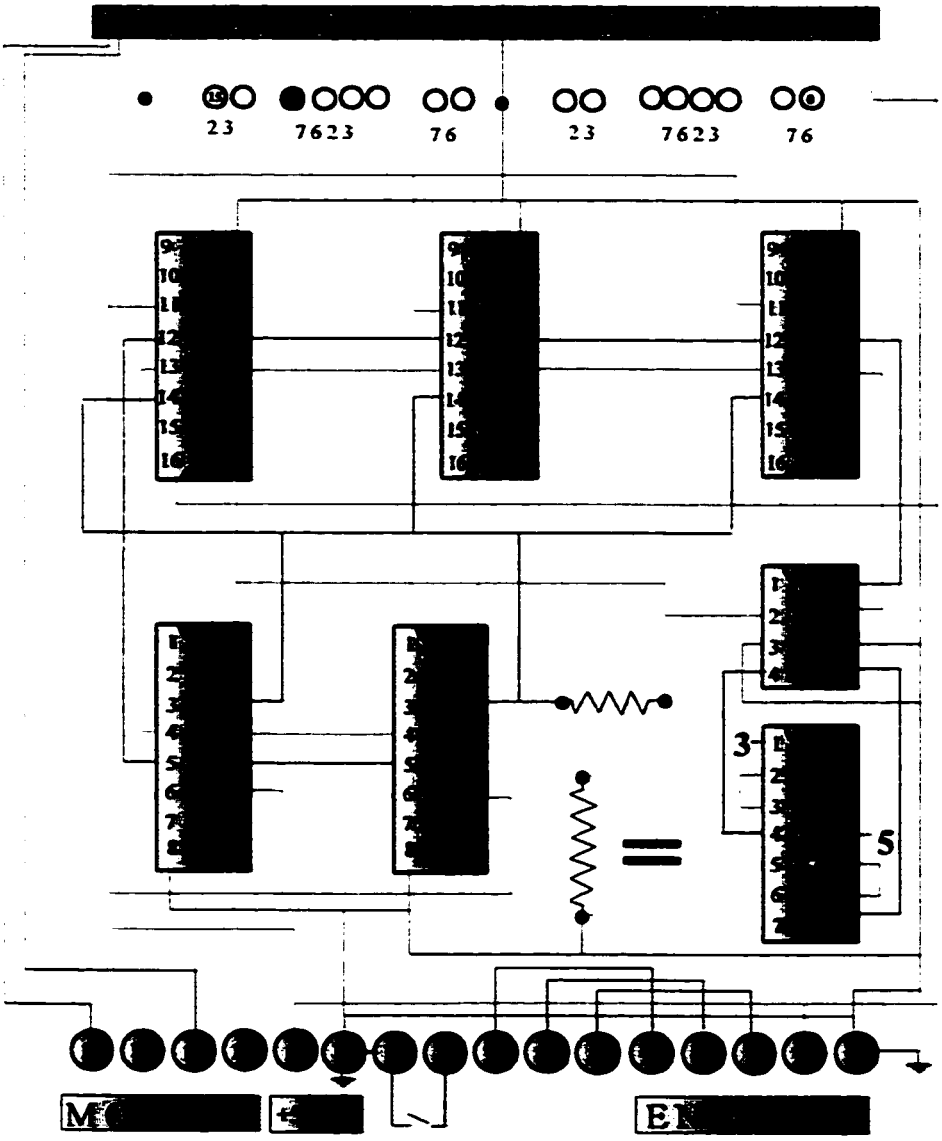

Figure D.1 Wiring arrangement of the up-down counter.

D.2 Wiring arrangement for the frequency to volt converter

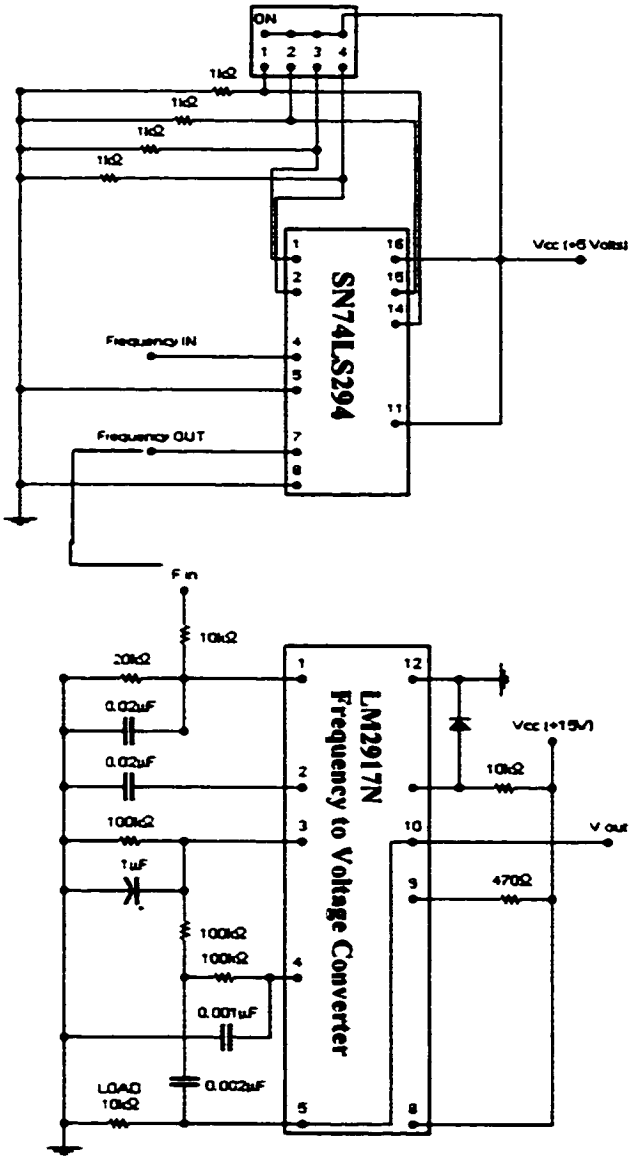

Figure D.2 Frequency to Volt converter.

APPENDIX E – The Relationship Between the Coordinates of the Rotating Arm of the Measuring Device and the Length of the Convergence Zone

APPENDIX E – The Relationship Between the Coordinates of the Rotating Arm of the Measuring Device and the Length of the Convergence Zone

Figure E.1 is a pictorial side view of the convergence zone. As shown in Figure 4.5, the convergence zone lies between the deposit plane, where all strands of fibre lie on the mandrel, and the guide plane. The plane C is parallel to the guide plane. This plane passes through the point where the rotating arm lies on the strands while passing through the zone. The mandrel is assumed to be axially symmetric. The line tangent to the mandrel, if rotated, would generate a conic surface. This surface is extended through the zone.

E.1. The Geometric Method

In order to derive the relationship between the coordinates of the rotating arm of the measuring device and the length of the convergence Zone, the following symbols are used;

r_c – radius of the base of the conic surface, tangent to the mandrel, at the plane C.

p , q – coordinates of the centre of rotation of the swinging arm with respect to the guide plane.

g , h – location of the point 'C' with respect to the guide plane.

L – length of the rotating arm.

x_c , R_C – coordinates of the point 'C' with respect to the deposit plan.

α_o – initial position of the rotation of the arm (value at zero).

α – deviation of the rotating arm from initial position.

With reference to Figure 4.5, the coordinates of the point, C , with respect to the deposit plane can be determined as follows:

$$x_c = D - g \tag{E.1}$$

where $g = L.\cos(\alpha+\alpha_0)+p$

Similarly,

$$R_c = R_G - h \tag{E.2}$$

where $h = L.\sin(\alpha+\alpha_0)-q$

Since $y_c = \sqrt{R_c^2 - r_c^2}$, $r_2 = (r_1 + D.\tan\gamma)$ *and* $r_c = (r_1 + x_c \cdot \tan\gamma)$

Also,

$$\begin{aligned}\tan\theta &= \frac{y_c}{x_c / \cos\gamma} \\ &= \frac{\sqrt{R_G^2 - r_2^2}}{D / \cos\gamma}\end{aligned} \tag{E.3}$$

Then, substituting the values of x_c, R_c *and* r_c in the Equation E.3 gives;

$$\tan\theta = \frac{\cos\gamma \cdot \sqrt{(R_G - h)^2 - (r_1 + (D-g)\cdot\tan\gamma)^2}}{D-g} \tag{E.4}$$

Similarly, by substituting the values of the coordinates of the point *C*, the relationship between the measured angle, α, and the braid angle, θ, could be obtained as follows;

$$\theta = \tan^{-1}\left(\frac{\cos\gamma \cdot \sqrt{\left(R_G - (L\cdot\sin(\alpha+\alpha_o)-q)\right)^2 - \left(r_1 \cdot \left(D - (L\cdot\cos(\alpha+\alpha_o)+p)\right)\tan\gamma\right)^2}}{D - \left(L\cdot\cos(\alpha+\alpha_o)+p\right)}\right) \tag{E.5}$$

As shown in Equation E.5, for a given value of the measured angle, α, the braid angle, θ, is dependent on the radius of the mandrel at the deposit plane and the length of the convergence zone, and consequently, could be evaluated by iteration.

E.2 Vector Analysis Method

The coordinates of the point C with respect to the deposit plane can also be derived using vector analysis. In this method, the intersection of a strand of fibre represented by the vector AB and the path of the rotating arm of the measuring device will be considered. Reference to Figure E2, the coordinates of the points A, B, and C could be described as follows;

$$A = \{0,\ r_1 \cdot \sin\varphi,\ r_1 \cdot \cos\varphi\} \tag{E.6}$$

$$B = \left\{D, \left(\cos\varphi\sqrt{R_G^2 - r_2^2} + r_2 \sin\varphi\right), \left(r_2 \cos\varphi - \sin\varphi \sqrt{R_G^2 - r_2^2}\right)\right\} \tag{E.7}$$

$$C = \{x_c, R_c, 0\} \tag{E.8}$$

Then, the vector $A\bar{B}$ representing the strand is given by:

$$A\bar{B} = \left\{D, (r_2 - r_1)\sin\varphi + \cos\varphi \cdot \sqrt{R_G^2 - r_2^2}, (r_2 - r_1)\cos\varphi - \sin\varphi \cdot \sqrt{R_G^2 - r_2^2}\right\} \tag{E.9}$$

Consequently, the direction numbers are:

$a = D$

$b = \left\{(r_2 - r_1)\sin\varphi + \cos\varphi \sqrt{R_G^2 - r_2^2}\right\}$

$c = \left\{(r_2 - r_1)\cos\varphi - \sin\varphi \sqrt{R_G^2 - r_2^2}\right\}$

And, the symmetric equation passing through the point A is given by:

$$\frac{x-0}{D} = \frac{y - r_1 \cdot \sin\varphi}{(r_2 - r_1)\sin\varphi + \cos\varphi \sqrt{R_G^2 - r_2^2}} = \frac{z - r_1 \cdot \cos\varphi}{(r_2 - r_1)\cos\varphi - \sin\varphi \sqrt{R_G^2 - r_2^2}} \tag{E.10}$$

When $z = 0$, i.e. at point where the strand of fibre intersect the x-y plane, the coordinates of point C are given by :

$$\frac{x_c}{D} = \frac{-r_1 \cdot \cos\varphi}{(r_2 - r_1).\cos\varphi - \sin\varphi.\sqrt{R_G^2 - r_2^2}} \tag{E.11}$$

and,

$$\frac{R_c - r_1 \cdot \sin\varphi}{(r_2 - r_1).\sin\varphi + \cos\varphi.\sqrt{R_G^2 - r_2^2}} = \frac{-r_1 \cdot \cos\varphi}{(r_2 - r_1).\cos\varphi - \sin\varphi.\sqrt{R_G^2 - r_2^2}} \tag{E.12}$$

Equation (E.12) could be rearranged to read:

$$(r_2 - r_1).\cos\varphi - \sin\varphi.\sqrt{R_G^2 - r_2^2} = \frac{-r_1 \cdot \sqrt{R_G^2 - r_2^2}}{R_c} \tag{E.13}$$

Substituting in Equation (E.11);

$$\frac{x_c}{D} = \frac{R_c \cdot \cos\varphi}{\sqrt{R_G^2 - r_2^2}} \tag{E.14}$$

But since $\cos\varphi = \dfrac{\sqrt{(R_G - h)^2 - r_c^2}}{R_G - h}$ *and* $\tan\theta = \dfrac{\sqrt{R_G^2 - r_2^2}}{D/\cos\gamma}$ and by substituting for the values of x_c and r_c, then Equation (E.14) becomes;

$$\tan\theta = \frac{\cos\gamma \cdot \sqrt{(R_G - h)^2 - \left(r_1 + (D - g) \cdot \tan\gamma\right)^2}}{D - g} \tag{E.15}$$

As can be seen, Equation (E.15) is similar to Equation (E.4).

E.3 The Relationship Between the Length of the Conversion Zone and the Measured Angle

In some cases, it is would be desired to evaluate the length of the conversion zone as a function of the rotation of the swinging arm. To this end, Equation E.14 could be rewritten as follows;

$$\frac{(D-g)^2}{D^2}=\frac{(R_G-h)^2-\left\{r_1+(D-g).\tan\gamma\right\}^2}{R_G^2-(r_1+D.\tan\gamma)^2} \tag{E.16}$$

Further simplification leads to:

$$\left(-2.R_G.h+h^2-2.r_1.g.\tan\gamma\right).D^2+\left\{2.g.\left(R_G^2-r_1^2\right)+2.r_1.g^2.\tan\gamma\right\}.D-g^2.\left(R_G^2-r_1^2\right)=0 \tag{E.17}$$

$$D^2.(R_G-h)^2-D^2\left\{r_1+(D-g).\tan\gamma\right\}^2-(D-g)^2R_G^2+(D-g)^2(r_1+D.\tan\gamma)^2=0 \tag{E.18}$$

$$D^2(R_G-h)^2-D^2r_1^2-(D-g)^2R_G^2+(D-g)^2r_1^2-2.r_1.D.g.(D-g)\tan\gamma=0 \tag{E.19}$$

Solving for D;

$$D=\frac{g\left(R_G^2-r_1^2+r_1.g.\tan\gamma\right)+g\sqrt{R_G^4+r_1^4+r_1^2.g^2.\tan^2\gamma-2.R_G^2.r_1^2-h\left(R_G^2-r_1^2\right)(2.R_G-h)}}{h(2.R_G-h)+2.r_1.g.\tan\gamma} \tag{E.20}$$

For cylindrical braiding, Equation (E.20) can be reduced to;

$$D=\frac{g\left(R_G^2-r_1^2\right)+g\sqrt{\left(R_G^2-r_1^2\right)^2-h\left(R_G^2-r_1^2\right)(2.R_G-h)}}{h(2.R_G-h)} \tag{E.21}$$

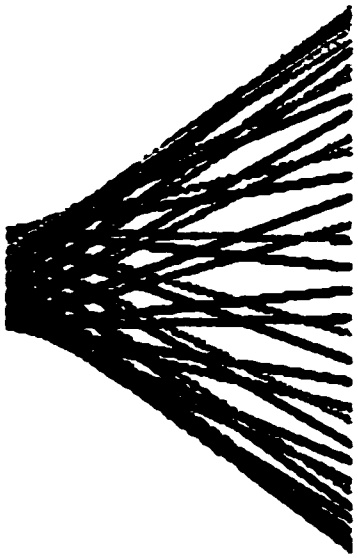

Figure E.1 Pictorial side view of the convergence zone

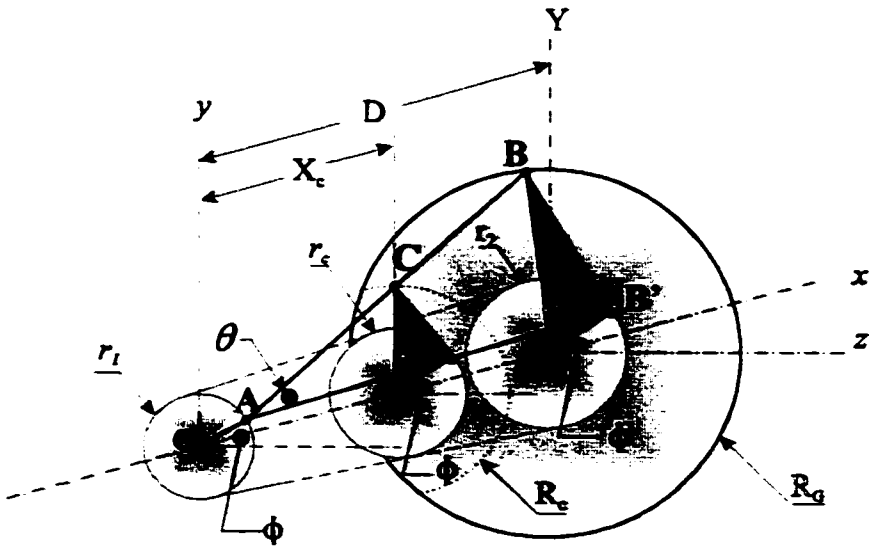

Figure E.2 Pictorial view of the vector *AB*, representing a strand in the convergence zone

APPENDIX F Sample of Computer Programs Outputs and Logic

F.1 Sample of an Output of a Program to Calculate the Braid Angle and to Determine the Corresponding set of Machine Speeds

Input data

STRAND WIDTH	: 3.14 mm	MANDREL RADIUS	: 1.270 cm
COVERAGE	: 100. %	RING RADIUS	: 10.305 cm
NUMBER OF SPOOLS	: 36.		
MAX. MANDREL SPEED	: 1.905 cm/sec.		
MAX. BRAID HEAD SPEED	: 1.570 rad/sec.		

Output data

RATIO = 1.993
THETA = 44.903 TANTHETA = .9966
GAMMA = 45.1223 TANGAMMA = 1.0043

Length of the convergence zone 'D' =10.261 cm
Contact point from the outside Rim = 9.218 cm

Braider head velocity		**Mandrel Velocity**	
rad/sec	**%**	**cm/sec**	**%**
0.149	9.52 %	0.190	10.00 %
0.299	19.04 %	0.381	20.00 %
0.448	28.57 %	0.571	30.00 %
0.598	38.09 %	0.762	40.00 %
0.747	47.61 %	0.952	50.00 %
0.897	57.13 %	1.143	60.00 %
1.046	66.65 %	1.333	70.00 %
1.196	76.17 %	1.524	80.00 %
1.345	85.70 %	1.715	90.00 %
1.495	95.22 %	1.905	100.00 %

Note: percentages are those of full speed

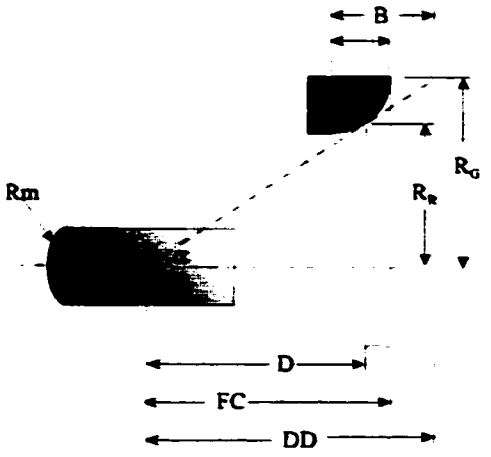

F.2 Sample of an Interactive Session for Off-line Calculation of Processing Data (File = braid8c.c)

PLEASE ENTER THE NAME AND PATH OF THE WORK PIECE DATA FILE:- **WP-DIMEN**

YOUR INPUT INFORMATION READS AS FOLLOWS:

Slice#	radius	Slice#	radius	Slice#	radius	Slice#	radius
1	0.500	7	0.916	13	1.354	19	1.062
2	0.500	8	0.989	14	1.427	20	0.916
3	0.624	9	1.062	15	1.500	21	0.770
4	0.697	10	1.135	16	1.500	22	0.624
5	0.770	11	1.208	17	1.354	23	0.500
6	0.843	12	1.281	18	1.208	24	0.500

THANK YOU... Please press any key to continue

FABRIC COVER FACTOR (i.e. ratio of 'covered' to total area) IS A FUNCTION OF BRAID ANGLE, Fibre WIDTH AND RADIUS OF MANDREL.

FOR A GIVEN MANDREL SIZE, ONLY TWO PARAMETERS COULD BE SELECTED AT ONE TIME. THE THIRD PARAMETER HAS TO BE CALCULATED. YOU HAVE THREE POSSIBLE CHOICES:

1. BRAID ANGLE & Fibre WIDTH
2. BRAID ANGLE & COVERAGE FACTOR
3. Fibre WIDTH & COVERAGE FACTOR

***PLEASE ENTER YOUR CHOICE OF TWO PARAMETERS ONLY ***
(note that the initial value of the third parameter is ZERO)

STRAND WIDTH (in mm.) **3.14**
COVERAGE FACTOR (as a fraction -- 1.0 for full coverage) **1**
BRAID ANGLE (in degrees) **0**

ALSO, PLEASE ENTER:

RING DISTANCE FROM BRAIDER HEAD:- **3.22**
ANGULAR VELOCITY OF BRAIDER HEAD (as a percent of its max.) **30**

THE BASIC PROCESSING PARAMETERS ARE GIVEN AS FOLLOWS:-

strand width	: 3.14 mm	Mandrel radius	: 0.500 in.
Coverage	: 1.00	Ring radius	: 4.057 in.
Theta	: to be calculated	Braider Head radius	: 18.656 in.
Increment	: 0.250	Braider Head distance	: 3.220 in.
Delta_R	: to be calculated	B. Head angular speed	: 0.471 in/s

... Please press any key to continue

Step #	Inc.	Theta	Cone Angle	Radius	Speed ratio	V_t %	ω %	contact Point
1	0.500	44.903	40.540	0.500	1.993	0.236	0.471	3.618
2	0.500	50.938	48.933	0.500	2.392	0.197	0.471	2.773
3	0.500	57.576	53.549	0.624	2.496	0.189	0.471	2.290
4	0.500	61.130	56.790	0.697	2.575	0.183	0.471	2.002
5	0.500	63.952	59.365	0.770	2.629	0.179	0.471	1.783
6	0.500	66.255	61.454	0.843	2.668	0.177	0.471	1.608
7	0.500	68.173	63.192	0.916	2.697	0.175	0.471	1.466
8	0.500	69.797	64.645	0.989	2.719	0.173	0.471	1.345
9	0.500	71.192	65.885	1.062	2.736	0.172	0.471	1.244
10	0.500	72.404	66.955	1.135	2.749	0.171	0.471	1.156
11	0.500	73.467	67.875	1.208	2.759	0.171	0.471	1.079
12	0.500	74.407	68.670	1.281	2.768	0.170	0.471	1.009
13	0.500	75.245	69.365	1.354	2.775	0.170	0.471	0.948
14	0.500	75.996	69.976	1.427	2.780	0.169	0.471	0.892
15	0.500	76.343	69.542	1.500	2.744	0.172	0.471	0.888
16	0.500	75.630	68.716	1.500	2.498	0.189	0.471	0.923
17	0.500	73.951	67.302	1.354	2.464	0.191	0.471	1.048
18	0.500	71.819	65.416	1.208	2.420	0.195	0.471	1.206
19	0.500	69.017	62.866	1.062	2.357	0.200	0.471	1.413
20	0.500	65.159	59.294	0.916	2.264	0.208	0.471	1.705
21	0.500	59.462	53.998	0.770	2.113	0.223	0.471	2.153
22	0.500	50.938	45.961	0.624	1.917	0.246	0.471	2.932
23	0.500	44.903	40.547	0.500	1.993	0.236	0.471	3.623

*** DO YOU WANT TO CONSIDER NEW INPUT VALUES (Y or N) ***

NOTE: The above table, saved in 'file WPDATAxx.IN', contains the input parameters required to control the Braiding process.

Other messages with respect to the check and balance steps imbedded in the program would appear as appropriate.

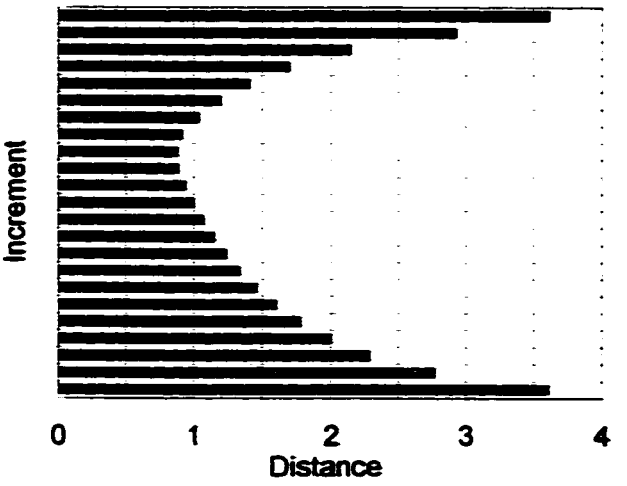

Distance along the mandrel from the strand's contact point to the guide plane at 12.7cms increments.

F.3 – Programming Logic to take into Account the Curvature of the Guide Ring

The steps and formulae introduced in the computer programs to take into consideration the large curvature of the guide ring are:

1. from the user's input information (i.e. braid angle, cover factor, strand width) and the mandrel profile, a set of speed ratios are generated.

2. at every increment of the mandrel and assuming an initial value (between the inner and the outer diameter of the guide ring) for the diameter of the ring, R_R, passing through the point of tangency, calculate the length of the convergence zone, D.

3. compute the value of the angle, α, using the relation:

$$\tan\alpha = \frac{R_R \cdot \tan\theta}{\cos\gamma \sqrt{R_R^2 - (r_1 + D \cdot \tan\gamma)^2}}$$

4. compute a new value of, R_R, using the relation: $R_R = R_G - \cos\alpha$

5. perform necessary iterations to obtain an acceptable value for R_R.

6. compute the offset distance between the point of tangency and the edge of the guide ring as well as the fibre contact point on the work piece.

7. record the pertinent results in a file for input, as a look-up table, during the braiding operation.

F.4 Sample of an Interactive Braiding Session
(File = BRD21.C)

Please enter the NAME and PATH of the conversion data file: **SENSOR2.IN**

YOUR CONVERSION DATA READS AS FOLLOWS:

DEG_AT_ZERO	xxxx	PULSE_TO_RAD	xxxx
TVSPD_AT_ZERO	xxxx	PULSE_TO_INCH	xxxx
BHSPD_AT_ZERO	xxxx	VOLTS_TO_INCH	xxxx
RAWCOUNT_TO_VOLTS	xxxx	VOLTS_TO_RAD	xxxx
RAWCOUNT_TO_DEGREE	xxxx	VOLTS_TO_DEG	xxxx
RAWCOUNT_TO_TVSPD	xxxx	VOLTS_TO_0	xxxx
RAWCOUNT_TO_BHSPD	xxxx		

Please press any key to continue

Please enter the NAME and PATH of the Workpiece data File **WPDATAxx.IN**

PLEASE MAKE SURE THAT THE DISTANCE OF THE FIBRE CONTACT POINT
FROM THE OUTER SIDE OF THE RING = xx inches

Use the manual mode for calibration and press any key to continue
The cone angle should read .....xx.xxx degrees

NOW, FIX THE WORKPIECE ONTO THE MANDRELAND <enter> ITS DISTANCE
FROM THE FIBRE CONTACT POINT. (At least 5 inches away) **xxxxxxxxxx**

PLEASE ENTER THE DESIRED 'TAIL END' STRAIGHT BRAIDING

THANK YOU ..... Please press any key to continue

Press 'R' to start the process or <SPACE> to quit

Press 'P' to activate the 'PAUSE' feature

Angle Raw counts	=40496	Cone Angle	= 53.838
Mandrel Raw Counts	= 32928	Mandrel Vel.	= 0.188 m/sec
B. Head Raw Counts	= 32896	B. Head Vel.	= 0.628 rad/sec
Mandrel travel R count	= 11317	Overall Dist	= 19.231 in
B. Head revs in RC	= 9778	Revolutions	= 10 revs & 6.639 deg

Braid Parameters ..... Braid Angle = 59.771 degrees
Contact point = 1.756 in

**** 2186 11354 274 1 *****

As well, this session produces an output file "**BRD21_xx.OUT**" to store the pertinent information of the session.

F.5 Verification of the Expression Developed to Derive the Variable Pitch Length of the Braided Strands During the Transient State Using the Vector Analysis Approach

A vector approach was used to calculate the pitch lengths of the braided strands during the transient state. The intention was to verify that the angle between the tangent to the helix, represented by the spiralling fibre strand, and the vector $\bar{V}_3$ is always equal to zero (reference to Figure 6.3) when modelling the braiding process during its transient state. The following is an excerpt of the output of a computer program written for that purpose (data from experiment #7 were used as input to the program).

Summary of computation:

Rev.	a_n	α° of T1	α° of V3	α° of (T1-V3)	
1	3.675	65.262	65.262	0	
2	4.282	61.786	61.786	0	
3	4.577	60.161	60.161	0	R_m = 1.270
4	4.722	59.383	59.383	0	R_G = 7.765
5	4.793	59.007	59.007	0	c = 0.510
6	4.829	58.824	58.824	0	X = 2.344
7	4.845	58.734	58.734	0	Pitch = 4.862
8	4.854	58.69	58.69	0	
9	4.856	58.669	58.669	0	
10	4.859	58.658	58.658	0	
11	4.862	58.653	58.653	0	
12	4.862	58.651	58.651	0	
13	4.862	58.65	58.65	0	
14	4.862	58.649	58.649	0	
15	4.862	58.649	58.649	0	
16	4.862	58.648	58.649	0	
17	4.862	58.648	58.649	0	
18	4.862	58.648	58.648	0	
19	4.862	58.648	58.648	0	
20	4.862	58.648	58.648	0	
21	4.862	58.648	58.648	0	
22	4.862	58.648	58.648	0	

Note:- α, β and γ, are the direction angles of a vector.

a_n is the distance travelled along the axis of the mandrel, i.e. pitch.

Detailed computation:

a) Vector, $\vec{V}_1$, representing a helix spiralling up the mandrel's surface and its tangent.

Rev.	α° of V1	β° of V1	γ° of V1	a_n	α° of T1	β° of T1	γ° of T1
1	19.056	90	70.944	**3.675**	65.262	24.738	90
2	9.068	90	80.933	**1.686**	61.786	28.214	90
3	5.785	90	84.215	**4.577**	60.161	29.840	90
4	4.209	90	85.791	**4.722**	59.383	30.617	90
5	3.296	90	86.704	**4.793**	59.007	30.993	90
6	2.705	90	87.295	**4.829**	58.824	31.176	90
7	2.293	90	87.708	**4.845**	58.734	31.266	90
8	1.989	90	88.012	**4.854**	58.690	31.310	90
9	1.756	90	88.244	**4.856**	58.669	31.331	90
10	1.571	90	88.429	**4.859**	58.658	31.342	90
11	1.422	90	88.578	**4.862**	58.653	31.347	90
12	1.299	90	88.701	**4.862**	58.651	31.349	90

b) Vector, $\vec{V}_2$, and the tangent to the helix at the guide ring.

Rev.	α° of V2	β° of V2	γ° of V2	Pitch	α° of T2	β° of T2	γ° of T2
1	47.138	43.687	83.114	**7.206**	84.309	80.633	169.013
2	32.759	57.736	84.923	**12.068**	84.309	80.633	169.013
3	24.639	65.714	86.090	**16.929**	84.309	80.633	169.013
4	19.613	70.662	86.853	**21.791**	84.309	80.633	169.013
5	16.243	73.982	87.378	**26.652**	84.309	80.633	169.013
6	13.842	76.349	87.758	**31.514**	84.309	80.633	169.013
7	12.050	78.115	88.043	**36.375**	84.309	80.633	169.013
8	10.664	79.482	88.266	**41.237**	84.309	80.633	169.013
9	9.561	80.569	88.443	**46.098**	84.309	80.633	169.013
10	8.664	81.454	88.588	**50.960**	84.309	80.633	169.013
11	7.919	82.188	88.709	**55.822**	84.309	80.633	169.013
12	7.292	82.807	88.811	**60.683**	84.309	80.633	169.013

Detailed computation (cont.):

c) Vector, $\vec{V}_3$, representing the fibre strand.

Rev.	α° of V3	β° of V3	γ° of V3
1	65.262	24.738	90
2	61.786	28.214	90
3	60.161	29.840	90
4	59.383	30.617	90
5	59.007	30.993	90
6	58.824	31.176	90
7	58.734	31.266	90
8	58.690	31.310	90
9	58.669	31.331	90
10	58.658	31.342	90
11	58.653	31.347	90
12	58.651	31.349	90

APPENDIX G -- The General Algorithm Relating the Length of the Conversion Zone to Mandrel and Machine Parameters

In this appendix, a Vector Analysis approach will be used in developing a general algorithm for the length of the convergence zone i.e. the point of formation of the braid, to the geometry of the mandrel. Figure G.1, shows a pictorial view of the convergence zone extending between the deposit plane and the guide plane. The point A represents the point of tangency of the strand to the mandrel at the deposit plane. It also represents the tip of the vector $\vec{V}_1$ which when rotated forms the helical curve that describes the path of the strand along the mandrel. The inclination of the vector $\vec{V}_1$ to the horizontal is given by the angle ϕ. The path of the strand AB in the convergence zone is represented by $\vec{V}_3$, while $\vec{V}_2$ represents the line tangent to the mandrel at point A.

The coordinates of the points A, B, and C were developed in Appendix E (Equations E11, E12, and E13) and are reintroduced here for reference:

$$A \rightarrow (0,\ r_1.\sin\varphi,\ r_1.\cos\varphi)$$

$$B \rightarrow (D,\ r_2.\sin\varphi,\ r_2.\cos\varphi)$$

$$C \rightarrow \left\{D,\ \left(\cos\varphi\sqrt{R_G^2-r_2^2}+r_2.\sin\varphi\right),\ \left(r_2.\cos\varphi-\sin\varphi.\sqrt{R_G^2-r_2^2}\right)\right\}$$

The equations for the vectors $\vec{V}_2$ and $\vec{V}_3$ and their magnitudes can then be derived as follows:

$$\vec{V}_2=\left\{D,\left(r_2-r_1\right)\sin\varphi,\left(r_2-r_1\right)\cos\varphi\right\} \qquad \textbf{(G.1)}$$

$$\left|\vec{V}_2\right| = \sqrt{D^2 + (r_2 - r_1)^2} \tag{G.2}$$

$$\vec{V}_3 = \left[D, \left\{(r_2 - r_1).\sin\varphi + \cos\varphi.\sqrt{R_G^2 - r_2^2}\right\}, \left\{(r_2 - r_1).\cos\varphi - \sin\varphi.\sqrt{R_G^2 - r_2^2}\right\}\right] \tag{G.3}$$

$$\left|\vec{V}_3\right| = \sqrt{D^2 + \left(R_G^2 - r_2^2\right) + (r_2 - r_1)^2} \tag{G.4}$$

Thus, the fabric braid angle, θ, i.e. the angle between the two vectors $\vec{V}_2$ *and* $\vec{V}_3$ can be calculated as follows;

$$\cos\theta = \frac{\vec{V}_2.\vec{V}_3}{\left|\vec{V}_2\right|.\left|\vec{V}_3\right|} \tag{G.5}$$

$$\begin{aligned}\cos\theta = {} & \frac{D^2 + \left[(r_2 - r_1)\sin\varphi\left\{(r_2 - r_1)\sin\varphi + \cos\varphi\sqrt{R_G^2 - r_2^2}\right\}\right]}{\left(\sqrt{D^2 + (r_2 - r_1)^2}\right)\left(\sqrt{D^2 + \left(R_G^2 - r_2^2\right) + (r_2 - r_1)^2}\right)} \\ & + \frac{\left[(r_2 - r_1)\cos\varphi\left\{(r_2 - r_1)\cos\varphi - \sin\varphi\sqrt{R_G^2 - r_2^2}\right\}\right]}{\left(\sqrt{D^2 + (r_2 - r_1)^2}\right)\left(\sqrt{D^2 + \left(R_G^2 - r_2^2\right) + (r_2 - r_1)^2}\right)}\end{aligned} \tag{G.6}$$

Since $r_2 = r_1 + D \cdot \tan\gamma$, further simplification would lead to:

$$\cos\theta = \frac{D^2 + D^2\tan^2\gamma}{\left(\sqrt{D^2 + D^2\tan^2\gamma}\right)\left(\sqrt{D^2 + R_G^2 - r_1^2 - 2.r_1.D.\tan\gamma}\right)} \tag{G.7}$$

$$\cos\theta = \frac{\left(\sqrt{D^2 + D^2 \tan^2 \gamma}\right)}{\left(\sqrt{D^2 + R_G^2 - r_1^2 - 2.r_1.D.\tan\gamma}\right)} \qquad \textbf{(G.8)}$$

It should be noted that, as expected, the value of the angle, θ, is independent of the angle, ϕ.

For given values of θ and γ, the expression for the distance between the guide plane and the deposit plane could be written in the form $D = f(\theta, \gamma)$. Thus Equation (G.8), could be re-arranged as follows;

$$\cos^2\theta = \frac{D^2}{\cos^2\gamma \cdot \left(D^2 + R_G^2 - r_1^2 - 2.r_1.D.\tan\gamma\right)} \qquad \textbf{(G.9)}$$

Solving for D;

$$D^2 - \cos^2\theta \cdot \cos^2\gamma \cdot \left(D^2 + R_G^2 - r_1^2 - 2.r_1.D.\tan\gamma\right) = 0 \qquad \textbf{(G.10)}$$

further simplification leads to:

$$D = \frac{-r_1.\sin\gamma.\cos\gamma + \cos\gamma\sqrt{\left(R_G^2 - r_1^2\right).\tan^2\theta + R_G^2.\sin^2\gamma}}{\tan^2\theta + \sin^2\gamma} \qquad \textbf{(G.11)}$$

For cylindrical braiding, i.e. when $\gamma = 0$, Equation (G.11) reduces to:

$$D = \frac{\sqrt{\left(R_G^2 - r_1^2\right)}}{\tan\theta} \qquad \textbf{(G.12)}$$

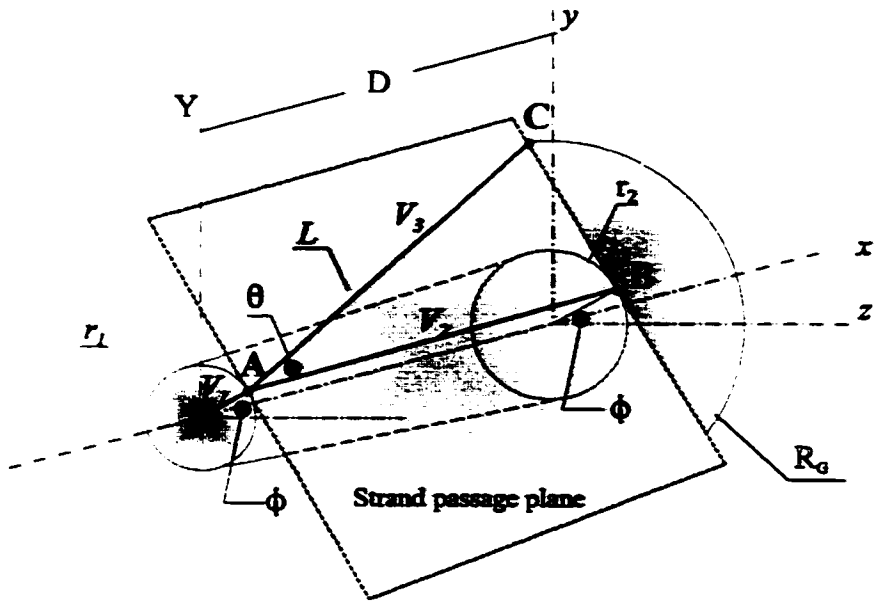

Figure G.1 General presentation of the strand passage in the convergence zone

APPENDIX H. Experimental Data and Results

H.1 Derived Pitch Lengths versus Experimental Data from the Lathe Simulation

Basic Data:

Rm	2.540
R_G	7.620
Pitch	2.540
Distance X	0.0

Rm	1.270
R_G	6.985
Pitch	2.540
Distance X	0.0

2.54 cm Rod

	a_n	Data points	deviation	
x	0	0	cm.	%
1	1.308	1.191	0.117	8.94
2	1.943	2.065	0.122	6.28
3	2.25	2.301	0.051	2.27
4	2.4	2.461	0.061	2.54
5	2.471			
6	2.507			
7	2.525			
8	2.532			
9	2.537			
10	2.537			
11	2.540			
12	2.540			
13	2.540			
14	2.540			
15	2.540			
16	2.540			
17	2.540			
18	2.540			
19	2.540			

1.27 cm Rod

a_n	Data points	deviation	
0	0	cm.	%
0.927	0.795	0.132	14.24
1.514	1.509	0.005	0.34
1.887	1.984	0.097	5.11
2.126	2.223	0.097	4.54
2.276	2.383	0.107	4.69
2.372	2.461	0.089	3.75
2.433			
2.471			
2.497			
2.512			
2.522			
2.53			
2.532			
2.535			
2.537			
2.537			
2.54			
2.540			
2.540			

H.2 Data Points Generated from Fourteen 2D Cylindrical Braiding Experiments (Table 6.1) and the Corresponding Derivation Result (Table 6.2)

Experiment No. 1

Basic data:

Rm	1.270	rpm (head)	674.9	1
R_G	7.765	rpm (mandrel)	136.6	
Pitch	7.840	Ratio (ω/v)	2.035	
Distance X	2.426			

	a_n derived	a_n measured	Deviation (absolute)
	2.426	2.426	
1	5.238	4.763	0.475
2	6.566	6.668	0.102
3	7.217	7.463	0.246
4	7.535	7.699	0.164
5	7.691	7.78	0.089
6	7.768		
7	7.805		
8	7.823		
9	7.832		
110	7.837		

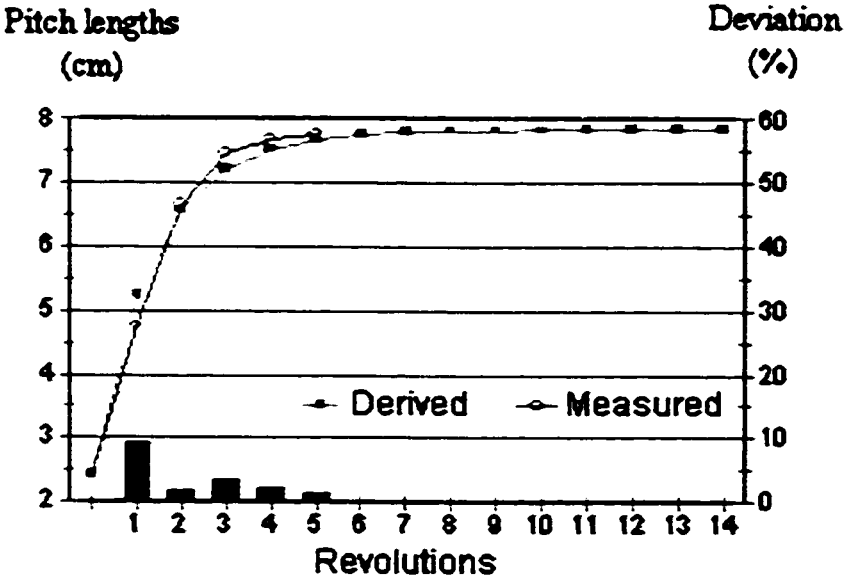

Figure H.1 Pitch lengths of the braided strands during the transient state – measured vs derived (exp #1). Percentage deviation given by bars

Experiment No. 2

Basic data:

Rm	1.270	rpm (head)	674.9	2
R_G	7.765	rpm (mandrel)	136.6	
Pitch	7.840	Ratio (ω/v)	2.035	
Distance X	13.462			

	a_n derived	a_n measured	Deviation (absolute)
	13.462	13.462	
1	10.869	12.065	1.196
2	9.324	9.682	0.358
3	8.567	8.334	0.233
4	8.197	8.016	0.181
5	8.015	7.938	0.077
6	7.926	7.859	0.067
7	7.883	7.859	0.024
8	7.861	7.859	0.002
9	7.851		
10	7.846		

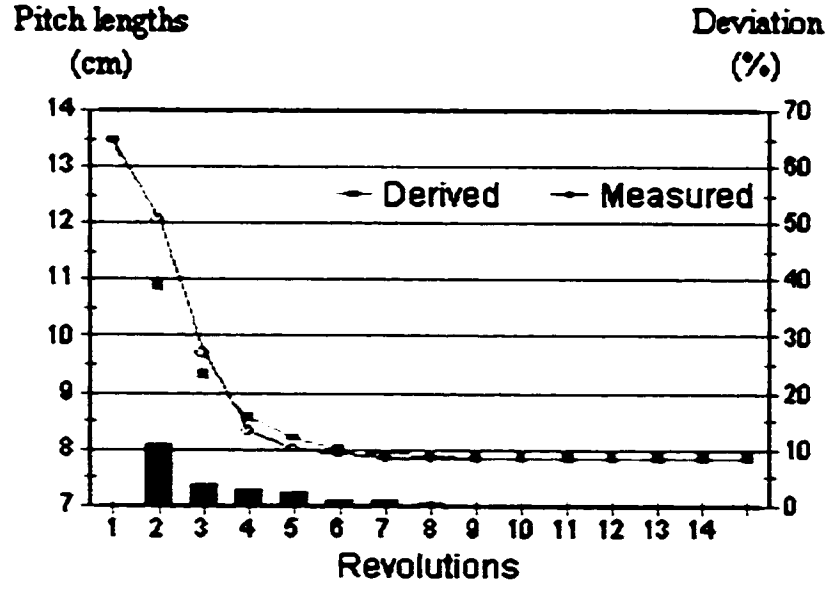

Figure H.2 Pitch lengths of the braided strands during the transient state – measured vs derived (exp #2). Percentage deviation given by bars

Experiment No. 3

Basic data:

Rm	1.270	rpm (head) 674.5	3
R_G	7.765	rpm (mandrel) 119.2	
Pitch	6.845	Ratio (ω/v) 2.331	
Distance X	2.51		

	a_n derived	a_n measured	Deviation (absolute)
	2.51	2.51	
1	4.773	4.524	0.249
2	5.830	6.114	0.284
3	6.348	6.429	0.081
4	6.602	6.708	0.106
5	6.726	6.784	0.058
6	6.787	6.784	0.003
7	6.817	6.784	0.033
8	6.831	6.784	0.047
9	6.838	6.784	0.054
10	6.842	6.784	0.058
11	6.844		
12	6.844		

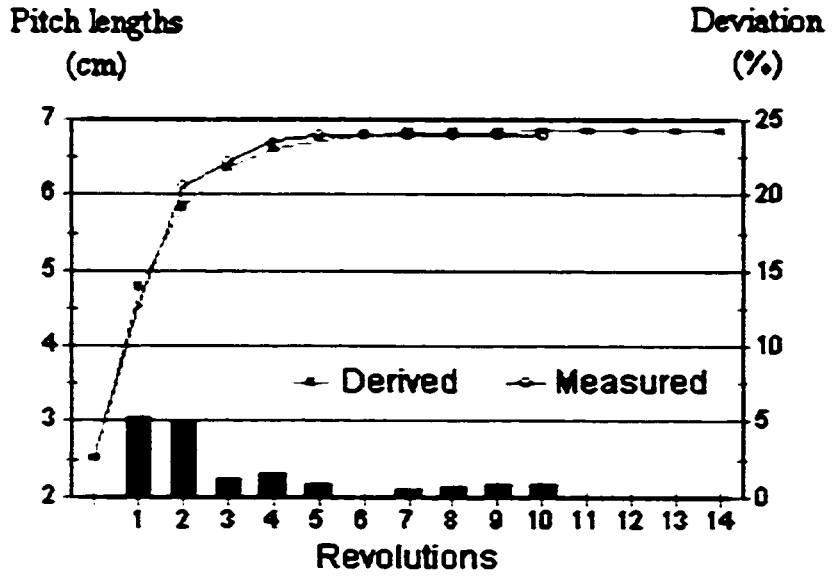

Figure H.3 Pitch lengths of the braided strands during the transient state – measured vs derived (exp #3). Percentage deviation given by bars

Experiment No. 4

Basic data:

Rm	1.270	rpm (head)	674.9	4
R_G	7.765	rpm (mandrel)	136.6	
Pitch	6.845	Ratio ω/v	2.035	
Distance X	1.859			

	a_n derived	a_n measured	Deviation (absolute)
	1.859	1.859	
1	4.441	4.247	0.194
2	5.668	5.913	0.245
3	6.269	6.51	0.241
4	6.563	6.668	0.105
5	6.707	6.708	0.001
6	6.778	6.746	0.032
7	6.812	6.828	0.016
8	6.829		
9	6.837		
10	6.841		
11	6.843		
12	6.844		

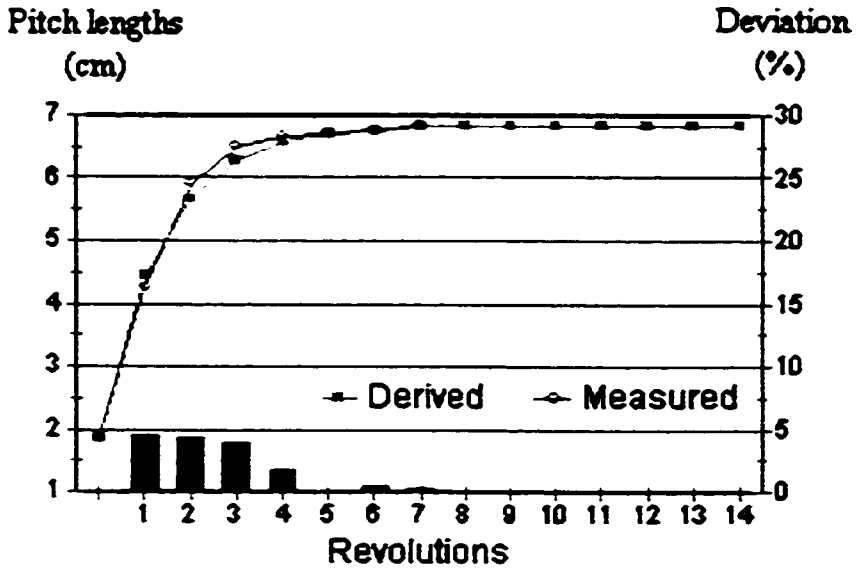

Figure H.4 Pitch lengths of the braided strands during the transient state – measured vs derived (exp #4). Percentage deviation given by bars

Experiment No. 5

Basic data:

Rm	1.270	rpm (head)	674.5	5
R_G	7.765	rpm (mandrel)	101.9	
Pitch	5.852	Ratio ω/v	2.727	
Distance X	3.675			

	a_n derived	a_n measured	Deviation (absolute)
	3.675	3.675	
1	4.861	5.08	0.219
2	5.367	5.555	0.188
3	5.614	5.715	0.101
4	5.736	5.872	0.136
5	5.795	5.872	0.077
6	5.824	5.872	0.048
7	5.838	5.794	0.044
8	5.845	5.872	0.027
9	5.849	5.794	0.055
10	5.851		
11	5.851		
12	5.852		

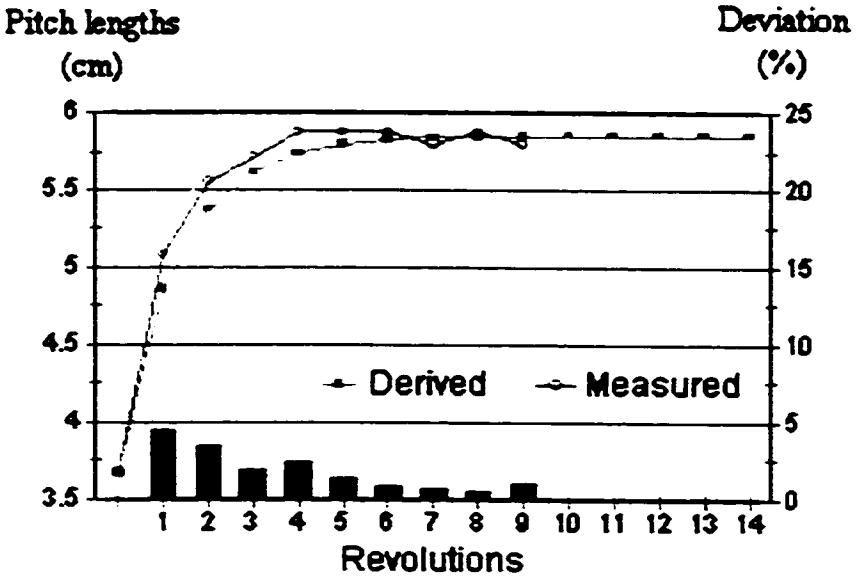

Figure H.5 Pitch lengths of the braided strands during the transient state – measured vs derived (exp #5). Percentage deviation given by bars

Experiment No. 6

Basic data:

Rm	1.270	rpm (head)	674.5	6
R_G	7.7657	rpm (mandrel)	101.9	
Pitch	5.853	Ratio ω/v	2.727	
Distance X	11.603			

	a_n derived	a_n measured	Deviation (absolute)
	11.603	11.603	
1	8.906	10.239	1.333
2	7.348	7.699	0.351
3	6.585	6.35	0.235
4	6.211	6.152	0.059
5	6.028	5.954	0.074
6	5.938	5.898	0.040
7	5.894	5.875	0.019
8	5.873	5.875	0.002
9	5.862	5.875	0.013
10	5.857		
11	5.855		
12	5.853		

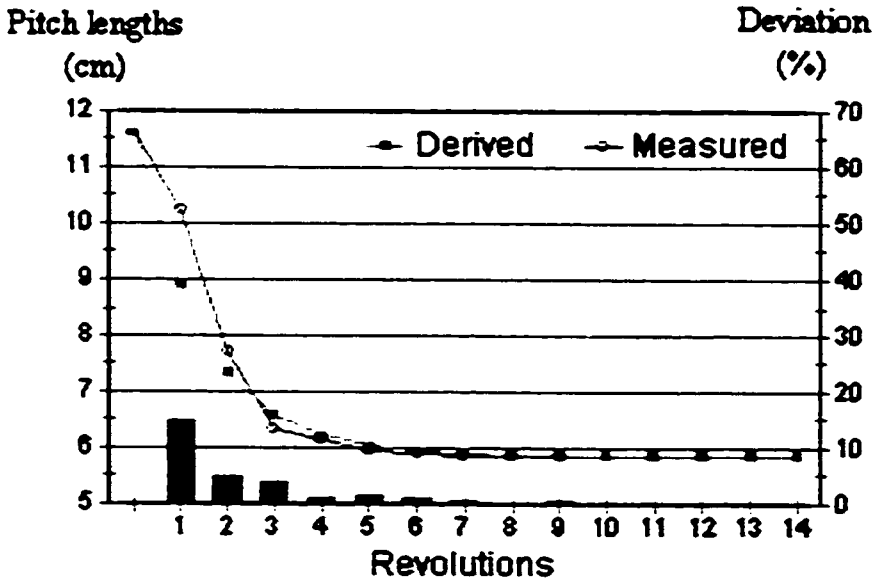

Figure H.6 Pitch lengths of the braided strands during the transient state – measured vs derived (exp #6). Percentage deviation given by bars

Experiment No. 7

Basic data:

Rm	1.270	rpm (head)	675.1	7
R_G	7.765	rpm (mandrel)	84.7	
Pitch	4.861	Ratio ω/v	3.283	
Distance X	2.344			

	a_n derived	a_n measured	Deviation (absolute)
	2.344	2.344	
1	3.677	3.81	0.133
2	4.281	4.445	0.164
3	4.577	4.684	0.107
4	4.722	4.763	0.041
5	4.793	4.803	0.01
6	4.828	4.841	0.013
7	4.845	4.841	0.004
8	4.854	4.841	0.013
9	4.858	4.841	0.017
10	4.860		
11	4.861		
12	4.861		

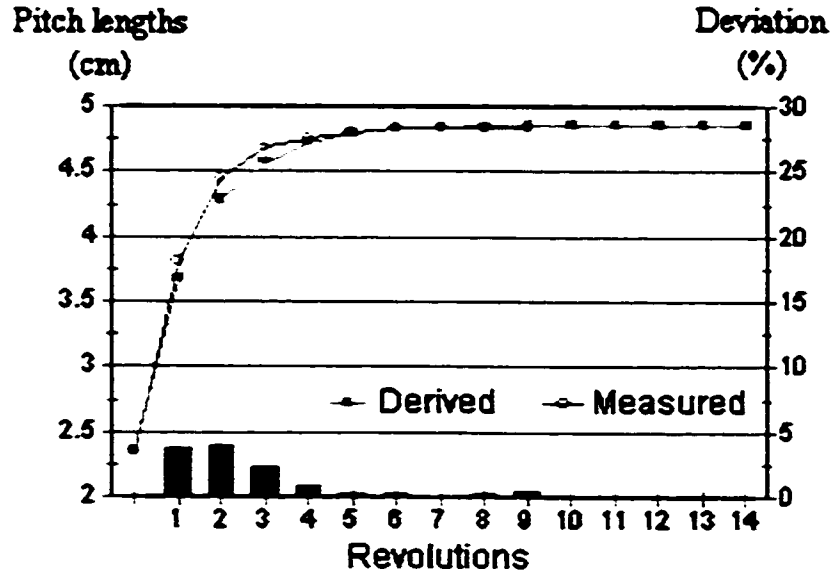

Figure H.7 Pitch lengths of the braided strands during the transient state – measured vs derived (exp #7). Percentage deviation given by bars

Experiment No. 8

Basic data:

Rm	1.270	rpm (head)	675.1	8
R_G	7.765	rpm (mandrel)	84.7	
Pitch	4.862	Ratio ω/v	3.283	
Distance X	9.055			

	a_n derived	a_n measured	Deviation (absolute)
	9.055	9.055	
1	7.100	7.653	0.553
2	5.958	6.033	0.075
3	5.399	5.357	0.042
4	5.125	5.08	0.045
5	4.990	4.92	0.070
6	4.925	4.841	0.084
7	4.892	4.841	0.051
8	4.877	4.841	0.036
9	4.869	4.841	0.028
10	4.865	4.841	0.024
11	4.863		
12	4.862		

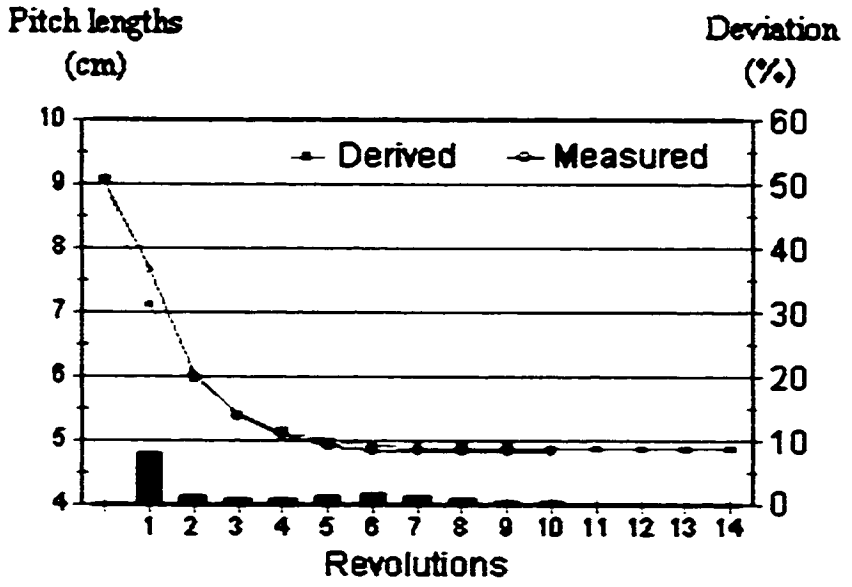

Figure H.8 Pitch lengths of the braided strands during the transient state – measured vs derived (exp #8). Percentage deviation given by bars

Experiment No. 9

Basic data:

Rm	1.270	rpm (head)	675.1	9
R_G	7.7657	rpm (mandrel)	67.4	
Pitch	3.866	Ratio ω/v	4.127	
Distance X	2.184			

	a_n derived	a_n measured	Deviation (absolute)
	2.184	2.184	
1	3.087	3.254	0.167
2	3.484	3.612	0.128
3	3.679	3.729	0.050
4	3.774	3.81	0.036
5	3.821	3.866	0.045
6	3.844	3.889	0.045
7	3.855	3.889	0.034
8	3.861	3.889	0.028
9	3.863	3.889	0.026
10	3.865	3.889	0.024
11	3.865		
12	3.866		

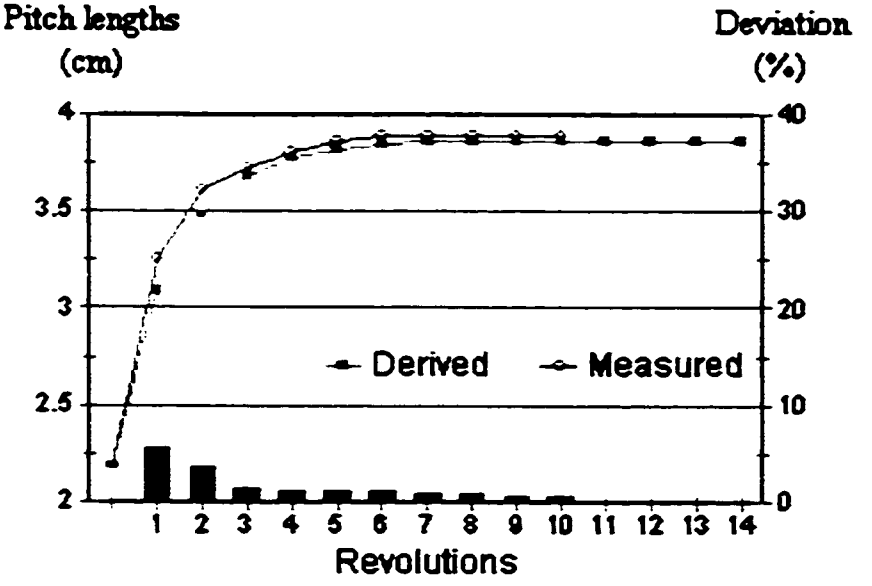

Figure H.9 Pitch lengths of the braided strands during the transient state – measured vs derived (exp #9). Percentage deviation given by bars

Experiment No. 10

Basic data:

Rm	1.270	rpm (head)	6745.1	10
R_G	7.765	rpm (mandrel)	67.4	
Pitch	3.866	Ratio ω/v	4.127	
Distance X	9.322			

	a_n derived	a_n measured	Deviation (absolute)
	9.322	9.322	
1	6.729	8.255	1.526
2	5.268	5.558	0.290
3	4.553	4.445	0.108
4	4.202	4.049	0.153
5	4.031	3.967	0.064
6	3.947	3.967	0.020
7	3.905	3.967	0.062
8	3.885	3.889	0.004
9	3.875	3.889	0.014
10	3.871		
11	3.868		
12	3.867		

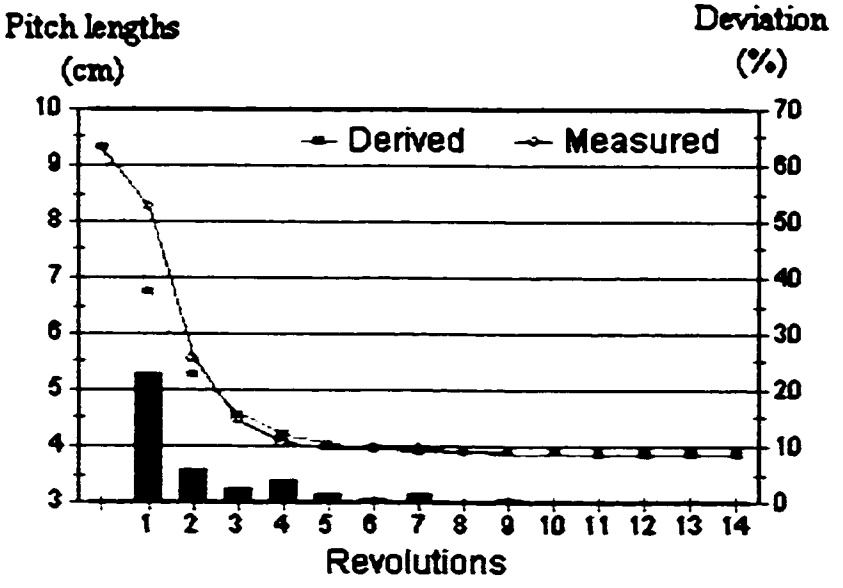

Figure H.10 Pitch lengths of the braided strands during the transient state – measured vs derived (exp #10). Percentage deviation given by bars

Experiment No. 11

Basic data:

Rm	1.270	rpm (head)	502.3	11
R_G	7.765	rpm (mandrel)	101.8	
Pitch	7.826	Ratio ω/v	2.039	
Distance X	2.672			

	a_n derived	a_n measured	Deviation (absolute)
	2.672	2.672	
1	5.356	5.08	0.276
2	6.616	6.746	0.130
3	7.233	7.541	0.308
4	7.536	7.78	0.244
5	7.684	7.777	0.093
6	7.756	7.699	0.057
7	7.792	7.699	0.093
8	7.809	7.699	0.110
9	7.818		
10	7.822		
11	7.824		
12	7.825		

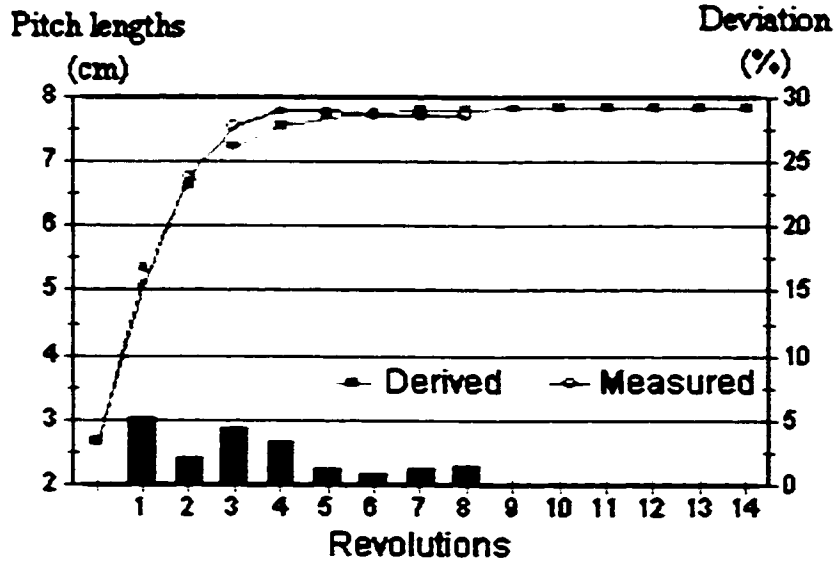

Figure H.11 Pitch lengths of the braided strands during the transient state – measured vs derived (exp #11). Percentage deviation given by bars

Experiment No. 12

Basic data:

Rm	1.270	rpm (head)	502.3	12
R_G	7.765	rpm (mandrel)	101.8	
Pitch	7.826	Ratio ω/v	2.039	
Distance X	11.773			

	a_n derived	a_n measured	Deviation (absolute)
	11.773	11.773	
1	10.000	10.478	0.478
2	8.890	9.208	0.318
3	8.347	8.176	0.171
4	8.081	8.098	0.017
5	7.951	7.859	0.092
6	7.887	7.777	0.110
7	7.856		
8	7.840		
9	7.833		
10	7.829		
11	7.827		
12	7.827		

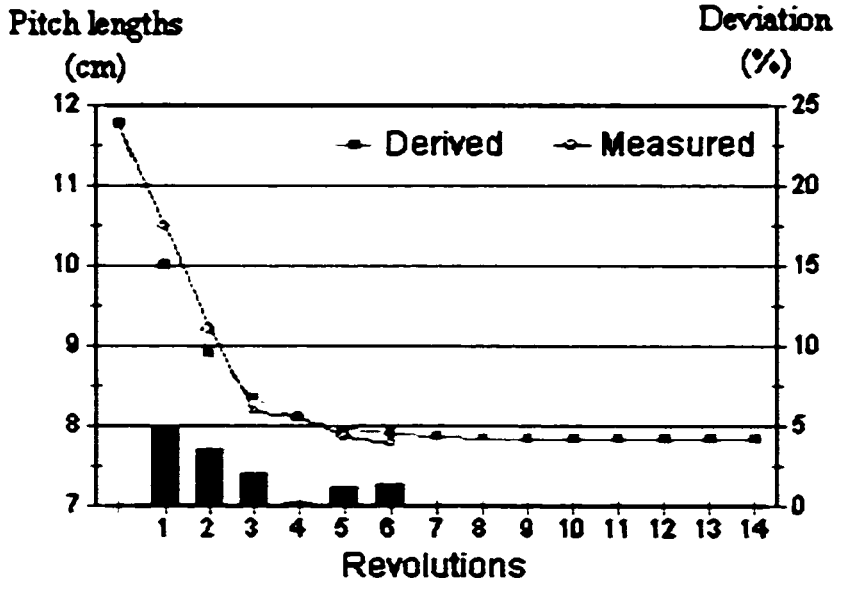

Figure H.12 Pitch lengths of the braided strands during the transient state – measured vs derived (exp #12). Percentage deviation given by bars

Experiment No. 13

Basic data:

Rm	1.270	rpm (head)	417.1	13
R_G	7.765	rpm (mandrel)	136.4	
Pitch	12.667	Ratio ω/v	1.260	
Distance X	2.022			

	a_n derived	a_n measured	Deviation (absolute)
	2.022	2.022	
1	7.494	6.787	0.707
2	10.134	10.518	0.384
3	11.426	11.908	0.482
4	12.059	12.383	0.324
5	12.369	12.543	0.174
6	12.521		
7	12.596		
8	12.632		
9	12.650		
10	12.659		
11	12.663		
12	12.663		

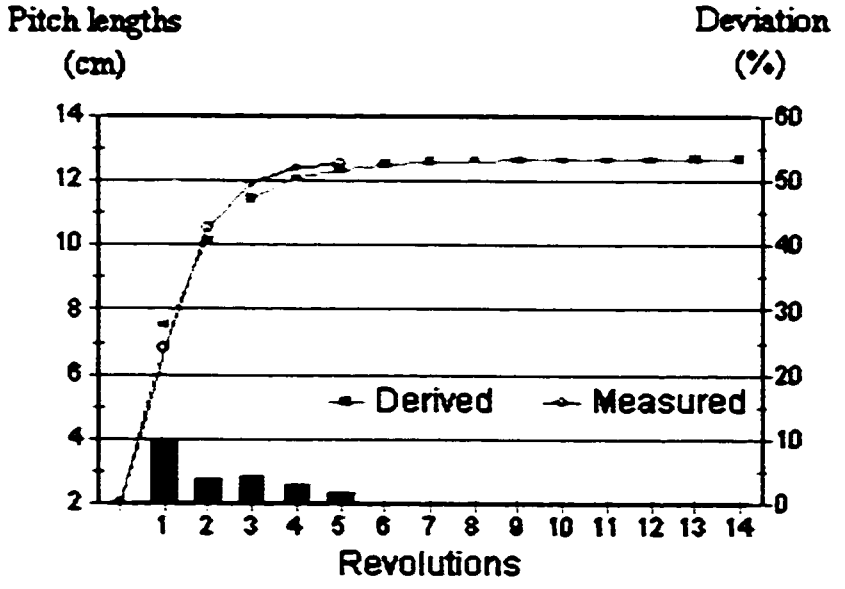

Figure H.13 Pitch lengths of the braided strands during the transient state – measured vs derived (exp #13). Percentage deviation given by bars

Experiment No. 14

Basic data:

Rm	1.270	rpm (head)	417.1
R_G	7.765	rpm (mandrel)	136.4
Pitch	12.667	Ratio ω/v	1.260
Distance X	0.246		

	a_n derived	a_n measured	Deviation (absolute)
	0.246	0.246	
1	6.589	6.589	0.000
2	9.690	9.921	0.231
3	11.209	11.826	0.617
4	11.953	12.304	0.351
5	12.317	12.543	0.226
6	12.496	12.543	0.047
7	12.583	12.543	0.040
8	12.626		
9	12.647		
10	12.657		
11	12.662		
12	12.665		

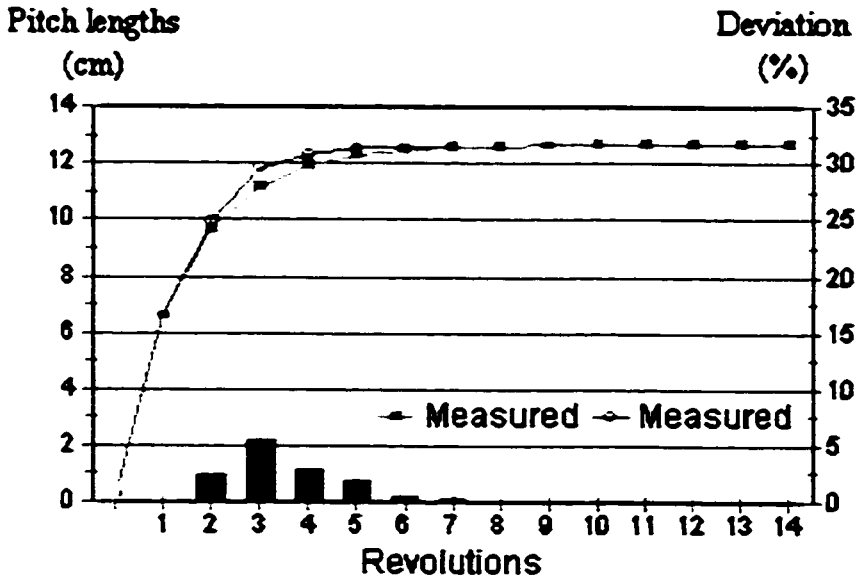

Figure H.14 Pitch lengths of the braided strands during the transient state – measured vs derived (exp #14). Percent deviation given by bars

H.3 Derived Pitch and Convergence Lengths, versus, Data Extracted from Du and Popper [10], Figure 12

Basic data:

Rm	1.875 cm	Rm	1.875 cm
R_G	15.00 cm	R_G	15.00 cm
Pitch	5.655 cm	Pitch	5.655 cm
h_o	24.00 cm	h_o	50.00 cm
h_∞	7.144 cm	h_∞	7.144 cm

	h_n	Data points	Deviation (cm)	Deviation (%)	h_n	Data points	Deviation (cm)	Deviation (%)
ho	24	24			50	50		
1	16.552	16.5	0.052	0.31	31.064	30	1.064	3.34
2	12.395	12	0.395	3.19	20.495	16.5	3.995	19.49
3	10.075	9.50	0.575	5.71	14.596	11.5	3.096	21.21
4	8.780	9.00	0.22	2.51	11.303	10	1.303	11.53
5	8.057	8.00	0.057	0.71	9.465	8.5	0.965	10.19
6	7.653	7.50	0.153	1.99	8.439	8.5	0.061	0.72
7	7.428	7.50	0.072	0.97	7.867	8.25	0.383	4.87
8	7.302	7.50	0.198	2.71	7.547	8.25	0.703	9.31
9	7.232				7.369	8	0.631	8.56
10	7.193				7.269	8	0.731	10.06
11	7.171				7.214	7.5	0.286	3.96
12	7.159				7.183	7.5	0.317	4.41
13	7.152				7.165	7	0.165	2.3
14	7.148				7.156	7	0.156	2.18
15	7.146				7.15	7	0.15	2.1
16	7.145				7.147			
17	7.144				7.146			
18	7.144				7.145			
19	7.144				7.144			
20	7.144				7.144			
21	7.144				7.144			
22	7.144				7.144			

The data points represent the lengths of the convergence zone at every multiple of 360° (data extracted from Du and Popper [10].

H.4 Comparison between continuous and discrete series (Experiment number 7)

Basic data:

Rm	1.270	rpm (head)	675.1
R_G	7.765	rpm (mandrel)	84.7
Pitch	4.861	Ratio ω/v	3.283
Distance X	2.344		

Continuous	Discrete	Difference	Continuous	Discrete	Difference	Continuous	Discrete	Difference
2.441	2.441	0.000	4.577	4.577	0.000	4.829	4.829	0.000
2.609	2.564	0.044	4.597	4.592	0.006	4.831	4.830	0.001
2.764	2.688	0.076	4.615	4.606	0.009	4.834	4.832	0.002
2.908	2.811	0.097	4.633	4.621	0.012	4.834	4.834	-0.000
3.043	2.935	0.108	4.648	4.635	0.013	4.836	4.836	0.001
3.167	3.058	0.109	4.663	4.649	0.014	4.839	4.837	0.001
3.284	3.182	0.103	4.676	4.664	0.012	4.839	4.839	-0.001
3.393	3.305	0.088	4.689	4.678	0.010	4.841	4.841	0.000
3.495	3.428	0.067	4.702	4.693	0.009	4.844	4.843	0.001
3.589	3.552	0.037	4.712	4.707	0.004	4.844	4.845	-0.001
3.675	3.675	0.000	4.722	4.722	0.000	4.846	4.846	0.000
3.759	3.736	0.023	4.732	4.729	0.003	4.846	4.847	-0.001
3.835	3.797	0.039	4.740	4.736	0.004	4.846	4.848	-0.002
3.904	3.857	0.046	4.750	4.743	0.007	4.849	4.849	0.000
3.970	3.918	0.052	4.757	4.750	0.007	4.849	4.849	-0.001
4.034	3.979	0.055	4.765	4.757	0.008	4.849	4.850	-0.001
4.089	4.040	0.050	4.770	4.765	0.006	4.851	4.851	0.001
4.14[illegible]	4.100	0.042	4.778	4.772	0.006	4.851	4.852	-0.000
4.191	4.161	0.030	4.783	4.779	0.004	4.851	4.852	-0.001
4.239	4.222	0.018	4.788	4.786	0.002	4.854	4.853	0.001
4.282	4.282	0.000	4.793	4.793	0.000	4.854	4.854	0.000
4.321	4.312	0.009	4.798	4.797	0.002	4.854	4.854	-0.000
4.359	4.341	0.017	4.803	4.800	0.003	4.854	4.854	-0.001
4.394	4.371	0.023	4.806	4.804	0.002	4.854	4.855	-0.001
4.425	4.400	0.024	4.811	4.807	0.004	4.856	4.855	0.002
4.455	4.430	0.025	4.813	4.811	0.003	4.856	4.855	0.001
4.483	4.459	0.024	4.818	4.814	0.004	4.856	4.855	0.001
4.509	4.489	0.020	4.821	4.818	0.003	4.856	4.856	0.001
4.534	4.518	0.016	4.823	4.821	0.002	4.856	4.856	0.001
4.557	4.548	0.009	4.826	4.825	0.001	4.856	4.856	0.000

Note: Data interval = 1/10 revolution

H.5 Derived Pitch Lengths versus Experimental Data Considering the Effect of Fibre Interlace

Basic data:

Rm	1.270
R_G	7.765
Pitch	4.826

With
Strand interlacing parameter 'ζ'

	a_n	Data points	Deviation	
			(cm)	(%)
X	2.057	2.057	0	0
1	3.995	3.967	0.28	0.7
2	4.496	4.524	0.028	0.62
3	4.707	4.684	0.23	0.59
4	4.796	4.773	0.33	0.69
5	4.834	4.826	0.08	0.16
6	4.849	4.826	0.023	0.47
7	4.856	4.826	0.03	0.63
8	4.859			
9	4.862			
10	4.862			
11	4.862			
12	4.862			
13	4.862			
14	4.862			
15	4.862			
16	4.862			